UNIVERSIDADE FEDERAL DE LAVRAS

DIEGO TASSINARI

COMPRESSIBILIDADE DO SOLO E PRESSÃO DE PRÉ-CONSOLIDAÇÃO: DETERMINAÇÃO, PREDIÇÃO E INTERAÇÕES

LAVRAS-MG
2019

DIEGO TASSINARI

COMPRESSIBILIDADE DO SOLO E PRESSÃO DE PRÉ-CONSOLIDAÇÃO:
DETERMINAÇÃO, PREDIÇÃO E INTERAÇÕES

Tese apresentada à Universidade Federal de Lavras, como parte das exigências do Programa de Pós-Graduação em Ciência do Solo, área de concentração em Recursos Ambientais e Uso da Terra, para a obtenção do título de Doutor.

Prof. PhD. Moacir de Souza Dias Junior
Orientador

LAVRAS-MG
2019

DIEGO TASSINARI

COMPRESSIBILIDADE DO SOLO E PRESSÃO DE PRÉ-CONSOLIDAÇÃO:
DETERMINAÇÃO, PREDIÇÃO E INTERAÇÕES
SOIL COMPRESSIBILITY AND PRECOMPRESSION STRESS:
DETERMINATION, PREDICTION AND INTERACTIONS

> Tese apresentada à Universidade Federal de Lavras, como parte das exigências do Programa de Pós-Graduação em Ciência do Solo, área de concentração em Recursos Ambientais e Uso da Terra, para a obtenção do título de Doutor.

APROVADA em 15 de Fevereiro de 2019.
Dr. Geraldo César de Oliveira   UFLA
Dr. Bruno Montoani Silva   UFLA
Dr. Wellington Willian Rocha   UFVJM
Dr. Eduardo da Costa Severiano   IF Goiano

Prof. PhD. Moacir de Souza Dias Junior
Orientador

Lavras-MG
2019

A meu pai, que acompanhou a labuta porém não seu desfecho,

dedico.

AGRADECIMENTOS

"− Coronel, esse relatório tem fundamento estatístico (...).

− E eu quero lá saber de Numerologia!"

(Tropa de Elite, 2007)

RESUMO

O estudo do comportamento mecânico do solo tem grande relevância na avaliação da compactação do solo em sistemas agrícolas. Mais comumente, a resistência mecânica do solo é avaliada a partir do seu comportamento compressivo, determinado pela curva de compressão do solo oriunda de ensaios de compressão uniaxial. A propriedade do solo mais comumente associada à sua resistência mecânica é a pressão de pré-consolidação (σ_p), considerada um indicativo da capacidade de suporte de carga do solo. O presente trabalho teve como objetivos verificar as mudanças que ocorrem nas propriedades do solo durante a compressão (artigo 1), comparar diferentes métodos para determinação da σ_p a partir da curva de compressão do solo (artigo 2), e verificar como a σ_p pode ser predita a partir de outros atributos (artigo 3). Durante a compressão, as amostras estiveram sujeitas tanto a compactação quanto a consolidação, esta principalmente nas amostras equilibradas à tensão de água (Ψ) de 10 kPa e sob as cargas aplicadas mais elevadas. O grau de compactação obtido ao longo de toda a faixa de pressões plicadas foi fortemente dependente da condição inicial do solo. O formato da curva de compressão, bi-linear ou sigmoidal, foi significativamente afetado pela Ψ e pela condição inicial da amostra. Observou-se interação entre o método de determinação da σ_p e o atributo usado para representar a curva de compressão. Além da não-linearidade entre densidade do solo e índice de vazios, o desempenho dos métodos avaliados também foi afetado pela relação direta ou inversa entre os atributos físicos e as pressões aplicadas durante a compressão. A determinação de σ_p pela interseção de duas retas (definidas pelos primeiros e pelos últimos três pontos da curva de compressão do solo) mostrou-se uma alternativa viável e segura. A predição da σ_p torna-se mais precisa quando atributos relativizados, como o grau de compactação, são empregados nos modelos, o que reduz a influência da variabilidade de atributos intrínsecos, como a textura do solo.

Palavras-chave: Ensaio de compressão uniaxial. Curva de compressão do solo. Compactação do solo. Grau de compactação.

ABSTRACT

The study of soil mechanical behavior is of great relevance in the assessment of soil compaction on agricultural systems. Most commonly, mechanical strength is evaluated from the soil compressive behavior, determined by the soil compression curve derived from uniaxial compression tests. The soil property most often associated to mechanical strength is the precompression stress (σ_p), considered an indicator of the soil load-bearing capacity. The present study aimed to assess the soil changes that take place during compression (article 1), compare different methods for determining σ_p from soil compression curves (article 2), and to verify how σ_p may be predicted from other attributes (article 3). During compression, soil samples were subjected to both compaction and consolidation, the latter majorly related to the water tension (Ψ) of 10 kPa and higher applied loads. The compaction degree observed throughout the role applied pressure range was strongly dependent on the soil initial condition. The shape of the compression curve, whether bi-linear or sigmoid, was significantly affected by Ψ a by the sample's initial condition. The method for determining σ_p and the soil attribute used for representing the compression curve interact to each other. Besides the nonlinear relation between bulk density and void ratio, method performance was also affected by the relation between the physical attribute and the applied pressure during compression, whether direct or inverse. Determination of σ_p from the intersection of two linear models (defined by the first and the last three points of the soil compression curve) proved to be a viable and reliable choice. Prediction of σ_p becomes more accurate when relative measures, such as the degree of compaction, are employed in the models, what reduces the effect of varying intrinsic attributes, like soil texture.

Keywords: Uniaxial compression test. Soil compression curve. Soil compaction. Degree of compaction.

SUMÁRIO

PRIMEIRA PARTE

1 INTRODUÇÃO

A resistência mecânica do solo depende de atributos intrínsecos, como textura e mineralogia, bem como de atributos dinâmicas, como umidade, histórico de tensões, dentre outros. A umidade do solo é o fator que sozinho exerce maior influência na suscetibilidade à compactação (DIAS JUNIOR, 2000), sendo que a capacidade de suporte de carga do solo (sua capacidade de tolerar a aplicação de pressões sem sofrer compactação adicional) decresce exponencialmente com o aumento do teor de água (DIAS JUNIOR, 1994).

A compactação do solo é grandemente influenciada pela sua estrutura, que representa o arranjo das partículas sólidas do solo e do espaço poroso entre elas (HILLEL, 1998); por exemplo, solos com estrutura em blocos são mais resistentes à compactação que solos com estrutura granular (AJAYI et al., 2009). A resistência mecânica do solo é consequência do histórico de tensões às quais ele foi submetido, estando gravada na estrutura do solo como a pressão de pré-consolidação (DIAS JUNIOR, 2000). Esta propriedade do solo representa a máxima pressão que o solo pode suportar sem sofrer compactação adicional (HORN; LEBERT, 1994).

A pressão de pré-consolidação é determinada a partir da curva de compressão do solo, existindo diferentes métodos para tanto. A própria curve de compressão do solo pode ser ajustada de diferentes maneiras, a partir de diversos atributos físicos que caracterizam quantitativamente o estado da estrutura do solo, como densidade do solo e índice de vazios porosidade total. Assim, um dos objetivos desse trabalho foi avaliar a interação entre a escolha do atributo físico e a escolha do método de determinação da pressão de pré-consolidação.

Na região do município de Lavras-MG, um manejo que incorre em grande risco de compactação do solo em profundidade é o cultivo de milho para silagem. Nessas lavouras, a colheita ocorre ainda no período chuvoso, em que o solo encontra-se úmido e com menor capacidade de suporte de carga. Diferentemente das lavouras de grão, para produção de silagem praticamente toda a parte aérea das plantas é colhida, o que demanda tráfego de maquinário muito carregado e a aplicação de pressões elevadas. Adicionalmente, o preparo convencional do solo com aração é costumeiramente aplicado todos os anos, o que favorece a ocorrência de compactação abaixo da camada arável.

2 REFERENCIAL TEÓRICO

2.1 Compactação do solo em lavouras de milho para silagem

A pecuária leiteira demanda a adoção de técnicas de conservação de forragens para o fornecimento de alimento volumoso ao longo de todo o ano aos rebanhos (OLIVEIRA et al., 2010). Adicionalmente, a estacionalidade na produção de forragens também reforça a necessidade de conservação de forragens, já que na região, a estação seca (abril a setembro) concentra apenas de 3 a 26 % da produção anual de forrageiras (BOTREL; ALVIM; XAVIER, 1999).

No estado de Minas Gerais, a área colhida de milho para produção de forragem é estimada em mais de 170.000 ha, o que representa quase 22% da área cultivada com esta lavoura no país, enquanto na microrregião de Lavras, o milho representa 84% das lavouras temporárias com finalidade de produção de forragens (INSTITUTO BRASILEIRO DE GEOGRAFIA E ESTATÍSTICA − IBGE, 2006). O milho é preferido para a produção de silagem por diversos fatores: possui sistema de produção já bem definido, pela facilidade de cultivo e colheita mecanizados, possui produção adequada de matéria seca, a fermentação durante o processo de ensilagem é facilitada, o valor energético da silagem é elevado, e o consumo voluntário da silagem pelos animais é elevado (EVANGELISTA; LIMA, 2002) e continuará sendo ainda por um bom tempo o principal suplemento volumoso fornecido para os rebanhos leiteiros (OLIVEIRA; OLIVEIRA, 2014).

A compactação do solo em lavouras de milho para silagem reduz a produtividade e a absorção de nitrogênio pelas plantas (NEVENS; REHEUL, 2002). Avaliando a dinâmica de tráfego durante a colheita em lavouras de milho para silagem, Duttmann, Brunotte e Bach (2013) observaram que mais de 60% da área cultivada foi trafegada pelos veículos de colheita e transporte, sendo que dois terços dessa área foram trafegados ao menos duas vezes. Comparando diferentes sistemas de preparo de solo para o cultivo de milho para silagem em um solo franco-argilossiltoso, Afzalinia e Zabihi (2014) observaram que a densidade do solo não diferiu entre os tratamentos (preparo convencional, preparo reduzido e plantio direto) após dois meses das operações de preparo. Resultado semelhante foi encontrado por Tassinari et al. (2015) em pastagens renovadas por integração com milho silagem, também não sendo observadas diferenças na densidade do solo entre o preparo convencional e a semeadura direta ao término do experimento. Esses resultados apontam que ao término dos ciclos de cultivo, o

efeito da compactação do solo encontra-se reestabelecido independentemente do preparo realizado. Assim, no presente trabalho de tese, será dada ênfase à condição do solo previamente às operações de colheita, representativo, portanto, não só do estado de compactação experimentado pela lavoura, mas também da resistência mecância do solo por ocasião do tráfego associado às atividades de colheita..

2.2 Compressibilidade do solo e pressão de pré-consolidação

A compactação é um processo de degradação do solo, comprometendo a sua qualidade e ameaçando a produção agrícola (RABOT et al., 2018). Considerar o comportamento compressivo do solo e a sua resistência mecânica pode ser bastante benéfico para a prevenção e a avaliação da compactação do solo (IMHOFF et al., 2016; KELLER et al., 2013; LEBERT; BÖKEN; GLANTE, 2007), já que esses parâmetros estão intimamente ligados às alterações estruturais do solo decorrentes da compactação e também se relacionam ao desenvolvimento das plantas (NUNES et al., 2019; SCHJØNNING et al., 2016).

2.2.1 Compressibilidade do solo

A relação entre pressões aplicadas e deformações resultantes caracteriza a compressibilidade ou comportamento compressivo do solo (HORN; LEBERT, 1994). O comportamento compressivo do solo tem sido avaliado de diferentes maneiras, incluindo métodos de campo (KELLER et al., 2004; NADERI-BOLDAJI et al., 2018) e de laboratório, sendo o ensaio de compressão uniaxial o método mais comum (e.g. LIMA et al., 2018; MARTINS et al., 2018; NUNES et al., 2019; SCHJØNNING et al., 2016). Nesse ensaio, realizado em equipamentos denominados consolidômetros, amostras confinadas em anéis metálicos são deformadas sob pressões sequenciais (DIAS JUNIOR; MARTINS, 2017). Convencionalmente, as pressões são aplicadas sequencialmente e sem descompressão, contudo, mais recentemente, ensaios de compressão cíclicos ou dinâmicos têm sido empregados na caracterização do comportamento compressivo do solo (HOLTHUSEN et al., 2018), com aplicação de pressões em ciclos de 30 s.

A compressibilidade do solo não tem adoção universal na pesquisa em compactação do solo, mas encontra-se firmemente estabelecida nos nichos que ocupa. Essa técnica é mais comumente adotada como medida da resistência mecânica do solo em: lavouras sob

condições climáticas mais úmidas e, portanto, mais vulneráveis à compactação, como no Norte da Europa (KELLER et al., 2012; RÜCKNAGEL et al., 2017; SCHJØNNING et al., 2016) e no Sul do Brasil (NUNES et al., 2019; REICHERT et al., 2018); estudos de solos mais vulneráveis à compactação, como Latossolos, em especial os da região do Cerrado, Chernossolos e outros (AJAYI et al., 2014, 2013, 2010, 2009; IMHOFF et al., 2016; MOSADDEGHI et al., 2007, SEVERIANO et al., 2013, 2011); explorações agrícolas sujeitas a expressivo tráfego de maquinário, tanto pela intensidade de tráfego, como nas lavouras cafeeiras (ARAUJO JUNIOR et al., 2011; PAIS et al., 2013, 2011; KAMIMURA et al., 2012; MARTINS et al., 2012a; IORI et al., 2014, 2013), quanto pelas elevadas dimensões do maquinário empregado, como em florestas de eucalipto (ANDRADE et al., 2017; DIAS JUNIOR et al., 2005, 2007, 2008; MARTINS et al., 2013, 2018; SILVA; DIAS JUNIOR; LEITE, 2007, 2010) e lavouras de cana-de-açúcar (SOUSA et al., 2019; SOUZA et al., 2012; VISCHI FILHO et al., 2015).

2.2.2 Curva de compressão do solo

O comportamento compressivo do solo é representado pela sua curva de compressão (Figura 1), que é a expressão gráfica da relação entre pressão aplicada (em escala logarítmica) e alguma propriedade de relação massa-volume do solo, como índice de vazios (e), densidade do solo (ρ), e porosidade total (n). Existe variação entre os formatos das curvas de compressão do solo (TANG et al., 2009), sendo reconhecidos ao menos dois formatos gerais, (i) o sigmoidal, em que a taxa de deformação decresce nas maiores pressões; e (ii) o bi-linear, em que a taxa de deformação não decresce (Figura 1).

O formato sigmoidal representa um decréscimo da taxa de variação na compressão do solo nos últimos estágios do ensaio de compressão uniaxial, marcadamente no último incremento de carga aplicado. Já o formato bi-linear pode ser verificado sob duas condições distintas, uma em que a taxa de compressão na muda ao longo das últimas pressões do ensaio, e outra em que a taxa de compressão aumenta sequencialmente conforme aumentam as pressões (Figura 1).

Figura 1 − Diferentes formatos da curva de compressão do solo em função da taxa de variação da densidade do solo em função da pressão aplicada.
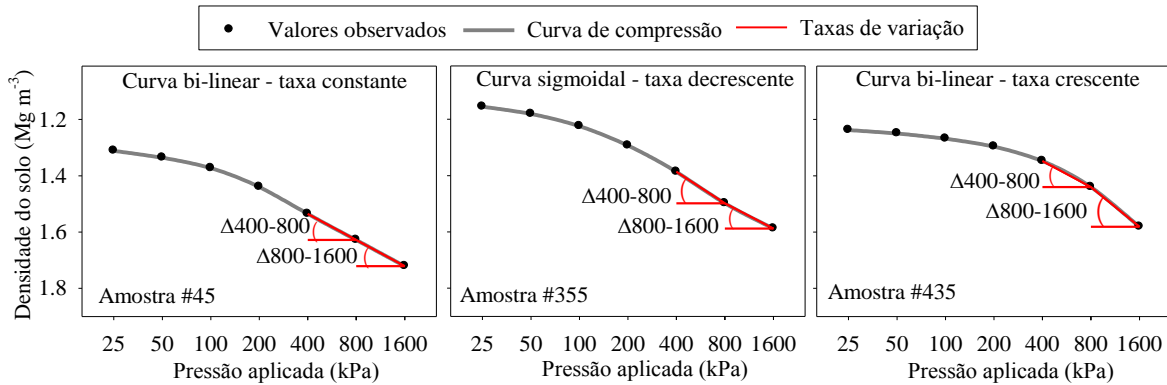
Fonte: Do autor.

2.2.3 Determinação da pressão de pré-consolidação

Quando se considera que o comportamento mecânico do solo é o de um meio sólido poroso perfeitamente elasto-plástico, assume-se que existe um determinado valor de pressão que separa as deformações que são elásticas e recuperáveis daquelas que são plásticas. Esse valor é a pressão de pré-consolidação do solo e representa a sua capacidade de suporte de carga. Evidências recentes sugerem que a escolha da propriedade física do solo na definição da curva de compressão afeta a subsequente determinação da pressão de pré-consolidação.

Originalmente determinada graficamente a partir da curva de compressão do solo (CASAGRANDE, 1936), essa propriedade tem sido atualmente determinada por métodos estatísticos e numéricos (DIAS JUNIOR; PIERCE, 1995; GREGORY et al., 2006; LAMANDÉ; SCHJØNNING; LABOURIAU, 2017), apesar de diversos trabalhos ainda empregarem o método original (REICHERT et al., 2018; HOLTHUSEN et al., 2018). Os métodos baseiam-se na proposição original de Casagrande (1936) tanto por procedimentos validados com o método original quanto pela aplicação do método em si estatística-, numérica- e algebricamente. Nesse caso, mais comumente ajusta-se uma equação à curva de compressão do solo (para estimativa dos parâmetros) a partir da qual se determina numericamente o ponto de máxima curvatura e então, os passos seguintes do método original são aplicados algebricamente. Contudo, estudos recentes têm demonstrado que o ponto de máxima curvatura da curva de compressão tem se aproximado mais de uma estimativa

experimentalmente corroborada da pressão de pré-consolidação (GREGORY et al., 2006; LAMANDÉ; SCHJØNNING; LABOURIAU, 2017).

Na proposição original de Casagrande (1936), representado na figura 2, inicialmente o ponto de máxima curvatura é determinado visualmente. A partir dele, são traçadas uma reta tangente e uma reta secante paralela à abcissa. Traça-se então a bissetriz dessas duas retas. A interseção dessa bissetriz com a projeção linear da curva de compressão virgem (definida pelos últimos pontos da curva de compressão) é projetada na abcissa, definindo assim o valor da pressão de pré-consolidação.

Figura 2 − Representação gráfica da determinação da pressão de pré-consolidação (σ_p) pelo método de Casagrande (1936).
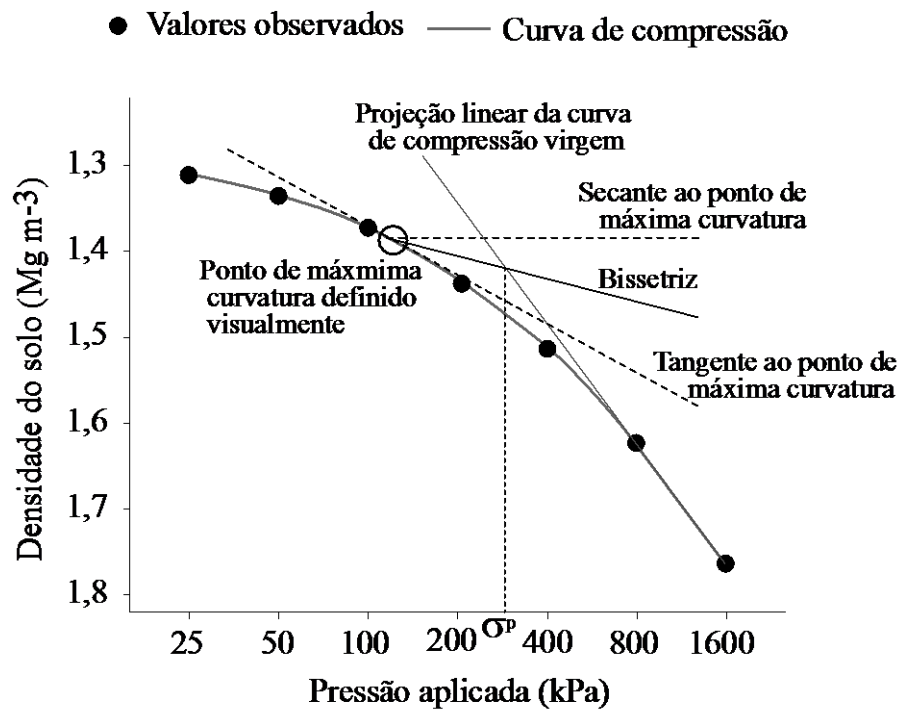
Fonte: Do autor.

Devido à subjetividade associada à definição visual do ponto de máxima curvatura e à morosidade da aplicação do método gráfico, Dias Junior e Pierce (1995) propuseram um método baseado em equações lineares associadas às regiões de compressão secundária e compressão virgem da curva de compressão do solo (Figura 3). Nesse método, a pressão de pré-consolidação é determinada a partir da interseção de duas retas, uma ajustada aos primeiros pontos da curva de compressão (região de compressão secundária) e outra ajustada aos últimos pontos da curva de compressão (região de compressão virgem). Nesse estudo,

validado em relação ao método gráfico de Casagrande (1936), os autores observaram que a concordância com o método gráfico original dependia do número de pontos escolhidos para ajustar a reta associada à compressão secundária (pontos iniciais da curva). Assim, os autores propuseram que, para amostras mais úmidas que a umidade na tensão de água do solo de 100 kPa, essa equação linear deveria se ajustada aos dois primeiros pontos da curva de compressão (associados às pressões de 25 e 50 kPa); enquanto para as amostras mais secas, a equação linear deveria ser ajustada aos quatro primeiros pontos da curva de compressão (associados às pressões de 25, 50, 100 e 200 kPa). Já para a projeção linear da curva de compressão virgem, os autores adotaram os dois últimos pontos da curva de compressão (associados às pressões de 800 e 1600 kPa).

Figura 3 − Determinação da pressão de pré-consolidação (σ_p) pelo método de Dias Junior e Pierce (1995).
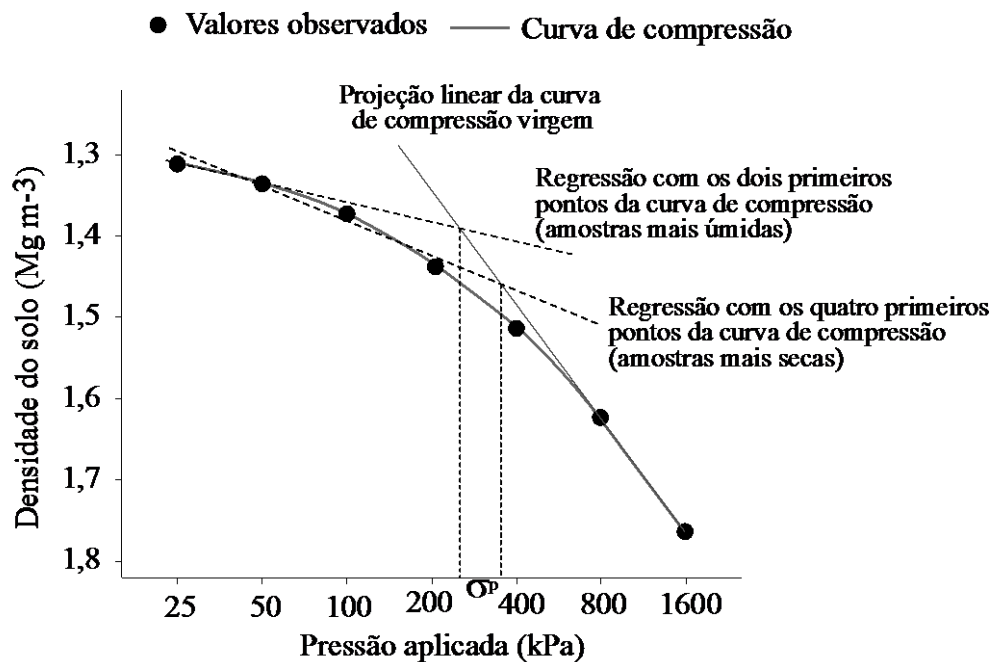
Fonte: Do autor.

Em anos mais recentes, tem se tornado mais comum o emprego de equações não lineares para ajuste da curva de compressão do solo e determinação da pressão de pré-consolidação. No trabalho seminal de Gregory et al. (2006), a equação sigmoidal de Gompertz (1825), equação 1, foi ajustada aos dados da curva de compressão (Figura 1). A partir dos parâmetros estimados, determinou-se o ponto de máxima curvatura numericamente

pela equação 2. Adicionalmente, os autores também verificaram experimentalmente que o ponto de máxima curvatura em si era um melhor indicador da pressão de pré-consolidação do que o valor definido pelas etapas subsequentes do método original de Casagrande (1936). Rapidamente essa proposição foi aceita e aplicada por trabalhos subsequentes (e.g. Cavalieri et al., 2008).

$$\sigma_p = a + b(e^{-e^{m(x-c)}}) \tag{1}$$

$$\kappa = \frac{|f''(x)|}{(1+(f'(x))^2)^{\frac{3}{2}}} \tag{2}$$

em que σp é a pressão de pré-consolidação, x é o logaritmo da pressão aplicada, *a*, *b*, *c* e *m* são os parâmetros de ajuste, κ é a função de curvatura e f'(x) e f''(x) são respectivamente a primeira e a segunda derivada.

Figura 4 − Determinação da pressão de pré-consolidação (σp) pelo método de Gregory et al. (2006). A curva de compressão é ajustada à equação sigmoidal de Gompertz (esquerda), indicada na equação 1, e os parâmetros ajustados são utilizados na determinação do ponto de máxima curvatura (direita) a partir da equação 2
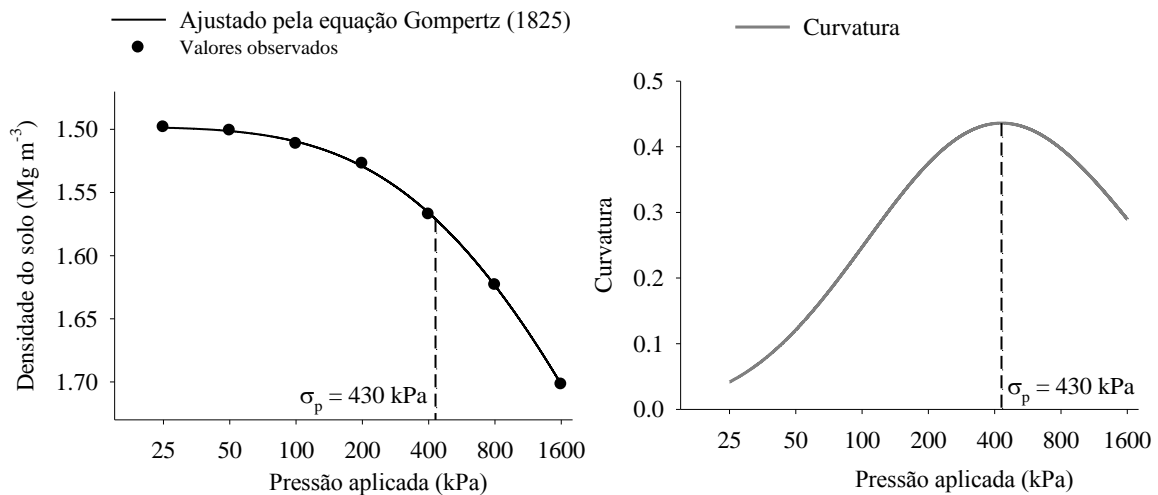
Fonte: Do autor.

A equação sigmoidal proposta por van Genuchten (1980) para ajustar os dados da curva de retenção de água também foi empregada por Cavalieri et al. (2008) para ajustar os dados da curva de compressão do solo e assim determinar a pressão de pré-consolidação. Nesse caso, os dados da curva de compressão são ajustados à equação 3 e o ponto de máxima curvatura também é definido a partir da equação 2, conforme ilustrado na figura 5.

$$\sigma_p = l + \frac{(u-l)}{(1+(a*x)^n)^{\left(1-\frac{1}{n}\right)}} \tag{3}$$

em que σ_p é a pressão de pré-consolidação, x é o logaritmo da pressão aplicada, *l*, *u*, *a*, *n* são os parâmetros de ajuste.

Figura 5 − Determinação da pressão de pré-consolidação (σ_p) pelo método de Cavalieri et al. (2008). A curva de compressão (à esquerda) é ajustada à equação sigmoidal de van Genuchten (1980), indicada na equação 3, e os parâmetros ajustados são utilizados na determinação do ponto de máxima curvatura (direita) a partir da equação 2.
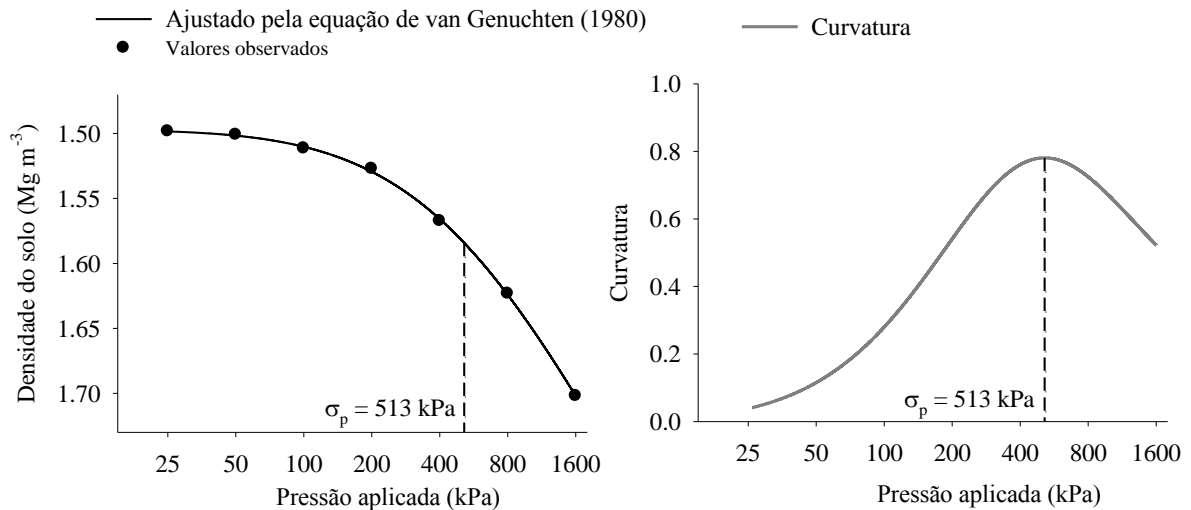
Fonte: Do autor.

Além do ajuste de modelos não-lineares aos dados da curva de compressão do solo, equações polinomiais, em particular de quarto grau (equação 4), também têm sido aplicadas, por exemplo nos trabalhos de Gregory et al. (2006) e Cavalieri et al. (2008) e no pacote *soilphysics* desenvolvido por Silva e Lima (2015) para emprego no *software* R. Novamente, a partir do ajuste dessa equação, a pressão de pré-consolidação é determinada pelo cálculo do ponto de máxima curvatura (Figura 6). Contudo, nesse caso esse ponto pode ser determinado numericamente a partir da equação 2 (GREGORY et al., 2006; CAVALIERI et al., 2008) ou igualando-se a terceira derivada a zero pela equação 5 (SILVA; LIMA, 2015).

$$\sigma_p = ax^4 + bx^3 + cx^2 + dx + e \tag{4}$$

$$f'''(x) = 24ax + 6b \tag{5}$$

em que σ_p é a pressão de pré-consolidação, x é o logaritmo da pressão aplicada, *a*, *b*, *c*, *d* e *e* são os parâmetros de ajuste e f'''(x) é a terceira derivada da equação 4.

Figura 6 − Determinação da pressão de pré-consolidação (σ_p) a partir do ajuste de polinomial de quarto grau. A curva de compressão (à esquerda) é ajustada à equação 4 e os parâmetros ajustados são utilizados na determinação da pressão de pré-consolidação por duas formas (à direita): determinando-se numericamente o ponto de máxima curvatura pela equação 2, ou igualando-se a terceira derivada (equação 5) a zero.
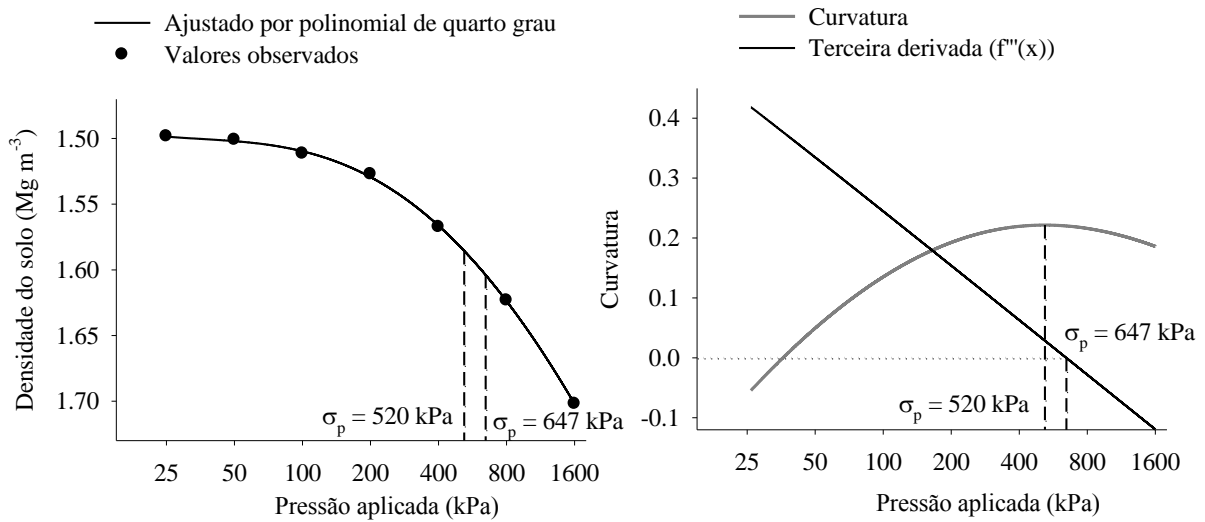
Fonte: Do autor.

O desenvolvimento mais recente em termos de método de determinação da pressão de pré-consolidação foi elaborado por de Lamandé, Schjønning e Labouriau (2017). Esse método foi proposto para uma condição de ensaio de compressão uniaxial com taxa de deformação constante e coleta automática de dados, resultando em um grande número números de pares ordenados (mas de 200 observações por ensaio). O método realiza uma varredura nos pontos observados, ajustando polinômios de segundo grau a inúmeros segmentos sequenciais, já que esta função é a mais simples que possibilita a determinação da curvatura. Dessa forma, esse método não sofre a limitação que dos métodos anteriores de necessitar do ajuste de uma equação a toda a curva de compressão, já que esta é seccionada em segmentos sequenciais aos quais é ajustado um modelo simples (polinômio de segundo grau). Contudo, a aplicação deste

método a dados obtidos por ensaios diferentes daquele para o qual o método foi desenvolvido exige uma adaptação, já que o método exige um grande número de pontos observacionais para ser aplicado. Assim, como estratégia adaptativa, é possível gerar um grande número de pontos a partir do ajuste de uma equação à curva de compressão e então aplicar o método proposto. Esse ajuste poderia ser feito, por exemplo, por uma equação polinomial de quarto grau, já que as equações lineares não apresentam problema de não convergência como as não-lineares, ou por regressão não-paramétrica, como uma regressão *spline* (Figura7).

Figura 7 − Determinação da pressão de pré-consolidação (σ_p) a partir da modificação do método numérico de Lamandé, Schjønning e Labouriau (2017). As curvas de compressão (à esquerda) foram ajustadas à equação 4 e por regressão *spline*. Os valores preditos a partir das equações ajustadas foram utilizados na determinação da pressão de pré-consolidação por duas formas pela busca numérica do ponto de máxima curvatura a partir do ajuste de equações de segundo grau sequenciais com 25 pontos em cada segmento (à direita).
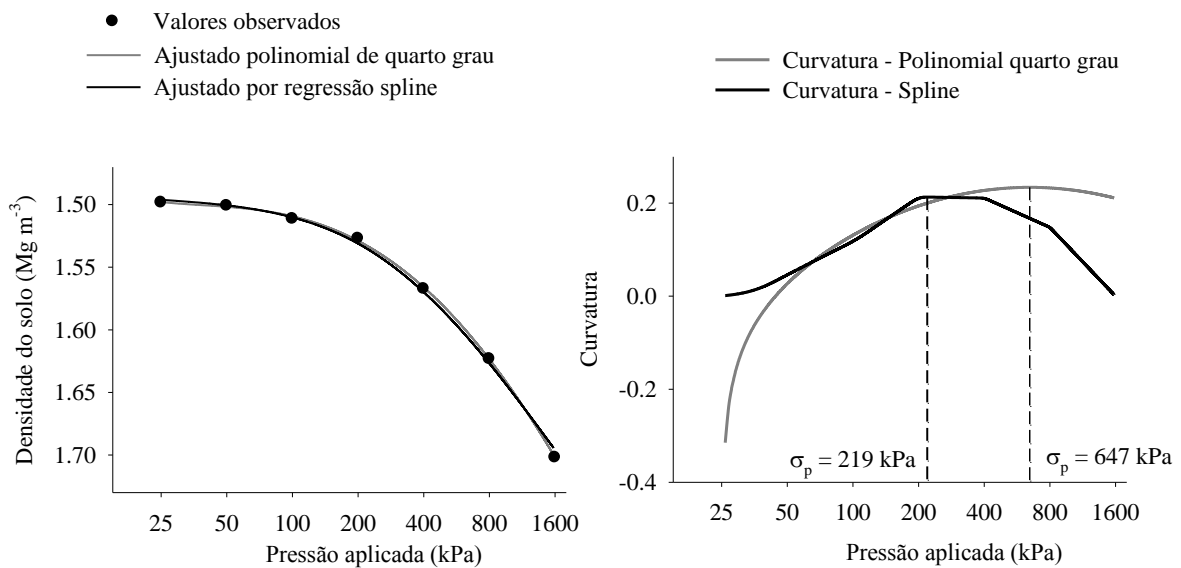
Fonte: Do autor.

2.3 Atributos físicos que afetam o comportamento compressivo do solo

Como ressaltado anteriormente, o comportamento compressivo do solo é afetado pelos seus atributos físicos. Assim, a partir do estabelecimento das relações entre esses atributos e o comportamento compressivo do solo ou a pressão de pré-consolidação, é possível desenvolver modelos preditivos para a resistência mecânica do solo. Quando esses modelos são construídos a partir de atributos de fácil determinação em campo, eles podem se tornar uma

ferramenta de manejo, indicando se determinado solo tem capacidade de suportar o tráfego de determinada máquina naquela condição.

2.3.1 Atributos relacionados ao teor de água do solo

Devido à influência preponderante da umidade do solo na pressão de pré-consolidação, a comparação entre diferentes solos ou manejos tem utilizado amostras previamente equilibradas em diferentes umidades (IORI et al., 2013; VISCHI FILHO et al., 2015), em diferentes potenciais matriciais (AJAYI et al., 2014; LIMA et al., 2018; REICHERT et al., 2018), em um único potencial matricial, frequentemente próximos à capacidade de campo, mais comumente 10 kPa (CAVALIERI et al., 2008; KELLER et al., 2004; KELLER et al., 2011; WATANABE et al., 2017). Também têm sido empregadas amostras com umidade de campo para avaliação do impacto do tráfego de maquinário agrícola (ANDRADE et al., 2017; MARTINS et al., 2018), avaliação da sazonalidade da resistência mecânica do solo (IORI et al., 2014) ou para comparação com outras de avaliações *in situ* (KELLER; ARVIDSSON, 2007).

A variação da pressão de pré-consolidação tem sido mais comumente modelada pela umidade do solo, relação funcional que define o modelo de capacidade de carga do solo (DIAS JUNIOR; MARTINS, 2017). Os modelos de capacidade de suporte de carga têm sido utilizados para avaliar a qualidade física do solo em diversos ambientes (IORI et al., 2012; MARTINS et al., 2012b) , avaliar a suscetibilidade do solo à compactação (AJAYI et al., 2009, 2010, 2013), e o efeito de práticas de manejo no estado de compactação do solo para diversas culturas (ANDRADE et al., 2017; MARTINS et al., 2018; VISCHI FILHO et al., 2015).

No presente trabalho, foram empregados os seguintes atributos físicos relacionados ao teor de água do solo (associados às tensões de água de 10 e 100 kPa): umidade com base em peso ou umidade gravimétrica (θ_g); umidade com base em volume ou umidade volumétrica (θ_v); grau de saturação(S); razão de água (*w*); relação entre a umidade gravimétrica e a umidade ótima de compactação pelo ensaio de Proctor Normal (θ_g/θ_{opt}); e relação entre a umidade gravimétrica e o limite de plasticidade (θ_g/θ_{PL}), definidos nas equações 6 a 11 respectivamente.

$$\theta_g \ (g \ g^{-1}) = \frac{Massa \ de \ água}{Massa \ de \ solo \ seco} \tag{6}$$

$$\theta_v \ (m^3 \ m^{-3}) = \frac{Volume \ de \ água}{Volume \ de \ solo} \tag{7}$$

$$S \ (\%) = 100 * \frac{\theta_v}{Porosidade \ total} \tag{8}$$

$$w = \frac{Volume \ de \ água}{Volume \ de \ sólidos} \tag{9}$$

$$\theta_g / \theta_{opt} = \frac{\theta_g}{Umidade \ ótima \ de \ compactação} \tag{10}$$

$$\theta_g / \theta_{PL} = \frac{\theta_g}{Limite \ de \ plasticidade} \tag{11}$$

2.3.2 Atributos relacionados às relações de massa/volume

Trabalhos recentes têm demonstrado que a escolha do atributo associado às relações massa/volume do solo na definição da curva de compressão afeta significativamente a determinação da pressão de pré-consolidação (GUBIANI et al., 2015; MOSADDEGHI et al., 2003; RÜCKNAGEL et al., 2010). A curva de compressão foi definida a partir do índice de vazios (*e*)(equação 12) como a variável na ordenada no método original de Casagrande (1936) para determinação da pressão de pré-consolidação, apesar desse método ter sido também aplicado empregando-se a densidade do solo (ρ_b)(equação 13) na ordenada da curva de compressão por Dias Junior e Pierce (1995) e Rücknagel et al. (2010). A compactação que ocorre durante o ensaio de compressão também pode ser representada pelo deslocamento vertical da amostra ou deformação registrada durante o ensaio de compressão(ε)(e.g. KELLER et al., 2012) ou ainda pelo volume específico do solo de acordo com Keller e Arvidsson (2007)(equação 14).

$$e = \frac{Volume \ de \ poros}{Volume \ de \ sólidos} \tag{12}$$

$$\rho_b \ (Mg \ m^{-3}) = \frac{Massa \ de \ solo \ seco}{Volume \ de \ solo} \tag{13}$$

$$v = \frac{\rho_b}{\rho_p} * \frac{H - \varepsilon}{H} \tag{14}$$

em que *e* é o índice de vazios (adimensional); ρ_b é a densidade do solo, ρ_p é a densidade de partículas, *v* é o volume específico do solo; *H* é a altura inicial da amostra e ε é a deformação registrada durante o ensaio de compressão.

As diferenças na determinação de pré-consolidação possivelmente advêm da não-linearidade existente entre esses atributos (Figura 8), conforme identificado inicialmente por Mosaddeghi et al. (2003) e demonstrado para diferentes métodos de cálculo por Rücknagel et al. (2010) e Gubiani et al. (2015).

Figura 8 − Relação entre diferentes atributos físicos do solo empregados na construção das curvas de compressão.
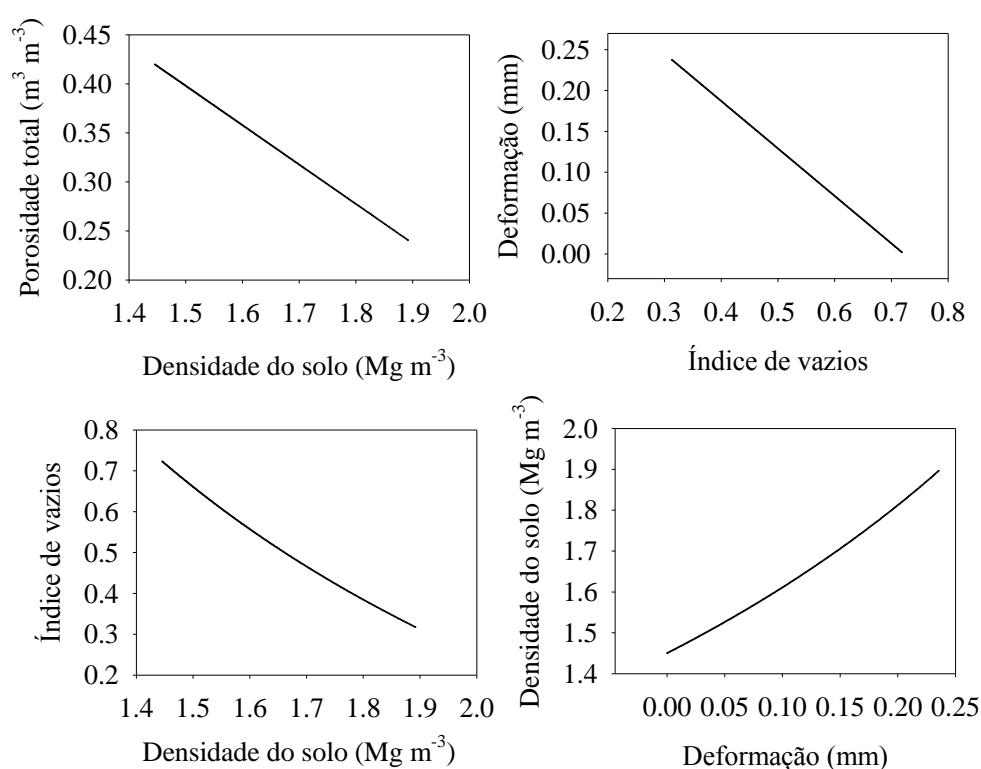
Fonte: Do autor.

3 CONSIDERAÇÕES GERAIS

A avaliação da resistência mecânica do solo por meio do seu comportamento compressivo e da pressão de pré-consolidação tem grande relevância nos estudos de compactação dos solos agrícolas, já que esse atributo físico do solo pode ser empregado como indicador da sua capacidade de suporte de carga. Não obstante, os inúmeros métodos de determinação e de definição da curva de compressão do solo podem afetar grandemente os

valores obtidos. Para tanto, torna-se importante que a interação entre esses dois fatores seja estudada com maior profundidade, o que ainda permanece por fazer nesse campo de pesquisa.

A relação entre pressão de pré-consolidação e outros atributos físicos do solo tem sido descrita de inúmeras maneiras, ora ressaltando-se a importância de um atributo, ora de outro. Nesse sentido, um estudo de maior abrangência também falta ainda na literatura especializada. Adicionalmente, por vezes a inclusão de solos muito diferentes em um único estudo pode afetar a importância relativa deste ou daquele atributo, o que também precisa ser avaliado a partir da comparação de medidas absolutas, como a densidade do solo, e de medidas relativas, como o grau de compactação. Desse modo, evita-se o confundimento entre o que é de fato efeito do grau de compacidade da estrutura e o que é efeito resultante dos diferentes atributos intrínsecos de cada solo.

REFERÊNCIAS

AFZALINIA, S; ZABIHI, J. Soil compaction variation during corn growing season under conservation tillage. **Soil and Tillage Research**, Amsterdam, v. 137, p. 1–6, 2014. Disponível em: <https://doi.org/10.1016/j.still.2013.11.003>. Acesso em: 4 abr. 2019.

AJAYI, A. E. et al. Assessment of vulnerability of Oxisols to compaction in the Cerrado region of Brazil. **Pedosphere**, v. 20, n. 2, p. 252–260, 2010. Disponível em: <https://doi.org/10.1016/S1002-0160(10)60013-6>. Acesso em: 4 abr. 2019.

AJAYI A. E. et al. Compressive response of some agricultural soils influenced by mineralogy and moisture. **International Agrophysics**, Lublin, v. 27, p. 239-246, 2013. Disponível em: <https://doi.org/10.2478/v10247-012-0091-x>. Acesso em: 4 abr. 2019.

AJAYI, A. E. et al. Hydrophysical properties of Humic Latosols from Brazil. **International Agrophysics**, Lublin, v. 28, p. 395–402, 2014. Disponível em: <https://doi.org/10.2478/intag-2014-0030>. Acesso em: 4 abr. 2019.

AJAYI, A. E. et al. Strength attributes and compaction susceptibility of Brazilian Latosols. **Soil and Tillage Research**, Amsterdam, v. 105, n. 1, p. 122-127, 2009. Disponível em: <https://doi.org/10.1016/j.still.2009.06.004>. Acesso em: 4 abr. 2019.

ANDRADE, M. L. C. et al. Soil compaction caused by harvest and logging operations in eucalyptus forests in coarse-textured soils from northeastern Brazil. **Ciência e Agrotecnologia**, Lavras, v. 41, n. 2, p. 191–200, 2017. Disponível em: <http://dx.doi.org/10.1590/1413-70542017412036216>. Acesso em 4 abr. 2019.

ARAUJO JUNIOR C. F. et al. Capacidade de suporte de carga e umidade crítica de um Latossolo induzida por diferentes manejos. **Revista Brasileira de Ciência do Solo**, Viçosa, v. 35, n. 1, p. 115-131, 2011. Disponível em: <http://dx.doi.org/10.1590/S0100-06832011000100011>. Acesso em 4 abr. 2019.

BOTREL, M. A.; ALVIM, M. J.; XAVIER, D. F. Avaliação de gramíneas forrageiras na região Sul de Minas Gerais. **Pesquisa Agropecuária Brasileira**, Brasília, v. 34, n. 4, p. 683-689, 1999. Disponível em <http://dx.doi.org/10.1590/S0100-204X1999000400021>. Acesso em: 02 abr. 2019.

CASAGRANDE, A. Determination of the pre-consolidation load and its practical significance. In: International Conference on Soil Mechanics and Foundation Engineering, 1936, Cambridge. **Proceedings...** Cambridge: Harvard University; 1936. p. 60-64.

CAVALIERI, K. M. V. et al. Determination of precompression stress from uniaxial compression tests. **Soil and Tillage Research**, Amsterdam, v. 98, n. 1, p. 17-26, 2008. Disponível em: <https://doi.org/10.1016/j.still.2007.09.020>. Acesso em 4 abr. 2019

DIAS JUNIOR, M. S. **Compression of three soils under long term tillage and wheel traffic**. 1994. 114 p. Thesis (Ph.D. in Crop and Soil Sciences)−Michigan State University, East Lansing, 1994.

DIAS JUNIOR, M. S. Compactação do Solo. In: NOVAIS, R. F.; ALVAREZ, V. H. V.; CHAEFER, C. E. G. R (Ed.). **Tópicos em Ciência do Solo**. Viçosa: Ed. UFV, 2000. p. 55-94.

DIAS JUNIOR, M. S. et al. Assessment of the soil compaction of two Ultisols caused by logging operations. **Revista Brasileira de Ciência do Solo**, Viçosa, v. 32, n. 6, p. 2245–2253, 2008. Disponível em: <http://dx.doi.org/10.1590/S0100-06832008000600004>. Acesso em 4 abr. 2019

DIAS JUNIOR, M. S. et al. Soil compaction due to forest harvest operations. **Pesquisa Agropecuária Brasileira**, Brasília, v. 42, n. 2, p. 257–264, 2007. Disponível em: <http://dx.doi.org/10.1590/S0100-204X2007000200015>. Acesso em 4 abr. 2019

DIAS JUNIOR, M. S. et al. Traffic effect on the preconsolidation pressure due to Eucalyptus harvest operations. **Scientia Agricola**, Piracicaba, v. 62, n. 3, p. 248-255, 2005. Disponível em: <http://dx.doi.org/10.1590/S0103-90162005000300008>. Acesso em 4 abr. 2019

DIAS JUNIOR, M. S.; MARTINS, P. C. C. Ensaio de compressão uniaxial e modelos de capacidade de suporte de carga do solo. In: TEIXEIRA, P. C. et al. (Eds). **Manual de Métodos de Análise de Solo.** 3ª ed. ver. e amp. Brasília: Embrapa, 2017. p. 152-171.

DIAS JUNIOR, M. S.; PIERCE, F. J. A simple procedure for estimating preconsolidation pressure from soil compression curves. **Soil Technology**, v. 8, n. 2, p. 139–151, 1995. Disponível em: <https://doi.org/10.1016/0933-3630(95)00015-8>. Acesso em 4 abr. 2019.

DUTTMANN, R.; BRUNOTTE, J.; BACH, M. Spatial analyses of field traffic intensity and modeling of changes in wheel load and ground contact pressure in individual fields during a silage maize harvest**. Soil and Tillage Research**, Amsterdam, v. 126, n. 2013, p. 100–111, 2013. Disponível em: <https://doi.org/10.1016/j.still.2012.09.001>. Acesso em 4 abr. 2019.

EVANGELISTA, A. R.; LIMA, J. A. **Silagem: do cultivo ao silo**. 2. ed. Lavras: Ed. UFLA, 2002. 212 p.

GREGORY, A. S. et al. Calculation of the compression index and precompression stress from soil compression test data. **Soil and Tillage Research**, Amsterdam, v. 89, n. 1, p. 45–57, 2006. Disponível em: <https://doi.org/10.1016/j.still.2005.06.012>. Acesso em: 4 abr. 2019.

GOMPERTZ, B. On the nature of the function expressive of the law of human mortality, and on a new mode of determining the value of life contingencies. **Philosophical Transactions of the Royal Society of London: Biological Sciences**. v. 182, p. 513–85, 1825.

GUBIANI, P. I. et al. Precompression stress and compression index depend on the property used to represent the soil deformation in the compression curve. **Ciência Rural**, Santa Maria, v. 46, n. 1, p. 76–82, 2015. Disponível em: <http://dx.doi.org/10.1590/0103-8478cr20141495>. Acesso em: 4 abr. 2019.

HILLEL, D. **Environmental soil physics**. San Diego: Academic Press, 1998. 771 p.

HOLTHUSEN, D. et al. Soil porosity, permeability and static and dynamic strength parameters under native forest/grassland compared to no-tillage cropping. **Soil and Tillage Research**, Amsterdam, v. 177, p. 113–124, 2018. Disponível em: <https://doi.org/10.1016/j.still.2017.12.003>. Acesso em 4 abr. 2019.

HORN, R.; LEBERT, M. Soil Compactability and compressibility. In: SOANE, B. D.; van OUWERKERK, C. (Ed.). **Soil compaction in crop production**. Amsterdam: Elsevier Science, 1994. p. 45-69.

IMHOFF, S. et al. Physical quality indicators and mechanical behavior of agricultural soils of Argentina. **PLoS ONE**, v. 11, n. 4, p. 1–21, 2016. Disponível em: <https://doi.org/10.1371/journal.pone.0153827>. Acesso em 4 abr. 2019.

INSTITUTO BRASILEIRO DE GEOGRAFIA E ESTATÍSTICA − IBGE. **Banco de Dados Agregados: Censo Agropecuário de 2006. Sistema IBGE de Recuperação automática - SIDRA**. Brasília, 2006. Disponível em <http://www.sidra.ibge.gov.br/bda/tabela/listabl.asp?z=t&o=24&i=P&c=932>. Acesso em 15 fev. 2016.

IORI, P. et al. Pressão de preconsolidação como ferramenta de análise da sustentabilidade estrutural de classes de solos com diferentes usos. **Revista Brasileira de Ciência do Solo**, Viçosa, v. 36, n. 5, p. 1448-1456, 2012. Disponível em: <http://dx.doi.org/10.1590/S0100-06832012000500009>. Acesso em 4 abr. 2019.

IORI, P. et al. Comparison of field and laboratory models of the load bearing capacity in coffee plantations. **Ciência e Agrotecnologia**, Lavras, v. 37, n. 2, p. 130–137, 2013. Disponível em: <http://dx.doi.org/10.1590/S1413-70542013000200003>. Acesso em 4 abr. 2019.

IORI, P. et al. Seasonal change of soil precompression stress in coffee plantation under sub-humid tropical condition. **Coffee Science**, Lavras, v. 9, n. 2, p. 145–154, 2014. Disponível em: <http://dx.doi.org/10.25186/cs.v9i2.568>. Acesso em 4 abr. 2019.

KAMIMURA K. M. et al. Capacidade de suporte de carga de um Latossolo Vermelho-Amarelo em uma lavoura cafeeira. **Revista Brasileira de Ciência do Solo**, Viçosa, v. 36, n. 5, p. 1457–1465, 2012. Disponível em: <http://dx.doi.org/10.1590/S0100-06832012000500009>. Acesso em 4 abr. 2019.

KELLER, T.; ARVIDSSON, J. Compressive properties of some Swedish and Danish structured agricultural soils measured in uniaxial compression tests. **European Journal of Soil Science**, Oxford, v. 58, n. 6, p. 1373-1381, 2007. Disponível em: <https://doi.org/10.1111/j.1365-2389.2007.00944.x>. Acesso em: 4 abr. 2019.

KELLER, T. et al. Analysis of soil compression curves from uniaxial confined compression tests. **Geoderma**, Amsterdam, v. 163, n. 1/2, p. 13-23, 2011. Disponível em: <http://dx.doi.org/10.1016/j.geoderma.2011.02.006>. Acesso em: 4 abr. 2019.

KELLER, T. et al. An interdisciplinary approach towards improved understanding of soil deformation during compaction. **Soil and Tillage Research**, Amsterdam, v. 128, n. 2013, p. 61–80, 2013. Disponível em: < https://doi.org/10.1016/j.still.2012.10.004>. Acesso em: 4 abr. 2019.

KELLER, T. et al. In situ subsoil stress-strain behavior in relation to soil precompression stress. **Soil Science**, Baltimore, v. 177, n. 8, p. 490–497, 2012. Disponível em: <https://doi.org/10.1097/SS.0b013e318262554e >. Acesso em: 4 abr. 2019.

KELLER, T. et al. Soil precompression stress II: a comparison of different compaction tests and stress-displacement behavior of the soil during wheeling. **Soil and Tillage Research**, Amsterdam, v. 77, n. 1, p. 97-108, 2004. Disponível em: <https://doi.org/10.1016/j.still.2003.11.003>. Acesso em 4 abr. 2004.

LEBERT, M.; BÖKEN, H.; GLANTE, F. Soil compaction indicators for the assessment of harmful changes to the soil in the context of the German Federal Soil Protection Act. **Journal of Environmental Management,** London, v. 82, n. 3, p. 388–97, fev. 2007. Disponível em: <https://doi.org/10.1016/j.jenvman.2005.11.022>. Acesso em: 4 abr. 2019.

LAMANDÉ, M.; SCHJØNNING, P.; LABOURIAU, R. A novel method for estimating soil precompression stress from uniaxial confined compression tests. **Soil Science Society of America Journal**, Madison, v. 81, n. 5, p. 1005-13, 2017. Disponível em: <https://doi.org/10.2136/sssaj2016.09.0274>. Acesso em: 4 abr. 2019.

LIMA, R. P. et al. Impact of initial bulk density and matric suction on compressive properties of two Oxisols under no-till. **Soil and Tillage Research**, Amsterdam, v. 175, p. 168–177, 2018. Disponível em: <https://doi.org/10.1016/j.still.2017.09.003>. Acesso em: 4 abr. 2019.

MARTINS, P. C. C. et al. Levels of induced pressure and compaction as caused by forest harvesting operations. **Cerne**, Lavras, v. 19, n. 1, p. 83–91, 2013. Disponível em: <http://dx.doi.org/10.1590/S0104-77602013000100011>. Acesso em: 4 abr. 2019.

MARTINS, P. C. C. et al. Soil compaction during harvest operations in five tropical soils with different textures under eucalyptus forests. **Ciência e Agrotecnologia**, Lavras, v. 42, n. 1, p. 58–68, 2018. Disponível em: <http://dx.doi.org/10.1590/1413-70542018421005217>. Acesso em: 4 abr. 2019.

MARTINS, P. C. C. et al. Compaction caused by mechanized operations in a Red-Yellow Latosol cultivated with coffee over time. **Ciência e Agrotecnologia**, Lavras, v. 36, n. 4, p. 391–398, 2012a. Disponível em: <http://dx.doi.org/10.1590/S1413-70542012000400002>. Acesso em 4 abr. 2019.

MARTINS, P. C. C. et al. Structural sustainability of Cambisol under different land use system. **Revista Brasileira de Ciência do Solo**, Viçosa, v. 36, n. 6, p. 1724–1732, 2012b. Disponível em: <http://dx.doi.org/10.1590/S0100-06832012000600006>. Acesso em 4 abr. 2019.

MOSADDEGHI, M. R. et al. Comparisons of different procedures of pre-compaction stress determination on weakly structured soils. **Journal of Terramechanics**, Oxford, v. 44, n. 1, p. 53–63, 2007. Disponível em: <https://doi.org/10.1016/j.jterra.2006.01.008>. Acesso em: 4 abr. 2019.

MOSADDEGHI, M. et al. Pre-compression stress and its relation with the physical and mechanical properties of a structurally unstable soil in central Iran. **Soil and Tillage Research**, Amsterdam, v. 70, n. 1, p. 53–64, 2003. Disponível em: <https://doi.org/10.1016/S0167-1987(02)00120-4 >. Acesso em: 4 abr. 2019.

NADERI-BOLDAJI, M. et al. Finite element simulation of plate sinkage, confined and semi-confined compression tests: A comparison of the response to yield stress. **Soil and Tillage Research**, Amsterdam, v. 179, p. 63–70, 2018. Disponível em: <https://doi.org/10.1016/j.still.2018.02.003>. Acesso em: 4 abr. 2019.

NEVENS, F.; REHEUL, D. The consequences of wheel-induced soil compaction and subsoiling for silage maize on a sandy loam soil in Belgium. **Soil and Tillage Research**, Amsterdam, v. 70, p. 175–184, 2002. Disponível em: <https://doi.org/10.1016/S0167-1987(02)00140-X>. Acesso em 4 abr. 2019.

NUNES, M. R. et al. Dynamic changes in compressive properties and crop response after chisel tillage in a highly weathered soil. **Soil and Tillage Research**, Amsterdam, v. 186, p. 183–190, 2019. Disponível em: <https://doi.org/10.1016/j.still.2018.10.017>. Acesso em: 4 abr. 2019.

OLIVEIRA, P. S.; OLIVEIRA, J. S. **Produção de Silagem de Milho para Suplementação do Rebanho Leiteiro**. Comunicado Técnico 74. Juiz de Fora: Embrapa Gado de Leite, 2014. 10 p.

OLIVEIRA, J. S. et al. **Cultivares de milho para silagem: Recomendações para as Regiões Sul, Sudeste e Brasil-Central**. Circular Técnica 103. Juiz de Fora: Embrapa Gado de Leite, 2010. 8 p.

PAIS, P. S. M. et al. Compactação causada pelo manejo de plantas invasoras em Latossolo Vermelho-Amarelo cultivado com cafeeiros. **Revista Brasileira de Ciência do Solo**, Viçosa, v. 35, n. 6, p. 1949–1957, 2011. Disponível em: < http://dx.doi.org/10.1590/S0100-06832011000600011>. Acesso em: 4 abr. 2019.

PAIS, P. S. M. et al. Load-bearing capacity of a Red-Yellow Latosol cultivated with coffee plants subjected to different weed managements. Ciência e Agrotecnologia, Lavras, v. 37, n. 2, p. 145–151, 2013. Disponível em: <http://dx.doi.org/10.1590/S1413-70542013000200005>. Acesso em 4 abr. 2019.

RABOT, E. et al. Soil structure as an indicator of soil functions: A review. **Geoderma**, Amsterdam, v. 314, n. October 2017, p. 122–137, 2018. Disponível em: <https://doi.org/10.1016/j.geoderma.2017.11.009>. Acesso em 4 abr. 2019.

REICHERT, J. M. et al. Compressibility and elasticity of subtropical no-till soils varying in granulometry organic matter, bulk density and moisture. **Catena**, Amsterdam, v. 165, p. 345–357, 2018. Disponível em: <https://doi.org/10.1016/j.catena.2018.02.014>. Acesso em: 4 abr. 2019.

RÜCKNAGEL, J. et al. Uniaxial compression behaviour and soil physical quality of topsoils under conventional and conservation tillage. **Geoderma**, Amsterdam, v. 286, p. 1–7, 2017. Disponível em: <http://dx.doi.org/10.1016/j.geoderma.2016.10.015>. Acesso em: 4 abr. 2019.

RÜCKNAGEL, J. et al. Variance of mechanical precompression stress in graphic estimations using the Casagrande method and derived mathematical models. **Soil and Tillage Research**, Amsterdam, v. 106, n. 2, p. 165–170, 2010. Disponível em: <https://doi.org/10.1016/j.still.2009.11.001>. Acesso em: 4 abr. 2019.

SCHJØNNING, P. et al. Soil precompression stress, penetration resistance and crop yields in relation to differently-trafficked, temperate-region sandy loam soils. **Soil and Tillage Research**, Amsterdam, v. 163, p. 298–308, 2016. Disponível em: <http://dx.doi.org/10.1016/j.still.2016.07.003>. Acesso em: 4 abr. 2019.

SEVERIANO E. C. et al. Preconsolidation pressure, soil water retention characteristics, and texture of Latosols in the Brazilian Cerrado. **Soil Research**, Rome, v. 51, p. 193–202, 2013. Disponível em: <https://doi.org/10.1071/SR12366>. Acesso em 4 abr. 2019.

SEVERIANO, E. C. et al. Structural changes in latosols of the cerrado region: II - soil compressive behavior and modeling of additional compaction. **Revista Brasileira de Ciência do Solo**, Viçosa, v. 35, n. 3, p. 783-791, 2011. Disponível em: <http://dx.doi.org/10.1590/S0100-06832011000300014>. Acesso em 4 abr. 2019.

SILVA, A. R., DIAS JUNIOR, M. S., LEITE, F. P. Camada de resíduos florestais e pressão de preconsolidação de dois latossolos. Pesquisa Agropecuária Brasileira, Brasília, v. 42, n. 1, p. 89-93, 2007. Disponível em: <http://dx.doi.org/10.1590/S0100-204X2007000100012>. Acesso em 4 abr. 2019.

SILVA, A. R., DIAS JUNIOR, M. S., LEITE, F. P. Propriedades físicas e mecânicas de latossolos em diferentes manejos florestais. Ciência e Agrotecnologia, Lavras, v. 34, n. 6, p. 1483-1491, 2010. Disponível em: <http://dx.doi.org/10.1590/S1413-70542010000600019>. Acesso em 4 abr. 2019.

SILVA, A. R.; LIMA, R. P. *soilphysics*: An R package to determine soil preconsolidation pressure. **Computers and Geosciences**, New York, v. 84, p. 54–60, 2015. Disponível em: <http://dx.doi.org/10.1016/j.cageo.2015.08.008>. Acesso em: 4 abr. 2019.

SOUSA, A. C. M. et al. Soil load-bearing capacity and development of root system in area under sugarcane with traffic control in Brazil. **Sugar Tech**, v. 21, p. 153–161, 2019. Disponível em: <https://doi.org/10.1007/s12355-018-0636-9>. Acesso em 4 abr. 2019.

SOUZA, G. S. et al. Compressibilidade do solo e sistema radicular da cana-de açúcar em manejo com e sem controle de tráfego. **Pesquisa Agropecuária Brasileira**, Brasília, v. 47, n. 4, p. 603-612. Disponível em: <http://dx.doi.org/10.1590/S0100-204X2012000400017>. Acesso em 4 abr. 2019.

TANG, A. et al. Analysing the form of the confined uniaxial compression curve of various soils. **Geoderma**, Amsterdam, v. 148, n. 3–4, p. 282–290, 2009. Disponível em: <http://dx.doi.org/10.1016/j.geoderma.2008.10.012>. Acesso em: 4 abr. 2019.

TASSINARI, D. et al. Short term changes on soil physical quality after different pasture renovation methods on a clayey oxidic Red Latosol. **Revista Brasileira de Ciências Agrárias (Agrária)**, Recife, v. 10, n. 4, p. 485–491, 2015. Disponível em: <http://dx.doi.org/10.5039/agraria.v10i4a4689>. Acesso em: 4 abr. 2019.

VAN GENUCHTEN, M. T. A closed-form equation for predicting the hydraulic conductivity of unsaturated soils. **Soil Science Society of America Journal**, Madison, v. 44, n. 5, p. 892–898, 1980. Disponível em: <http://dx.doi.org/10.2136/sssaj1980.03615995004400050002x>. Acesso em: 4 abr. 2019.

VISCHI FILHO, O. J. et al. Capacidade de suporte de carga de Latossolo Vermelho cultivado com cana-de-açúcar e efeitos da mecanização no solo. **Pesquisa Agropecuária Brasileira**, v. 50, n. 4, p. 322–332, 2015. Disponível em: <http://dx.doi.org/10.1590/S0100-204X2015000400008>. Acesso em: 4 abr. 2019.

WATANABE, R. et al. Soil compressibility under irrigated perennial and annual crops in a semi-arid environment**. Revista Brasileira de Ciência do Solo**, v. 41, 2017. Disponível em: <http://dx.doi.org/10.1590/18069657rbcs20160206>. Acesso em: 4 abr. 2019.

SEGUNDA PARTE − ARTIGOS

RELATING SOIL PHYSICAL ATTRIBUTES TO COMPRESSION CURVE SHAPE AND CHANGES DURING COMPRESSION

Preparado de acordo com as normas do periódico Soil and Tillage Research
(versão preliminar)

ABSTRACT

Soil compressive properties are commonly employed in soil compaction studies because of their importance for assessing soil mechanical strength. Soil conditions affect soil behavior during compression and may also influence the shape of the soil compression curve. The aim of the present study was to assess the influence of bulk density (ρ_b), water potential (Ψ), degree of compaction (DC), water content (θ_g) and degree of saturation (S) upon the soil compressive behavior. Undisturbed soil cores from fields cultivated with silage maize were equilibrated at $\Psi = 10$ kPa and $\Psi = 100$ kPa and then submitted to confined drained uniaxial compression tests. Changes in soil DC during compression were majorly affected by the initial DC and the applied pressure, whereas ρ_b was also affected by the sampling field, indicating it is more strongly influenced by intrinsic soil attributes. Changes in S during compression, apart from the mentioned factors, were also significantly affected by water tension (Ψ) and water content. A single value of applied pressure could not be identified to determine the maximum bulk density (similar to the one derived from the Proctor test) since DC equals to 100% was observed for several applied pressures depending on Ψ and initial DC. The applied uniaxial compression tests incurred on both compaction and consolidation, the latter being much more common for samples at $\Psi = 10$ kPa. Compression curve shape, as indicated by the attribute VCLratio (defined as the ratio between the rates of change in ρb from 800-1600 kPa and from 400-800 kPa) was significantly affected by Ψ, water content and initial DC.

Keywords: water content, degree of compaction, bulk density, degree of saturation.

1 INTRODUCTION

Soil compaction poses a threat to soil quality and crop production (Rabot et al., 2018). The prevention and assessment of soil compaction may greatly benefit from considering soil compressive behavior and its mechanical strength (Imhoff et al., 2016; Keller et al., 2013; Lebert et al., 2007), since these are tightly linked to structural changes due to compaction and are also related to plant growth (Nunes et al., 2019; Schjønning et al., 2016).

Soil compressive strength has been assessed by many different methods, including field methods, such as vertical stress transmission (Holthusen et al., 2018; Naveed et al., 2016) and plate-sinkage (Keller et al., 2004; Naderi-Boldaji et al., 2018); and laboratory methods, most commonly confined uniaxial compression tests performed under different conditions and methodologies (Holthusen et al., 2018a; Nunes et al., 2019; Reichert et al., 2018; Rücknagel et al., 2017; Watanabe et al., 2017; Dias Junior and Martins, 2017). Soil compression is most commonly adopted as a strength measurement in croplands under wet climate conditions, such as in Northern Europe (Keller et al., 2012; Rücknagel et al., 2017; Schjønning and Lamandé, 2018) and Southern Brazil (Nunes et al., 2019; Reichert et al., 2018); in the study of vulnerable soils, such as Oxisols, Mollisols and others (Ajayi et al., 2010; Imhoff et al., 2016; Mosaddeghi et al., 2007); and in forestry studies (Andrade et al., 2017; Martins et al., 2018).

Soil compressibility is strongly affected by the initial soil conditions, such as initial bulk density and water potential (Imhoff et al., 2016; Lima et al., 2018; Reichert et al., 2018). Nevertheless, it has been suggested that the soil compression curve from uniaxial compression tests can be used to assess the reference bulk density for calculating the degree of compaction (Reichert et al., 2009). Although this proposition has been well accepted within the Soil Physics scientific community (e.g. Rabot et al., 2018; Reichert et al., 2016), it has not yet been thoroughly evaluated.

The present study aimed to evaluate soil changes during compression and how these are controlled by initial soil conditions, also investigating their relation to the shape of the soil compression curve.

.

2 MATERIAL AND METHODS

2.1 Characterization of the studied sites and sampling

The present study was conducted with soil samples collected from three fields annually cultivated with maize for silage production located in the municipality of Lavras,

Southern Minas Gerais state, Southeastern Brazil (Figure 1). The fields belong to two different dairy farms and are managed under conventional tillage (annual disk-harrowing before seeding, with occasional subsoiling). The predominant soils classes in the studied sites are Oxisols (mainly Hapludox) and Inceptisols (Dystrudept) (FEAM - Fundação Estadual do Meio Ambiente, 2010; Soil Survey Staff, 2014). Local climate is classified as Cwa (mesothermic with rainy summer and warm winter) with mean annual precipitation of 1470 mm and average annual temperature of 22,3 °C (INMET-Instituto Nacional de Meteorologia, 2018). Sampling (Feb-Mar 2017) was performed prior to harvesting, in order to capture the soil physical condition to which the crop was submitted during most of the growing season and also to characterize soil strength before machinery traffic.
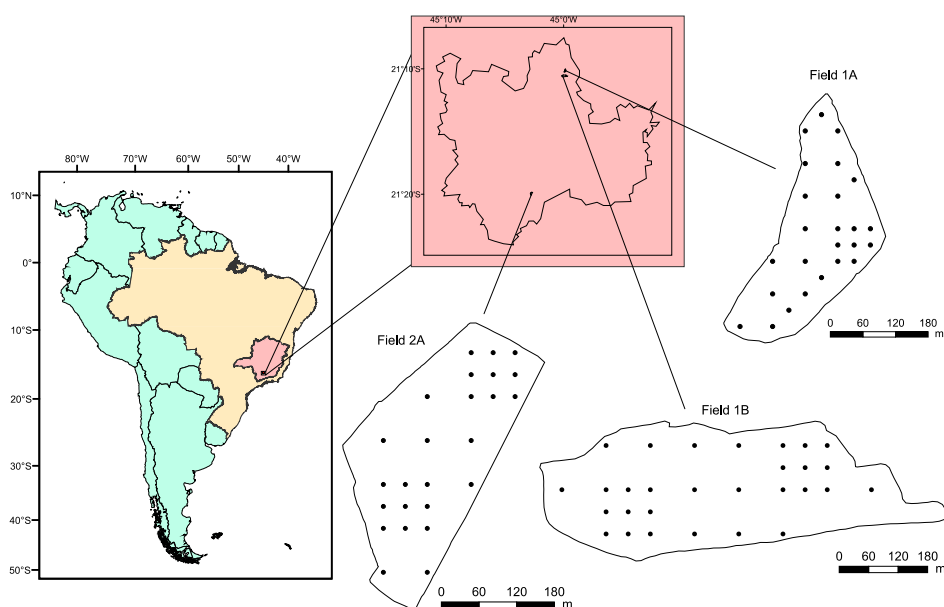
Figure 1. Location of the sampling points in the municipality of Lavras, southern Minas Gerais state, Southeastern Brazil.

The samples were collected according to a spatially-stratified design, aiming to systematically coverage the soil spatial variation. At each sampling point, six undisturbed soil samples were collected (within metallic cylinders 2.5 cm high and 6.4 cm wide), a replicate pair in each of the following depths: 0-5 cm, 10-15 cm, and 20-25 cm. A set of 76 sampling points was distributed in the three fields (field 1A: 22 points in 6.2 ha; field 1B: 29 points in 15.6 ha; field 2A: 25 points in 7.6 ha), totaling 456 samples.

2.2 Laboratory analysis and soil physical attributes

The undisturbed samples were initially prepared by removing the excess soil from the cylinders. This spare soil was air-dried and sieved (2.0 mm) for further analysis. Organic carbon was determined by wet combustion with $K_2Cr_2O_7$ and titration (Fontana and Campos, 2017). Soil texture was determined after dispersion with 1.0 mol L^{-1} NaOH and 16 h agitation (30 rpm) by the pipette method (Donagemma et al., 2017). Particle density was determined with deaerated water by the pycnometer method (Viana et al., 2017). Soil consistency was assessed by determining the plastic limit with soil sieved < 0.4 mm according to the procedure from McBride (2007).

Table 1. Soil texture (clay, sand and silt contents), organic carbon content (SOC), particle and bulk densities (ρ_p and ρ_b respectively), average water content at the water tensions of 10 and 100 kPa (θ_{10kPa} and θ_{100kPa}), and water content at the plastic limit (PL).

Field and depth	Clay	Sand	Silt	SOC	ρ_p	ρ_b	θ_{10kPa}	θ_{100kPa}	PL
	--------------- g kg^{-1} ---------------				---- Mg m^{-3} ----		---------- (g g^{-1}) ----------		
1A 0-5 cm	394	497	109	20.1	2.49	1.28	0.28	0.23	0.26
1A 10-15 cm	405	484	111	11.3	2.57	1.48	0.22	0.18	0.25
1A 20-25 cm	433	445	122	7.3	2.60	1.45	0.23	0.20	0.24
1B 0-5 cm	500	377	123	17.8	2.59	1.27	0.29	0.24	0.31
1B 10-15 cm	524	349	127	16.8	2.60	1.32	0.28	0.23	0.30
1B 20-25 cm	518	331	151	12.8	2.63	1.33	0.27	0.24	0.30
2A 0-5 cm	579	178	243	18.0	2.58	1.13	0.32	0.25	0.29
2A 10-15 cm	575	174	251	15.3	2.59	1.21	0.31	0.25	0.30
2A 20-25 cm	575	174	251	14.7	2.60	1.18	0.32	0.24	0.31

Following preparation, a nylon cloth was attached to the samples, which were put to saturate in plastic trays with distilled water. When saturation was reached, the samples were weighed and set to equilibrate at the water tensions (Ψ) of 10 or 100 kPa (half the samples at each) in porous plate extractors (Soil Moisture, USA). These water tensions were chosen because silage harvesting usually occurs during the rainy season and the soil is therefore expected to be moist.

After equilibrium, the undisturbed samples were weighed and submitted to drained, confined uniaxial compression tests on electric-pneumatic consolidometers (model S-450, Durham GeoSlope, USA) according to Dias Junior and Martins (2017). A stress sequence of 25, 50, 100, 200, 400, 800 and 1600 kPa was applied to the samples for eight minutes per load

step without decompression between each step. The resultant deformation was recorded by a dial gauge. This compression time was chosen because it ensures at least 90% of the maximum deformation per load step according to the square-root of time method (Taylor, 1948). Following compression, the samples were oven-dried (48 h at 105 °C) for determination of the soil dry mass, then used to calculate the soil mass/volume ratios and water content.

2.3 Soil physical attributes and statistical analysis

Soil changes during compression were investigated regarding changes in mass/volume ratios and water content. The former included bulk density (ρ_b) and degree of compaction (DC), which were calculated for each stress during compression. DC was calculated as the ratio between ρ_b and the maximum ρ_b from the standard Proctor test. This reference ρ_b was determined by a pedotransfer function from Dias Junior and Miranda (2000) derived from several soils within our study region.

To assess the changes in soil moisture during compression, we employed the ratio between the initial volumetric water content of the sample (θ_v) and its total porosity (n) at each applied stress during compression. The effects of sampling field and depth, Ψ, applied pressure (σ), initial DC (DC_i) and initial gravimetric water content (θ_g) on ρ_b, DC and θ_v/n were evaluated by analysis of variance. The effects of σ, θ_g and DC_i on DC and θ_v/n at each load step of the uniaxial compression test were further investigate by linear regressions (Equation 1), adjusting a different model for each Ψ.

$$DC \text{ or } {\theta_v}/{n} = a + b\sigma + c\theta_g + dDC_i \qquad (1)$$

where DC and θ_v/n are the degree of compaction and the ratio between the initial water content and the total porosity at each load step of the compression test, σ is the applied pressure at a given load step of the compression test, θ_g is the gravimetric water content of the sample prior to compression, DC_i is the initial degree of compaction of the sample and a, b, c, and d are the fitted parameters.

The shape of the compression curve was assessed by means of an attribute termed VCLratio based on the rates of change in soil ρ_b in the final steps of the uniaxial compression test (Figure 2). This term derives from virgin compression line (VCL) and this portion of the compression curve was chosen because it indicates its format, whether bi-linear or sigmoidal (Tang et al., 2009). The VCLratio was calculated as the ratio between the rate of change in ρ_b

at the load step 800-1600 kPa (Δ800-1600 in Figure 2) and the rate of change in ρ_b at the load step of 400-800 kPa (Δ400-800 in Figure 2). This attribute may be used to identify compression curves of sigmoid (VCLratio < 1.0) and bi-linear shape (VCLratio > 1.0). The compression curve shape, as indicated by the VCLratio, was investigated by additive linear models based on Ψ (as a categorical variable), initial DC and water content (equation 2).

$$VCLratio = a + b\Psi\theta_g + c\Psi DC_i \qquad (2)$$

where θ_g is the initial gravimetric water content, DC_i is the initial degree of compaction and a, b and c are the adjusted parameters. All the statistical procedures were performed on RStudio (RStudioTeam, 2016).
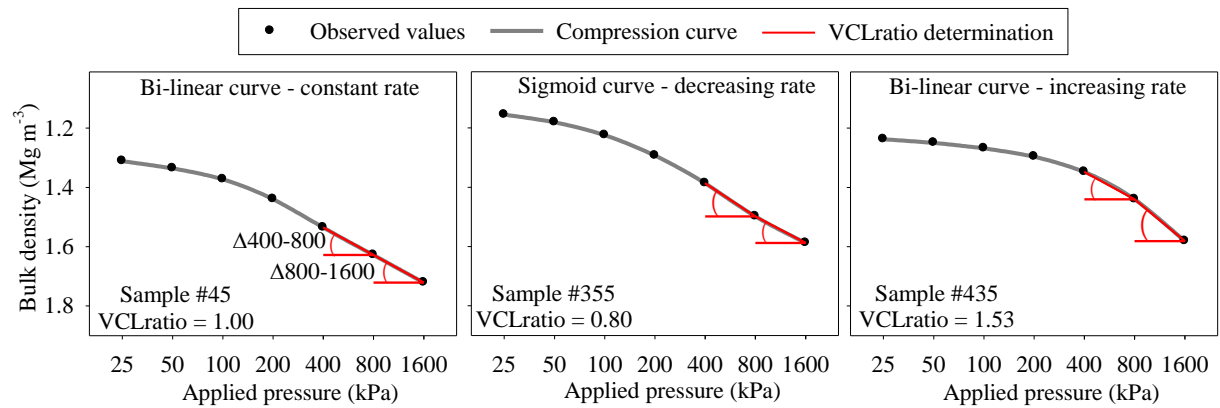
Figure 2. Determination of the VCLratio for three samples with differently-shaped compression curves (bi-linear and sigmoid) according to the rate of deformation during virgin compression (constant, decreasing and increasing rate).

3 RESULTS AND DISCUSSION

3.1 Soil changes during compression

The analyses of variance for bulk density (ρ_b), degree of compaction (DC), and the ratio between the initial volumetric water content of the sample and its total porosity at each applied stress during compression (θ_v/n) indicated that the factors sampling field and depth, water potential (Ψ), applied load (σ), initial degree of compaction (DC_i) and initial water content (θ_g) retained most of the total sum of squares (SSq), while the residue accounted for no more than 5.6% of the SSq (Table 2). This indicates that the major factors affecting the changes in soil properties during compression were indeed included in the analyses.

Even though the majority of the sources of variation were considered significant, several had little effect. Sampling field was a major source of variation only for ρ_b, accounting for 17% of the total SSq. As can be noted from Table 1, the fields differed in their textures, thus favoring the effect of this source of variation on ρ_b. The remaining attributes (DC and θ_v/n) were much less affected by sampling field, thus in the analyses of the following section the factors sampling field and depth were not included in the regression models. The interaction terms, although often significant, also contributed very little to explaining the variability in the data, retaining no more than 4% of the total SSq. Therefore, further analyses did not consider interactions between the predictors.

Table 2. Proportion of the total sum of squares retained by each of the sources of variation: sampling field and depth, water potential (Ψ), applied load (σ), initial degree of compaction (DC_i), gravimetric water content (θ_g) and interactions in the analyses of variance for bulk density (ρ_b), degree of compaction (DC), and the ratio between the initial volumetric water content of the sample and its total porosity at each applied stress during compression (θ_v/n).

Sources of variation	ρ_b	DC	θ_v/n
Field	17.3	3.13	5.17
Depth	1.54	3.62	0.42
Field*depth	0.34	0.09	0.67
Ψ	5.12	5.64	6.99
σ	52.8	60.8	29.0
DC_i	15.0	17.3	32.6
θ_g	0.72	0.69	18.9
$\Psi^*\sigma$	0.28	0.42	0.14
Ψ^*DC_i	0.02	0.03	0.02
$\Psi^* \theta_g$	0.00	0.00	0.46
σ^*DC_i	0.85	0.82	0.12
$\sigma^* \theta_g$	1.12	1.59	0.64
Other interactions	0.21	0.24	0.11
Residuals	4.71	5.57	4.73

The DC reached at each load step during the compression test was significantly dependent on DC_i (Table 3 and Figure 2). The compaction effect of each applied pressure

varied according to Ψ until up to 800 kPa (Table 3), being substantially higher for the samples equilibrated at Ψ = 10 kPa; while the coefficient value for the applied pressure of 1600 kPa was very similar for both Ψ (25.8 and 25.1 for Ψ equals to 10 and 100 kPa respectively). The effect of DC_i on the DC reached at each applied pressure was also distinct. For samples at Ψ = 10 kPa, each 1% increase in DC_i resulted in an increase of 0.7 in DC during compression; while this same unitary increase resulted in an increase in DC of 0.8 for samples at Ψ = 10 kPa.

Table 3. Coefficient values for the model $DC = a + b\sigma + c\theta g + dDC_i$ (Equation 1).

Coefficient values[1]	Soil water tension	
	10 kPa	100 kPa
a	20.4[**]	9.9[**]
b	22.6[**]	36.3[**]
c for σ = 50 kPa	1.80[**]	1.08[**]
c for σ = 100 kPa	4.7[**]	2.9[**]
c for σ = 200 kPa	8.9[**]	5.9[**]
c for σ = 400 kPa	14.2[**]	10.6[**]
c for σ = 800 kPa	20.0[**]	17.2[**]
c for σ = 1600 kPa	25.8[**]	25.1[**]
d	0.71[**]	0.80[**]

[1]Applied pressure (σ) entered the models as a categorical variable. [**]: Significant at 1%.

The maximum bulk density (ρ_{bmax}) from the standar Proctor test, reached at DC = 100%, was attained at several pressure values for both Ψ = 10 kPa and Ψ = 100 kPa (Figure 2). For the samples at Ψ = 10 kPa, ρ_{bmax} (DC = 100%) was reached at the load values of 100, 200, 400, 800 and 1600 kPa for samples with DC_i values of respectively 95%, 90%, 80%, 75% and 65% (Figure 2). For the samples at Ψ = 100 kPa, ρ_{bmax} was reached at higher DC_i values for these same loads. Under the applied loads of 200, 400, 800 and 1600 kPa, ρ_{bmax} was reached at DC_i values of 95%, 90%, 80% and 70%.

The present results suggest that, although uniaxial compression tests with undisturbed soil samples can indeed be used to calculate ρ_{bmax}, there are several factors which need to be considered for doing so. It does not suffice to choose a standard pressure and moisture condition (for example, close to field capacity) because the initial DC of the undisturbed samples will significantly affect the resulting DC at each load step. The use of uniaxial

compression tests for determining the reference ρ_b for calculating DC was originally proposed by (Hakansson and Lipiec, 2000) with disturbed soil samples and this was later extended to undisturbed samples by (Reichert et al., 2009). The latter authors suggested that undisturbed samples close to field capacity could be properly used for determining the reference bulk density for calculating DC, but our results do not corroborate this proposition.
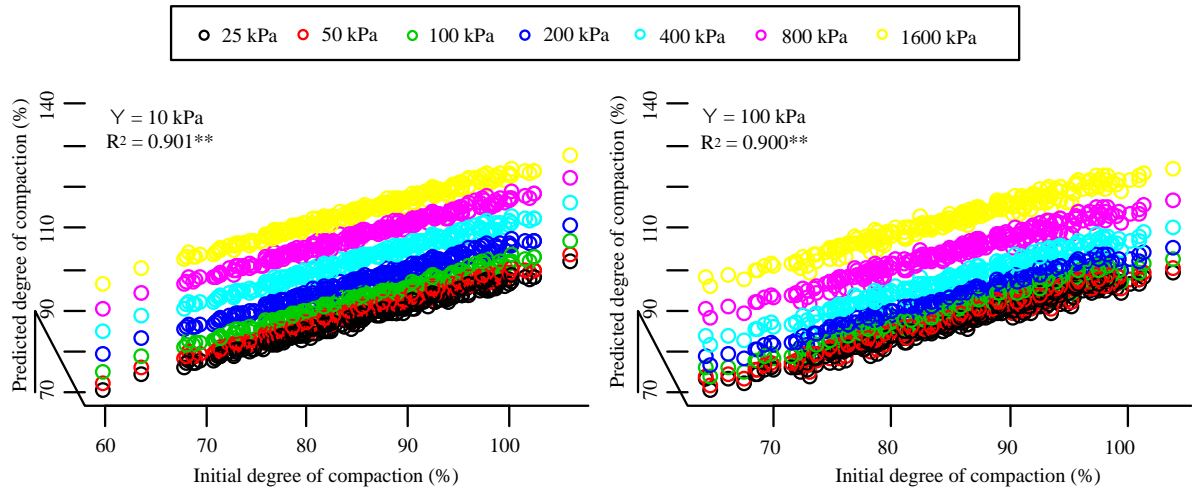
Figure 2. Effect of the initial degree of compaction (DC) on the DC reached at each applied load during compression (25, 50, 100, 200, 400, 800 and 1600 kPa), predicted according to the additive linear model from Equation 1 (DC = a + bσ + cθg + dDC$_i$) for two soil water tensions (Ψ), 10 and 100 kPa.

The usefulness of DC is precisely to cope with the natural influence of intrinsic attributes upon ρ_b (this is illustrated in Table 2 by the substantial differences on the effect of field depending on the physical attribute) and it was clear that using undisturbed samples under uniaxial compression for doing so produces results biased by the initial condition of the soil. We then suggest that reference ρ_b should be determined from pedotransfer functions based on intrinsic soil properties (soil texture, organic matter content) rather than attempting to determine it from this procedure with undisturbed samples. Therefore, studies focused on obtaining these pedotransfer functions, as those by Dias Junior and Miranda (2000) for soils within our study region, Marcolin and Klein (2011) for soil from Southern Brazil and Keller and Håkansson (2010) for Swedish soils should be greatly encouraged.

For samples equilibrated at Ψ = 10 kPa, compression shifted from compaction to consolidation during the final stages of the tests (Figure 3), as can be seen from the values of θ_v/n higher than unity. Since θ_v/n is the ratio between the pore volume occupied by water in

relation to the total pore volume, the values greater than unity actually indicate water expelled from the soil during the compression tests (developed under drained conditions). Because the soil pores were completely filled by water, the process is called consolidation rather than compaction, while compression is a broader term encompassing both these processes (Horn and Lebert, 1994).
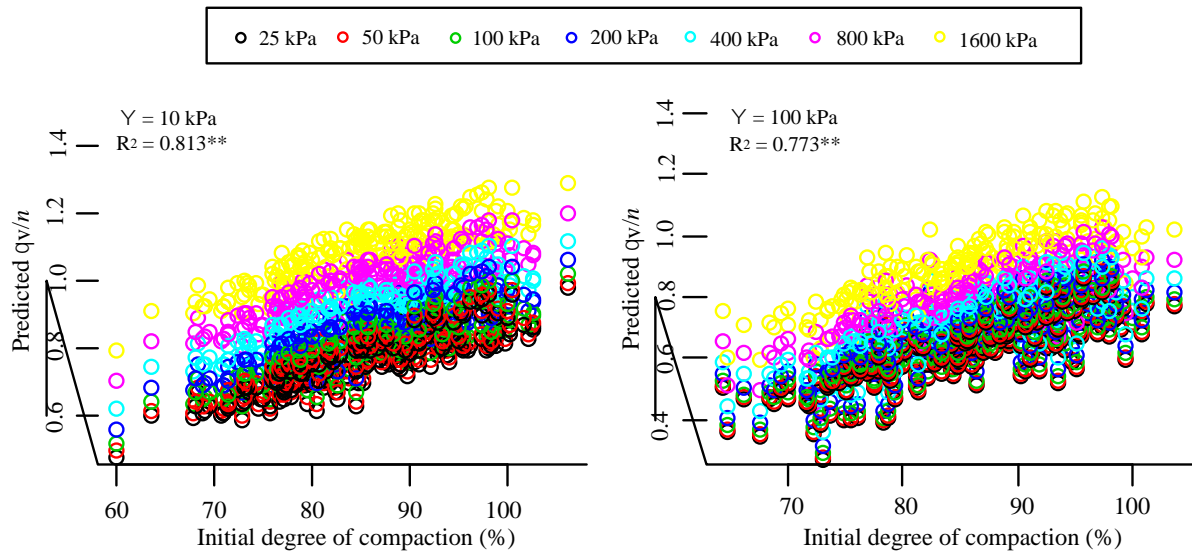
Figure 3. Relation between the initial degree of compaction (DC_i) and θ_v/n at each applied load during compression (25, 50, 100, 200, 400, 800 and 1600), predicted according to the additive linear model from Equation 1 ($\theta_v/n = a + b\sigma + c\theta g + dDC_i$) for two soil water tensions (Ψ), 10 and 100 kPa.

The change from compaction to consolidation may be related to the occurrence of sigmoid-shaped compression curves, commonly observed for samples close to field capacity (Arvidsson and Keller, 2004; Tang et al., 2009). During consolidation, the compression rate is governed by the saturated hydraulic conductivity, because decrease in pore volume can only take place if the corresponding volume of water is expelled from the soil (Horn and Lebert, 1994). The higher the DC_i, the lower the pressure value in which θ_v/n became greater than unity. Performing compression tests with samples as moist as at $\Psi = 10$ kPa may lead to consolidation under applied pressures of 200, 400, 800 and 1600 kPa for DC_i values of respectively 95%, 90, 80% and 75%. The applied pressure of 1600 kPa may incur in consolidation also for samples at $\Psi = 100$ kPa, but usually only for those with DC_i values above 90%.

3.2 Analysis of compression curve shape

Sigmoid curves were much more common for samples equilibrated at 10 kPa water tension, as can be seen from the scattered points in Figure 4 below the line for VCLratio equals to 1.0. This is in agreement with the findings of Tang et al. (2009) and may be related to the occurrence of consolidation in these samples, as discussed in the previous section. Since the compression change from compaction to consolidation, the rate of change in bulk density also changes, because consolidation is limited by the hydraulic conductivity of the soil. Therefore, the rate of change in compression diminishes for these moistest samples under the higher loads, resulting in sigmoid-shaped curves. Nevertheless, it should be noted that the VCLratio, although often below unity, was still very close to it. This evidence indicates that it is feasible to define the virgin portion of the compression curve by linear regression, but it would be advisable to fit it to more than just a single pair of points.
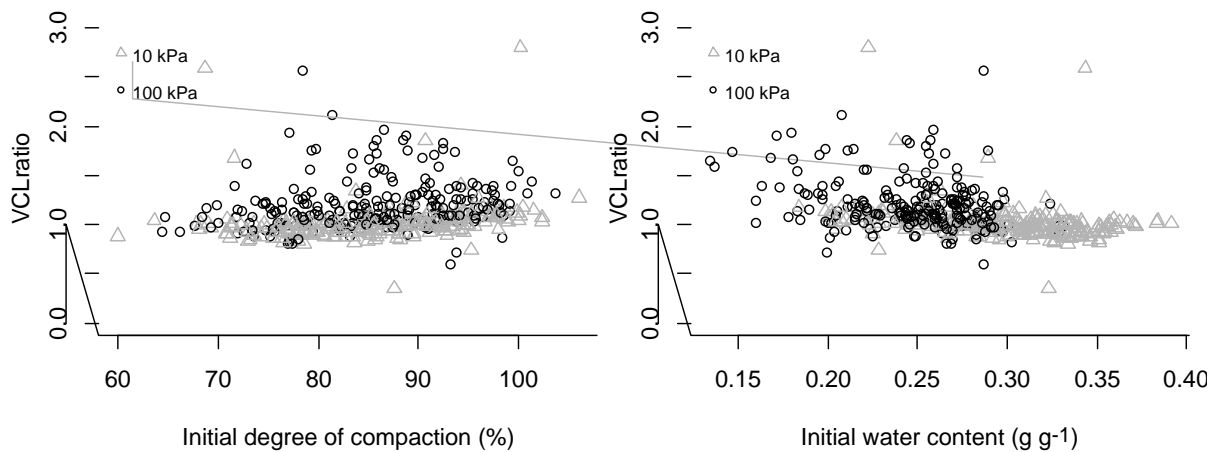
Figure 4. Relation between VCLratio and the initial degree of compaction and between VCL ratio and the initial water content according to the soil water tension (10 and 100 kPa).

The shape of the compression curve, as indicated by the attribute VCLratio, was significantly related to water content and initial degree of compaction, but the significance and effect of each of these parameters depended upon the soil water tension (Table 3). The initial degree of compaction (DC_i) had a significant effect over VCLratio only for samples equilibrate at $\Psi = 100$ kPa, indicating that the higher DC_i the higher the VCLratio. For samples at $\Psi = 10$ kPa, the linear effect of DC_i was non-significant, but Figure 4 indicates that bi-linaer curves became more common for DC_i values above 90% and became dominant for DC_i above 95%. Water content (θ_g) had a significant effect for both Ψ, but its effect over the VCLratio was more pronounced for $\Psi = 100$ kPa than for $\Psi = 10$ kPa, as can be seen from the

fitted parameters in table 3. Additionally, figure 4 indicates that sigmoid curves became much more common for water content values above 0.30 g g^{-1}.

Table 3. Parameter values (a, b and c) and coefficient of determination (R^2) for the models relating the VCLratio to soil water tension (Ψ), water content (θ_g) and degree of compaction (DC) according to equation 2 (VCLratio= a + b$\Psi\theta_g$ + cΨDC).

Model parameters	$\Psi = 100$ kPa	$\Psi = 10$ kPa
a	1.33^{**}	1.33^{**}
b	-1.72^{**}	-1.18^{**}
c	0.0035^{*}	0.0004^{ns}
R^2	0.211***	

**: significant at 1%; *: significant at 1%; ^{ns}: non-significant.

4 CONCLUSIONS

Changes in soil structure during compression were significantly affected by water tension (Ψ), applied pressure, water content and initial degree of compaction (DC). A single value of applied pressure could not be identified to determine the maximum bulk density since DC equals to 100% was observed for several applied pressures depending on Ψ and initial DC.

The applied uniaxial compression tests incurred on both compaction and consolidation, the latter being much more common for samples at $\Psi = 10$ kPa.

Compression curve shape, as indicated by the attribute VCLratio (defined as the ratio between the rates of change in ρ_b from 800-1600 kPa and from 400-800 kPa) was significantly affected by Ψ, water content and initial DC.

Sigmoid compression curves were more common for samples equilibrated at $\Psi = 10$ kPa, whereas higher initial DC and lower water content favored bi-linear compression curves.

5 ACKNOWLEDGEMENTS

6 REFERENCES

Ajayi, A.E., Dias Junior, M.S., Curi, N., Okunola, A., Souza, T.T.T., Pires, B.S., 2010. Assessment of vulnerability of oxisols to compaction in the Cerrado region of Brazil. Pedosphere 20, 252–260. doi:10.1016/S1002-0160(10)60013-6

Andrade, M.L.C., Tassinari, D., Dias Junior, M.S., Martins, R.P., Rocha, W.W., Souza, Z.R., 2017. Soil compaction caused by harvest and logging operations in eucalyptus forests in coarse-textured soils from Northeastern Brazil. Ciência e Agrotecnologia 41, 191–200. doi:10.1590/1413-70542017412036216

Arvidsson, J., Keller, T., 2004. Soil precompression stress I. A survey of Swedish arable soils. Soil Tillage Res. 77, 85–95. doi:10.1016/j.still.2004.01.003

Dias Junior, M.S., Miranda, E.É.V., 2000. Comportamento da curva de compactação de cinco solos da região de Lavras (MG). Ciência e Agrotecnologia 24, 337–346.

Dias Junior, M.S., Martins, P.C.C., 2017. Ensaio de compressão uniaxial e modelos de capacidade de suporte de carga do solo, In: Teixeira, P.C., Donagemma, G.K., Fontana, A., Teixeira, W.G. (Eds.), Manual de métodos de análise de solo. Embrapa, Brasília, pp. 152–171.

Donagemma, G.K., Viana, J.H.M., Almeida, B.G., Ruiz, H.A., Klein, V.A., Dechen, S.C.F., Fernandes, R.B.A., 2017. Análise granulométrica, In: Teixeira, P.C., Donagemma, G.K., Fontana, A., Teixeira, W.G. (Eds.), Manual de métodos de análise de solo. Embrapa, Brasília, pp. 95–116.

FEAM - Fundação Estadual Do Meio Ambiente, 2010. Mapa de solos de Minas Gerais: legenda expandida. FEAM, Belo Horizonte.

Fontana, A., Campos, D.V.B., 2017. Carbono orgânico, In: Teixeira, P.C., Donagemma, G.K., Fontana, A., Teixeira, W.G. (Eds.), Manual de métodos de análise de solo. Brasília, pp. 360–367.

Hakansson, I., Lipiec, J., 2000. A review of the usefulness of relative bulk density values in studies of soil structure and compaction. Soil Tillage Res. 53, 71–85.

Holthusen, D., Brandt, A.A., Reichert, J.M., Horn, R., 2018a. Soil porosity, permeability and static and dynamic strength parameters under native forest/grassland compared to no-tillage cropping. Soil Tillage Res. 177, 113–124. doi:10.1016/J.Still.2017.12.003

Holthusen, D., Brandt, A.A., Reichert, J.M., Horn, R., Fleige, H., Zink, A., 2018b. Soil functions and in situ stress distribution in subtropical soils as affected by land use, vehicle type, tire inflation pressure and plant residue removal. Soil Tillage Res. 184, 78–

92. doi:10.1016/J.Still.2018.07.009

Horn, R., Lebert, M., 1994. Soil compactability and compressibility, In: Soane, B.D., Van Ouwerkerk, C. (Eds.), Soil Compaction In Crop Production. Elsevier Science, Amsterdam.

Imhoff, S., Silva, A.P., Ghiberto, P.J., Tormena, C.A., Pilatti, M.A., Libardi, P.L., 2016. Physical quality indicators and mechanical behavior of agricultural soils of Argentina. Plos One 11, E0153827. doi:10.1371/Journal.Pone.0153827

INMET - Instituto Nacional de Meteorologia, 2018. Normais Climatológicas do Brasil: 1981-2010. INMET, Brasília.

Keller, T., Arvidsson, J., Dawidowski, J.B., Koolen, A.J., 2004. Soil precompression stress II. a comparison of different compaction tests and stress–displacement behaviour of the soil during wheeling. Soil Tillage Res. 77, 97–108. doi:10.1016/J.Still.2003.11.003

Keller, T., Arvidsson, J., Schjønning, P., Lamandé, M., Stettler, M., Weisskopf, P., 2012. In situ subsoil stress-strain behavior in relation to soil precompression stress. Soil Sci. 177, 490–497. doi:10.1097/Ss.0b013e318262554e

Keller, T., Håkansson, I., 2010. Estimation of reference bulk density from soil particle size distribution and soil organic matter content. Geoderma 154, 398–406. doi:10.1016/J.Geoderma.2009.11.013

Keller, T., Lamandé, M., Peth, S., Berli, M., Delenne, J.Y., Baumgarten, W., Rabbel, W., Radja, F., Rajchenbach, J., Selvadurai, A.P.S., Or, D., 2013. An interdisciplinary approach towards improved understanding of soil deformation during compaction. Soil Tillage Res. 128, 61–80. doi:10.1016/J.Still.2012.10.004

Lebert, M., Böken, H., Glante, F., 2007. Soil compaction indicators for the assessment of harmful changes to the soil in the context of the German Federal Soil Protection Act. J. Environ. Manage. 82, 388–397. doi:10.1016/J.Jenvman.2005.11.022

Lima, R.P., Silva, A.P., Giarola, N.F.B., Silva, A.R., Rolim, M.M., Keller, T., 2018. Impact of initial bulk density and matric suction on compressive properties of two Oxisols under no-till. Soil Tillage Res. 175, 168–177. doi:10.1016/J.Still.2017.09.003

Marcolin, C.D., Klein, V.A., 2011. Determinação da densidade relativa do solo por uma função de pedotransferência para a densidade do solo máxima. Acta Sci. Agron. 33, 349–354. doi:10.4025/Actasciagron.V33i2.6120

Martins, P.C.C., Dias Junior, M.S., Ajayi, A.E., Takahashi, E.N., Tassinari, D., 2018. Soil compaction during harvest operations in five tropical soils with different textures under

Eucalyptus forests. Ciência E Agrotecnologia 42, 58–68. doi:10.1590/1413-70542018421005217

Mcbride, R.A., 2007. Soil consistency: upper and lower plastic limits, In: Carter, M.R., Gregorich, E.G. (Eds.), Soil sampling and methods of analysis. Crc Press, Boca Raton, pp. 761–770.

Mosaddeghi, M.R., Koolen, A.J., Hemmat, A., Hajabbasi, M.A., Lerink, P., 2007. Comparisons of different procedures of pre-compaction stress determination on weakly structured soils. J. Terramechanics 44, 53–63. doi:10.1016/J.Jterra.2006.01.008

Naderi-Boldaji, M., Hajian, A., Ghanbarian, D., Bahrami, M., 2018. Finite element simulation of plate sinkage, confined and semi-confined compression tests: a comparison of the response to yield stress. Soil Tillage Res. 179, 63–70. doi:10.1016/J.Still.2018.02.003

Naveed, M., Schjønning, P., Keller, T., Jonge, L.W., Moldrup, P., Lamandé, M., 2016. Quantifying vertical stress transmission and compaction-induced soil structure using sensor mat and x-ray computed tomography. Soil Tillage Res. 158, 110–122. doi:10.1016/J.Still.2015.12.006

Nunes, M.R., Pauletto, E.A., Denardin, J.E., S. Suzuki, L.E.A., Van Es, H.M., 2019. Dynamic changes in compressive properties and crop response after chisel tillage in a highly weathered soil. Soil Tillage Res. 186, 183–190. doi:10.1016/J.Still.2018.10.017

Rabot, E., Wiesmeier, M., Schlüter, S., Vogel, H.-J., 2018. Soil structure as an indicator of soil functions: a review. Geoderma 314, 122–137. doi:10.1016/J.Geoderma.2017.11.009

Reichert, J.M., Rosa, V.T., Vogelmann, E.S., Rosa, D.P., Horn, R., Reinert, D.J., Sattler, A., Denardin, J.E., 2016. Conceptual framework for capacity and intensity physical soil properties affected by short and long-term (14 years) continuous no-tillage and controlled traffic. Soil Tillage Res. 158, 123–136. doi:10.1016/J.Still.2015.11.010

Reichert, J.M., Mentges, M.I., Rodrigues, M.F., Cavalli, J.P., Awe, G.O., Mentges, L.R., 2018. Compressibility and elasticity of subtropical no-till soils varying in granulometry organic matter, bulk density and moisture. Catena 165, 345–357. doi:10.1016/J.Catena.2018.02.014

Reichert, J.M., Suzuki, L.E.A.S., Reinert, D.J., Horn, R., Håkansson, I., 2009. Reference bulk density and critical degree-of-compactness for no-till crop production in subtropical highly weathered soils. Soil Tillage Res. 102, 242–254. doi:10.1016/J.Still.2008.07.002

Rstudioteam, 2016. Rstudio: Integrated Development For R.

Rücknagel, J., Rademacher, A., Götze, P., Hofmann, B., Christen, O., 2017. Uniaxial

compression behaviour and soil physical quality of topsoils under conventional and conservation tillage. Geoderma 286, 1–7. dDoi:10.1016/J.Geoderma.2016.10.015

Schjønning, P., Lamandé, M., 2018. Models for prediction of soil precompression stress from readily available soil properties. Geoderma 320, 115–125. doi:10.1016/J.Geoderma.2018.01.028

Schjønning, P., Lamandé, M., Munkholm, L.J., Lyngvig, H.S., Nielsen, J.A., 2016. Soil precompression stress, penetration resistance and crop yields in relation to differently-trafficked, temperate-region sandy loam soils. Soil Tillage Res. 163, 298–308. doi:10.1016/J.Still.2016.07.003

Soil Survey Staff, 2014. Keys To Soil Taxonomy. Washington, Dc.

Tang, A., Cui, Y., Eslami, J., Défossez, P., 2009. Analysing the form of the confined uniaxial compression curve of various soils. Geoderma 148, 282–290. doi:10.1016/J.Geoderma.2008.10.012

Viana, J.H.M., Teixeira, W.G., Donagemma, G.K., 2017. Densidade de partículas, In: Teixeira, P.C., Donagemma, G.K., Fontana, A., Teixeira, W.G. (Eds.), Manual de métodos de análise de solo. Embrapa, Brasília, pp. 76–81.

Watanabe, R., Figueiredo, G.C., Silva, A.P., Neves, J.C.L., Oliveira, T.S., 2017. Soil compressibility under irrigated perennial and annual crops in a semi-arid environment. Rev. Bras. Ciência do Solo 41. doi:10.1590/18069657rbcs20160206

DETERMINATION METHOD AND STRAIN-ATTRIBUTE INTERACT IN THE CALCULATION OF PRECOMPRESSION STRESS FROM SOIL COMPRESSION CURVES

Preparado de acordo com as normas do periódico Soil and Tillage Research
(versão preliminar)

ABSTRACT

Determination of soil precompression stress (σ_p) from compression curves has markedly changed in recent decades, with several available methods of varying complexity and computational effort. The graphical procedure proposed more than eight decades ago remains a standard, though it is now emulated by statistical and numerical procedures. We tested nine determination methods based on linear, polynomial (fourth order), nonlinear (sigmoid equations) and spline regressions, some of which included the numerical determination of the point of maximum curvature. Four physical attributes were used to represent soil deformation during compression (strain-attributes): bulk density (ρ_b), void ratio (*e*), total porosity (*n*) and strain (ε). Undisturbed soil samples from silage-maize fields were equilibrated at two water tensions (10 and 100 kPa) and submitted to confined, drained uniaxial compression tests. The experimental factors (determination method, strain-attribute and water tension) interacted in the determination of σ_p. Sigmoid equations fitted by nonlinear regressions only converged for 84% up to 95% of the compression curves. Methods based on fourth-degree polynomials resulted in several values outside the range 10-1550 kPa (from 10% up to more than 90% of the values depending on the strain-attribute). A fair agreement between σ_p values determined with ρ_b and ε was observed for several methods (fourth order polynomials and spline regression), indicating that differences between ρ_b and e are due not only to their nonlinear relation, but also because of their opposite behavior during compression (the former increasing and the latter decreasing). The linear intersection method (intersection between the regression lines fitted to 25-100 kPa and 400-1600 kPa) performed well with ρ_b. Spline regression resulted in clustering of σ_p close to the applied load values (more commonly 50, 100, 200 and 400 kPa) and performed better for ε.

Keywords: Casagrande method, preconsolidation pressure, compressibility, Gompertz equation, van Genuchten equation.

1 INTRODUCTION

Soil compaction poses a threat to soil quality and crop production (Rabot et al., 2018). Among the numerous ways in which it can be assessed, strength attributes related to soil mechanical behavior are leading choices in compaction studies at different environments. Soil compression is most commonly adopted as a strength measurement in croplands under wet climate conditions, such as in Northern Europe (Keller et al., 2012; Rücknagel et al., 2017; Schjønning et al., 2016) and Southern Brazil (Nunes et al., 2019; Reichert et al., 2018); in the study of vulnerable soils, such as Oxisols, Mollisols and others (Ajayi et al., 2010; Imhoff et al., 2016; Mosaddeghi et al., 2007); and in forestry studies (Andrade et al., 2017; Martins et al., 2018). Soil compressive strength has been assessed by many different methods, including field methods, such as vertical stress transmission and plate-sinkage; and laboratory methods, most commonly confined uniaxial compression tests performed under different conditions and methodologies.

Confined compression aims at determining the soil compression curve, from which the soil precompression stress (σ_p), a measure of the soil load-bearing capacity, can be calculated (Horn and Lebert, 1994; Koolen and Kuipers, 1983). Several methods are available for this, and the most common standard procedure was proposed more than eight decades ago by the civil engineer Arthur Casagrande for saturated samples under consolidation (Casagrande, 1936). This method is based on the graphical representation of the soil compression curve and begins by the visual determination of the point of maximum curvature. Nowadays, although this method is still applied in its original graphical form (e.g. Holthusen et al., 2018; Reichert et al., 2018; Silva et al., 2018), it has become increasingly more common to fit a equation to the compression curve data and then determine the point of maximum curvature numerically (Cavalieri et al., 2008; Imhoff et al., 2016; Keller et al., 2012), although this may not always agree to the graphical procedure (Rücknagel et al., 2010). The experimental study by Gregory et al., (2006) have shown that the point of maximum curvature *per se* is a better indicator of soil load bearing capacity, what has currently motivated its adoption as an estimator of precompression stress instead of following the whole subsequent procedure from the original method (Keller et al., 2011; Lamandé et al., 2017; Schjønning and Lamandé, 2018; Watanabe et al., 2017).

Also very common (e.g. Ajayi et al., 2014; Andrade et al., 2017; Martins et al., 2018) is the determination of σ_p at the intersection of two regression lines, one fitted to the first points of the compression curve and the other representing the linear expression of virgin

compression (VCL). This procedure was validated against the standard graphical procedure (Casagrande, 1936) in the study by Dias Junior and Pierce (1995) using bulk density (ρ_b) as the strain-attribute, but has also been applied to void ratio (*e*) by Cavalieri et al. (2008) and Gubiani et al. (2015). The number of points in each regression line varies, what affects results (Arvidsson and Keller, 2004; Cavalieri et al., 2008; Dias Junior and Pierce, 1995). The VCL may be fitted to two (Dias Junior and Pierce, 1995), three (Gubiani et al., 2015), five (Keller and Arvidsson, 2007) or to a variable number of points beyond σ_p (Arvidsson and Keller, 2004; Cavalieri et al., 2008). The other line is fitted to the initial points of the compression curve, commonly two, three, four or even five (Cavalieri et al., 2008; Dias Junior and Pierce, 1995; Gubiani et al., 2015). The most recent advance in determining σ_o from compression data was proposed by Lamandé et al (2017) and also applied by Schjønning and Lamandé (2018). It is based on a solely numerical approach. The compression curve (derived from a particular type of uniaxial compression test, with more than 200 data points) is divided into consecutive segments and a second-degree polynomial is fitted to each of these segments. This strategy allows determining the curvature at each of these segments, and then σ_o is also defined at the maximum curvature value.

Evidence has demonstrated that the strain-attribute chosen to define the compression curve significantly affects the determination of σ_p (Gubiani et al., 2015; Mosaddeghi et al., 2003). The compression curve was originally defined in terms of e as the variable in the ordinate axis (Casagrande, 1936), although this method has also been applied with ρ_b by Dias Junior and Pierce (1995) and Rücknagel et al. (2010). Deformation during compression may also be represented by the vertical displacement or strain (Keller et al., 2012) and soil specific volume (Keller and Arvidsson, 2007). Differences in the determination of σ_p are believed to arise from the non-linear relation between ρ_b and *e*, as identified by Mosaddeghi et al. (2003) and demonstrated by Rücknagel et al. (2010) and Gubiani et al. (2015) for graphical and intersection methods respectively.

The aims of the present study were to (i) compare different methods (based on linear, polynomial, nonlinear and spine regressions coupled to the numerical determination of the point of maximum curvature) for determining σ_o in a dataset (n = 456 samples) from tropical soils under silage-maize cultivation; and (ii) verify the influence of the choice of soil physical attribute used to define the soil compression curve (bulk density, void ratio, total porosity and strain).

2 MATERIAL AND METHODS

2.1 Characterization of the study sites and sampling

The studied sites are located in the municipality of Lavras, Southern Minas Gerais state, Southeastern Brazil (Figure 1). Three fields annually cultivated with maize for silage production were selected. The fields belong to two different dairy farms and are managed under conventional tillage (annual disk-harrowing before seeding, with occasional subsoiling). The predominant soils classes in the studied sites are Oxisols (mainly Hapludox) and Inceptisols (Dystrudept) (FEAM - Fundação Estadual Do Meio Ambiente, 2010; Soil Survey Staff, 2014). Local climate is classified as Cwa (mesothermic with rainy summer and warm winter) with mean annual precipitation of 1470 mm and average annual temperature of 22,3 °C (INMET-Instituto Nacional de Meteorologia, 2018). Sampling (Feb-Mar 2017) was performed prior to harvesting, in order to capture the soil physical condition to which the crop was submitted during most of the growing season.

The samples were collected according to a spatially-stratified design, aiming to systematically coverage the spatial variation. In each sampling point, six undisturbed soil samples were collected (within metallic cylinders 2.5 cm high and 6.4 cm wide), a replicate pair in each of the sampling depths: 0-5 cm, 10-15 cm, and 20-25 cm. A set of 76 sampling points was distributed in the three fields (field 1A: 22 points in 6.2 ha; field 1B: 29 points in 15.6 ha; field 2A: 25 points in 7.6 ha), totaling 456 samples.
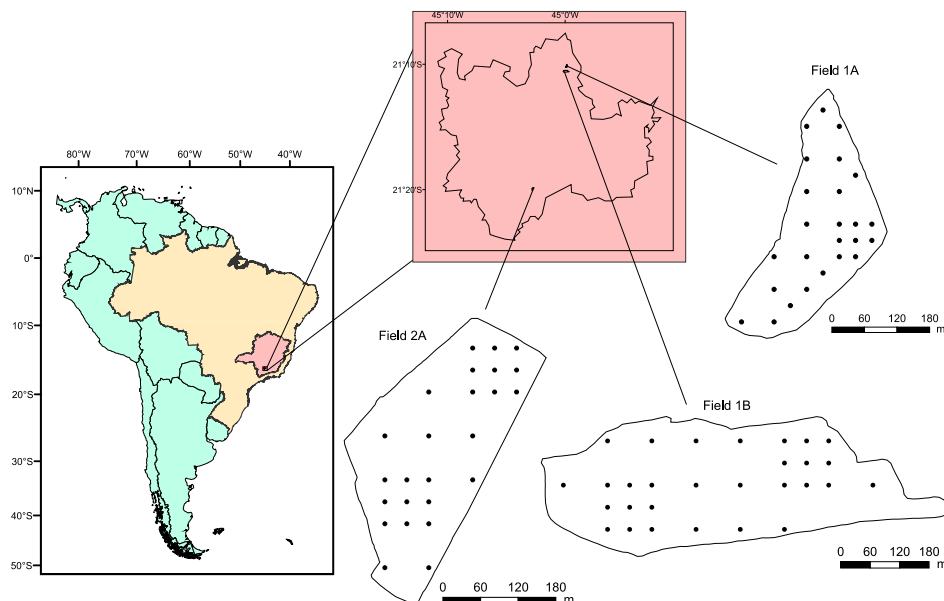
Figure 1. Location of the sampling points in the municipality of Lavras, southern Minas Gerais state, Southeastern Brazil.

2.2 Laboratory analysis and soil physical attributes

The undisturbed samples were initially prepared by removing the exceeding soil from the cylinders. This spare soil was air-dried and sieved (2.0 mm) for further analysis. Organic carbon was determined by oxidation with $K_2Cr_2O_7$ and titration (Fontana and Campos, 2017). Soil texture was determined after dispersion with 1.0 mol L^{-1} NaOH and 16h agitation (30 rpm) by the pipette method (Donagemma et al., 2017). Particle density was determined with deaerated water by the pycnometer method (Viana et al., 2017). Soil consistency was assessed by determining the plastic limit with soil sieved < 0.4 mm according to McBride (2007).

Table 1. Soil texture (clay, sand and silt contents), organic carbon content (SOC), particle and bulk densities (ρ_p and ρ_b respectively), average water content at the water tensions of 10 and 100 kPa (θ_{10kPa} and θ_{100kPa}), and water content at the plastic limit (PL).

Field and depth	Clay	Sand	Silt	SOC	ρ_p	ρ_b	θ_{10kPa}	θ_{100kPa}	PL
	--------------- g kg^{-1} ---------------				---- Mg m^{-3} ----		---------- (g g^{-1}) ----------		
1A 0-5 cm	394	497	109	20.1	2.49	1.28	0.28	0.23	0.26
1A 10-15 cm	405	484	111	11.3	2.57	1.48	0.22	0.18	0.25
1A 20-25 cm	433	445	122	7.3	2.60	1.45	0.23	0.20	0.24
1B 0-5 cm	500	377	123	17.8	2.59	1.27	0.29	0.24	0.31
1B 10-15 cm	524	349	127	16.8	2.60	1.32	0.28	0.23	0.30
1B 20-25 cm	518	331	151	12.8	2.63	1.33	0.27	0.24	0.30
2A 0-5 cm	579	178	243	18.0	2.58	1.13	0.32	0.25	0.29
2A 10-15 cm	575	174	251	15.3	2.59	1.21	0.31	0.25	0.30
2A 20-25 cm	575	174	251	14.7	2.60	1.18	0.32	0.24	0.31

Following preparation, a nylon cloth was attached to the samples, which were put to saturate in plastic trays with distilled water. When saturation was reached, the samples were weighed and set to equilibrate at water tensions of 10 or 100 kPa (half the samples at each water potential) in porous plate extractors (Soil Moisture, USA). These water tensions were chosen because silage harvesting usually occurs during the rainy season and the soil is therefore expected to be moist. After equilibrium, the undisturbed samples were weighed and submitted to drained, confined uniaxial compression tests on electric-pneumatic consolidometers (model S-450, Durham GeoSlope, USA) according to Dias Junior and Martins (2017). A stress sequence of 25, 50, 100, 200, 400, 800 and 1600 kPa was applied to the samples for eight minutes per load step without decompression between each step. The

resultant deformation was recorded by a dial gauge. This compression time was chosen because it ensures at least 90% of the maximum deformation per load step according to the square-root of time method (Taylor, 1948). Following compression, the samples were oven-dried (48 h at 105 °C) for determination of the soil dry mass, then used to calculate the soil mass/volume ratios and water content.

2.3 Determination of precompression stress (σ_p) and statistical analyses

Precompression stress was determined by nine different methods, summarized in Table 2. Each method was applied to the following strain-attributes: bulk density (ρ_b), void ratio (e), total porosity (n) and vertical strain (ε). Method I consists of the original method by Casagrande (1936) programmed into the R package "*soilphysics*" (Silva and Lima, 2015). This method fits a fourth-degree polynomial and finds the point of maximum curvature where the third derivative is equal to zero. The linear representation of the virgin compression curve (VCL) was fitted to the three last points of the compression curve (associated to the loads of 400, 800 and 1600 kPa). This method was also applied by Arvidsson and Keller (2004) and Cavalieri et al. (2008). Methods II and III define σ_p at the intersection of two linear equations, one fitted to first and the other to the last points of the compression curve. Method II used two points for each line, in accordance to the procedure tested by Dias Junior and Pierce (1995), while method III used three points (thus allowing for at least one degree of freedom in the regression residue of each regression line), also done in some other studies (Arvidsson and Keller, 2004; Cavalieri et al., 2008; Gubiani et al., 2015). Methods IV and V are based on nonlinear regression. Method IV was proposed for e by Gregory et al. (2006) and is based on the Gompertz (1825) growth model with four parameters (equation 1), from which the first and second derivatives (f' and f'' respectively) are used to determine σ_p at the point of maximum curvature (κ) from equation 2.

$$y = a + b[exp^{(-exp^{(-c((x)-d)))}}]} \tag{1}$$

$$\kappa = \frac{f''(x)}{\left(1 + \left(f'(x)\right)^2\right)^{3/2}} \tag{2}$$

where x is the logarithm of applied load and y is the strain-attribute (ρ_b, e, n and ε).

Method V, tested for *e* by Cavalieri et al. (2008), also makes use of equation 2 for determining the σ_p at the point of maximum curvature, but is based on the scaled sigmoid equation proposed by van Genuchten (1980) for the soil water retention curve. Methods VI, VII and VIII are all based on fourth-order polynomials, also employed for fitting compression data by Arvidsson and Keller (2004), Gregory et al. (2006), Cavalieri et al. (2008) and Silva and Lima (2015). Method VI used the point of maximum curvature determined by equation 2 for calculating σ_p, whereas method VII calculates the maximum curvature by making the third derivative of the polynomial equation equals to zero.

Method VIII adapts the recent development proposed by Lamandé et al. (2017), which consists in dividing the compression curve into consecutive segments and fitting a second-degree polynomial to each of these segments. This strategy allows for determining the curvature at each of these segments, and then σ_p is determined at the maximum curvature value. As the method was originally proposed for a specific type of uniaxial compression test resulting in 200 data points and because the tests we performed resulted in only seven ordinate pairs, we fitted fourth-degree polynomials to the original data and used them to predicted 1600 ordinate pairs of strain-attribute and log(load) in the range 1-1600 kPa. These predicted compression curve values were then used to apply the numerical approach by (Lamandé et al., 2017). Method IX also made use of this numerical procedure, but the soil compression curve was interpolated by a spline function. The numerical procedure was programmed to make use of 50 points in each segment, thus the minimum and maximum values are 26 and 1574 respectively.

Method I was applied using the "*soilphysics*" package (Silva and Lima, 2015) in RStudio (RStudio Team, 2016). Method II and III were programmed into Microsoft Excel® spreadsheets. RStudio was also used for fitting the nonlinear models from methods IV and V, the polynomials from methods VI, VII and VIII and the spline from method IX. The point of maximum curvature was found numerically for methods IV, V, VI, and VII, while RStudio was used to apply the numerical procedure by Lamandé et al. (2017) in methods VIII and IX. The spreadsheets employed and the scripts programmed are available as Supplementary Materials 1 and 2 respectively.

The methods were initially compared to each other by some summary statistics. Because σ_p sometimes reached unrealistically high values, the further analysis were performed by making all values above 1600 kPa equal to this, in order to allow for better graphical visualization. Kernel density distributions were derived in RStudio by the package

"sm" (Bowman and Azzalini, 2018). Princiapal components analysis (PCA) was also performed in RStudio and the biplot was constructed by using the package "factoextra" (Kassambara and Mundt, 2017).

Table 2. Summary of the different methods tested for determining precompression stress from soil compression curves.

ID	Procedure for determining σ_p	Reference
I	Casagrande procedure following fitting a fourth-degree polynomial	Casagrande (1936), Arvidsson and Keller (2004) and Silva and Lima (2015)
II	Intersection of two regression lines with two points each (the first two and the last two)	Dias Junior and Pierce (1995)
III	Intersection of two regression lines with three points each (the first two and the last two)	Modified from Dias Junior and Pierce (1995), Arvidsson and Keller (2004), Cavalieri et al. (2008) and Gubiani et al. (2015)
IV	Fitting the four-parameter Gompertz (1825) equation and finding the point of maximum curvature numerically	Gregory et al. (2006)
V	Fitting the van Genuchten (1980) equation and finding the point of maximum curvature numerically	Cavalieri et al (2008)
VI	Fitting a fourth- degree polynomial and finding the point of maximum curvature numerically	Gregory et al. (2006)
VII	Fitting a fourth- degree polynomial and finding the point of maximum curvature by making the 3rd derivative equals to 0 (y''' = 0)	modified from Arvidsson and Keller (2004) and Gregory et al. (2006)
VIII	Fitting a fourth- degree polynomial and finding the point of maximum curvature of the predicted compression curve by a numerical procedure	numerical procedure by (Lamandé et al., 2017)
IX	Fitting a smooth spline and finding the point of maximum curvature of the predicted compression curve by a numerical procedure	numerical procedure by (Lamandé et al., 2017)

ID: Identification of the method throughout the text.

3 RESULTS AND DISCUSSION

3.1 Descriptive statistics

Not only the different methods varied greatly in the estimated values of precompression stress (σ_p), but there was also a strong influence due to the strain-attribute (Table 3). The methods based on nonlinear regression (methods IV and V) failed to achieve convergence in all of the samples, with average convergence of 94% and 87% for methods IV and V, based on the sigmoid equations from Gompertz (1825) and van Genuchten (1980) respectively. Convergence failure was much more common for the samples equilibrated at 100 kPa water tension, which represented on average 92% and 84% of the convergence failure for methods IV and V respectively.

Other studies have not reported convergence failure for these nonlinear equations (Gregory et al., 2006; Cavalieri et al., 2008; Schjønning et al., 2016), probably because they employed samples close to field capacity, what may have favored sigmoidal compression curves (Tang et al., 2009) and successful convergence. Although the methods based on linear, polynomial and spline regressions (methods I, II, III, VI, VII, VIII and IX) always achieved 100% of regression convergence, they more or less commonly resulted in σ_p values outside the range 10-1550 kPa.

The method by Casagrande (1936) implemented in the R package "*soilphysics*" (method I) by Silva and Lima (2015) resulted in σ_p values higher than 1550 kPa in 8% of the samples, whereas the other methods based on fourth-degree polynomials performed more poorly, with 8.6%, 8.8% and 18.8% of σ_p values above 1550 kPa for methods VI, VII and VIII respectively; and 47.7%, 6.3% and 39.1% of exceedingly low values (below 10 kPa for methods VI and VII and equal to 26 kPa for method VIII, its minimum value). The linear intersection methods (methods II and III) and the spline method (method IX) also resulted in some unrealistic σ_p values, but majorly associated to void ratio (*e*) and strain (ε) for the former and *e* and total porosity (*n*) for the latter.

Table 3. Descriptive statistics (median, maximum and minimum values) for precompression stress, occurrence of extreme values and proportion of successful convergence for the different methods and soil physical attributes.

Method[1]	Median (kPa)	Maximum (kPa)	Minimum (kPa)	Values > 1550 kPa (%)	Exceedingly low values[2]	Convergence (%)
			Bulk density			
I	215.4	$8.33*10^{17}$	0.0	7.9	3.7 (2.6)	100
II	178.5	475.3	0.7	0.0	2.0 (0.4)	100
III	197.7	362.5	0.2	0.0	1.5 (0.4)	100
IV	103.5	1600	0.0	0.7	3.1	91.2
V	151.0	624	0.0	0.0	0.0	87.1
VI	161.5	1600	2.0	5.9	18.0 (13.4)	100
VII	188.0	$1.47*10^{19}$	0.0	9.4	9.0 (5.5)	100
VIII	190.0	1574	26.0	14.9	12.3	100
IX	202.0	802	60.0	0.0	0.0	100
			Void ratio			
I	215.4	$8.33*10^{17}$	0.0	7.9	6.1 (0.7)	100
II	117.4	$1.98*10^{5}$	0.0	2.0	18.9 (11.0)	100
III	161.5	$1.6*10^{91}$	0.0	2.6	9.0 (5.3)	100
IV	151.5	1600	0.0	0.4	4.4 (0.9)	95.4
V	98.5	603	0.0	0.0	1.8	88.0
VI	5.0	1600	2.0	13.2	83.3 (70.2)	100
VII	156.0	$2.8*10^{30}$	0.0	8.1	11.2 (7.0)	100
VIII	26.0	1574	26.0	30.5	56.1	100
IX	802.0	1574	26.0	31.6	20.2	100
			Total porosity			
I	261.2	$9.85*10^{90}$	0.0	7.9	3.7 (2.6)	100
II	178.5	475.3	0.7	0.0	2.0 (0.4)	100
III	197.7	362.5	0.2	0.0	1.5 (0.4)	100
IV	257.0	1600	0.0	2.0	0.2	94.7
V	268.0	1600	0.0	0.9	0.0	84.4
VI	2.0	1600	2.0	9.9	86.8 (85.5)	100
VII	188.0	$1.47*10^{19}$	0.0	9.4	9.0 (5.5)	100
VIII	26.0	1574	26.0	21.5	66.7	100
IX	806.0	1574	26.0	39.9	38.6	100
			Strain			
I	215.4	$8.33*10^{17}$	0.0	7.9	6.1 (0.7)	100
II	117.4	$1.98*10^{5}$	0.0	2.0	18.9 (11.0)	100
III	161.5	$1.6*10^{91}$	0.0	2.6	9.0 (5.3)	100
IV	74.0	1600	0.0	3.3	5.5 (0.4)	94.1
V	174.5	1283	0.0	0.0	0.0	88.8
VI	123.5	1600	2.0	5.3	26.1 (21.5)	100
VII	156.0	$2.8*10^{30}$	0.0	8.1	11.2 (7.0)	100
VIII	138.0	1574	26.0	8.3	21.1	100
IX	186.0	411	54.0	0.0	0.0	100

[1]Method identification according to Table 2.

[2]Below 10 kPa for methods I to VII and equal to 26 kPa for methods VIII and IX (the minimum of the numerical approach since it searches at 25 points intervals).

Artifact values can be readily spotted by analyzing σ_p minimum and maximum values (Table 3). Maximum values reached several dozens of magnitude (up to 10^{91} kPa) depending on both method and strain-attribute. Methods I, II, III and VII resulted in such extreme values for both e and ε. For ρ_b and n these extremely high values occurred only for methods I and VII (both based on the third derivative of fourth degree polynomials to find the point of maximum curvature). Method V performed well for ρ_b and e and the zero values shown in Table 3 are due to non-convergence (the latter also true for method V).

Methods I, II, III, VI, and VII also depicted minimum σ_p values close to zero, but at varying amounts and dependable upon the strain-attribute. Some methods limited the maximum and minimum values because of some intrinsic aspect of the method: sigmoidal equations and local search for the point of maximum curvature within the range 1-1600 kPa forcedly resulted in values within this range. These maximum values (1600 kPa for methods IV, V, VI and 1574 for methods VIII and IX) also constitute methodological artifacts as the aforementioned extreme values from methods I, II, III, VII. Because of this and to facilitate further comparisons, all σ_p values above 1600 kPa were set to this value.

Method IX presented well-behaved maximum and minimum values for ρ_b and especially for ε. For ρ_b, the maximum value of 802 kPa may be due to much higher rates of deformation from 800 to 1600 kPa, forcing the spline to shift the point of maximum curvature to immediately after 800 kPa. For ε, the smaller rate of variation at higher pressures (as clearly demonstrated for *e* by Gubiani et al., 2015) favored the spline to limit the point of maximum curvature right after 400 kPa.

3.2 Frequency distributions for σ_p

The kernel density empirical distributions for σ_p also indicated that method of determination and strain-attribute interacted to each other, as can be noted by the different shapes and positions of the curves from Figure 2. Some methods portrayed distinct distributions for all the four strain-attributes (methods IV, V, VIII and IX), while the distributions in the others clustered according to the pairs ρ_b together with *n* and *e* close to ε (methods I, II, III, VI, and VII). For methods I, II, III and VII, the distributions of σ_p determined from e and ε were located to the left of the curves for ρ_b and *n*. This indicates that the former attributes more commonly resulted in lower σ_p values in comparison to the latter. This same trend was also verified by Mosaddeghi et al. (2003) using the Casagrande (1936) procedure fitted numerically, by Rücknagel et al. (2010) for the graphical procedure from
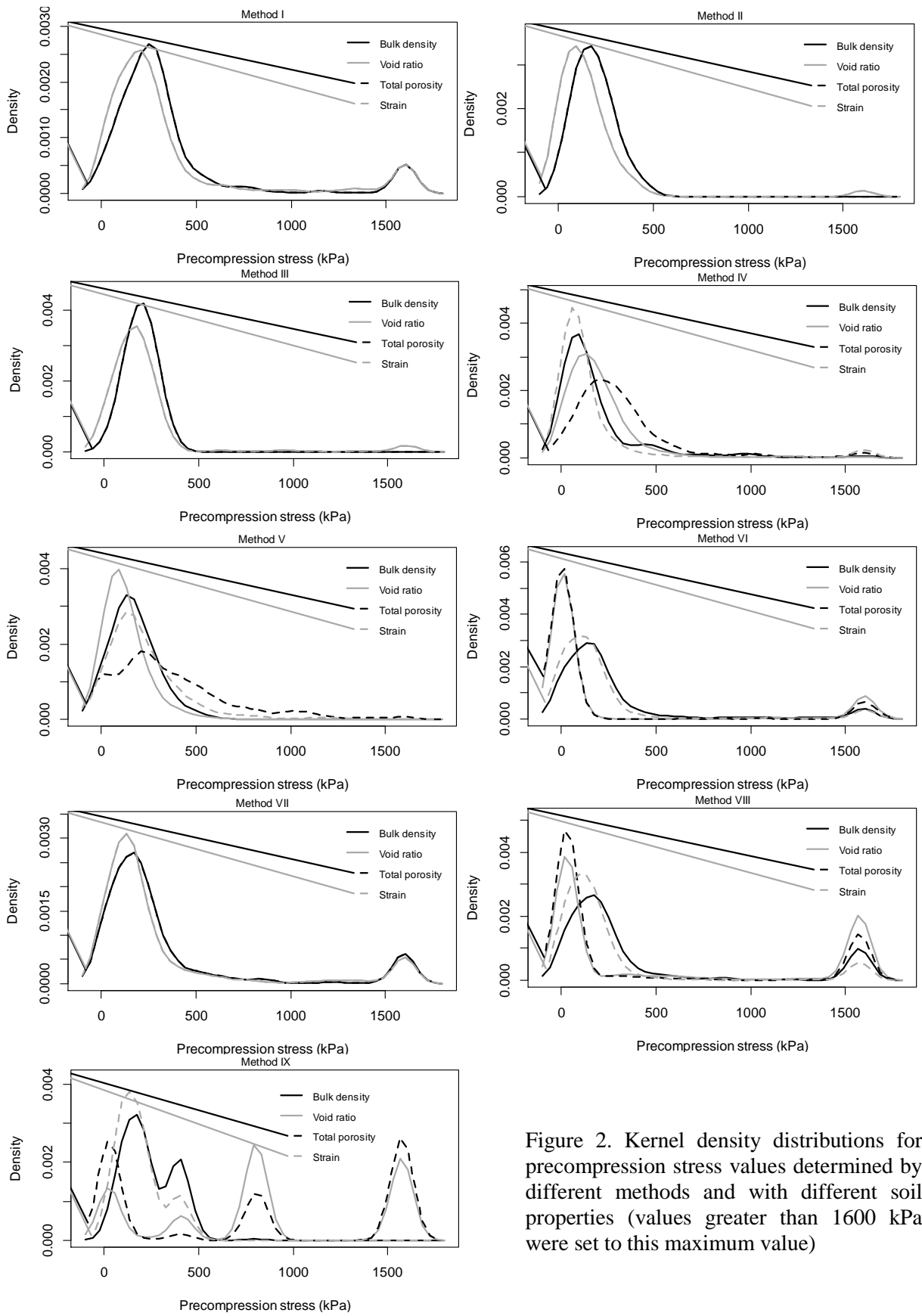
Figure 2. Kernel density distributions for precompression stress values determined by different methods and with different soil properties (values greater than 1600 kPa were set to this maximum value)

Casagrande (1936) and by Gubiani et al. (2015) with a bi-linear intersection method modified from Dias Junior and Pierce (1995). These observations were for ρ_b and e in these studies and we also confirmed them for n and ε as well. Among these methods, III and VII showed a smaller gap between the distributions of these two pairs of soil physical attributes.

The fourth-degree polynomial methods were influenced by the way of determining the point of maximum curvature and whether the compression curve increases or decreases (strain-attribute positively or negatively related to pressure). Methods VI, VIII and IX evidenced the effect of increasing and decreasing compression curves. For these methods, the distributions clustered according to the behavior of the strain-attribute: whether increasing (ρ_b and ε) or decreasing (e and n). This effect was also observable in methods IV and V (mainly between ρ_b and ε). A peak in the distribution close to 1600 kPa is clearly identifiable in methods I, VI, VII, VIII and IX, although not for all the strain-attributes (for method IX, only for e and n).

3.3 Relation between methods and effect of water potential

Principal component analysis (Figure 3) granted a wider perspective for the data depicted in Figure 2, also indicating that water potential was a major factor affecting σ_p determination. Although the first two principal components (PC) accounted for not more than half of the total variance, this can be considered a fair result given the amount of data (456 samples x 9 determination methods x 4 strain-attributes = 16,416 σ_p values). The majority of the methods were well correlated, but some methods depicted contrasting trends depending on the strain-attribute. The first PC was correlated to most of the methods, while the second PC was more related to methods I, V, VII and VIII for some strain-attributes. The arrows clustered along the first PC and pointing to the left indicate positive and stronger correlation between the σ_p values, including methods II and III for ρ_b and n, method VI, VIII and IX for ρ_b and ε, and method IV for all of the strain-attributes (although the latter with narrower arrows, indicating worse representation in the biplot and smaller contribution to the construction of the PC).

Methods VIII and IX had arrows pointing at opposite directions, depending on the behavior of the strain-attribute during compression: σ_p determined for ρ_b and ε were located to the left of the biplot, along the majority of the other methods, while e and n were oppositely located and negatively correlated to the first PC. This reinforces how the behavior of the soil physical attribute also affects determination of σ_p, although most studies usually focus only on

the nonlinear relation between these strain attributes (Gubiani et al., 2015; Mosaddeghi et al., 2003; Rücknagel et al., 2010).

The individuals located in the vicinity of the PC are those which portrayed more extreme values for σ_p (either too low or too high, depending on the location in comparison to the arrows of the methods), majorly scattered in the first and second quadrants. These more extreme values of σ_p indicate an interaction between method, strain-attribute and water potential. The points scattered in the first and second quadrants further away from the first PC axis represent well these extreme values and indicate that the methods based on bi-linear intersection and fourth-degree polynomials tended to result in excessively high values for samples at 100 kPa and exceedingly low values for samples at 10 kPa. Because water potential is a major factor affecting the shape of the compression curve (Tang et al., 2009) and since the shape of the curve significantly affects the determination of σ_p (Arvidsson and Keller, 2004; Gubiani et al., 2015), we further investigated the effect of this factor.
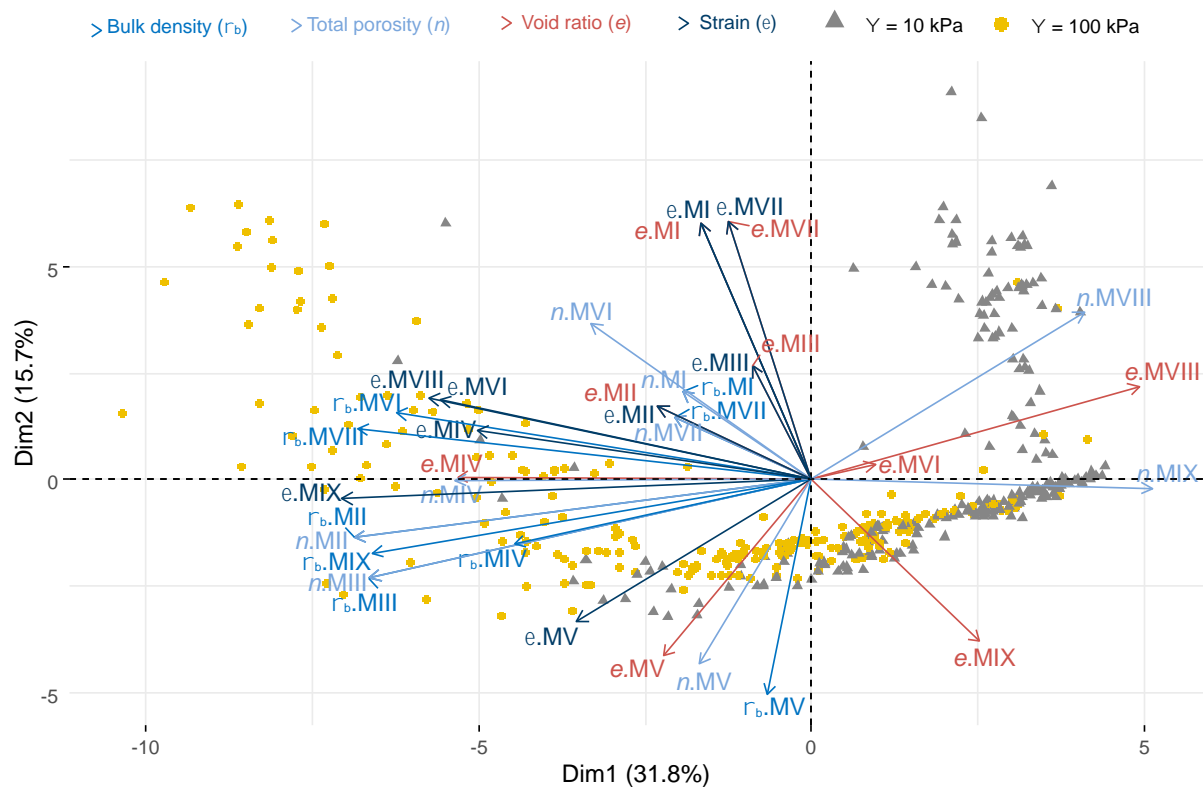

Figure 3. Principal components analysis biplot for 456 observations (colored according to the water tension during the compression test). Depicted variables are σ_p determined by different methods (MI to MIX) and for different strain-attributes.

3.4 Effect of compression curve shape

The shape of the compression curve is indicated by the relation between the compression rates at the last load steps of the compression test, associated to the virgin compression curve. The ratio between the compression rate at 800-1600 kPa and the compression rate at 400-800 kPa can thus be used as a numerical indicator of the compression curve shape (termed VCLratio in this paper). In a comprehensive study, Tang et al. (2009) reported two shapes of compression curve, the S-shaped or sigmoid curve, and the bi-linear one. Sigmoid compression curves are related to lower values of VCLratio (compression rate decreases from 400-800 kPa to 800-1600 kPa, making the VCLratio lower than unity), whereas bi-linear curves are related to higher values of VCLratio.

The VCLratio indicated that compression curve shape influenced the determination of σ_p depending on the method (Figure 4). Values close to zero and to 1600 kPa were more common the higher the VCLratio, indicating a greater difficulty of the majority of the methods to cope with bi-linear compression curves. This may have been overlooked in previous study because the majority of them focused on water contents close to field capacity (e.g. Arvidsson and Keller, 2004; Cavalieri et al., 2008) which favor sigmoid curves (Tang et al., 2009). For ρ_b, Methods VI, VII and VIII struggled with bi-linear curves resulting in σp whether too low (close to zero) or to high (close to 1600 kPa). To a lesser extent, method I also resulted in extreme σ_p values when VCLratio was approximately 1.2. Above this value, the nonlinear regression methods (IV and V) also presented spurious results, whether σ_p values too high (for method IV) or convergence failure and σ_p equals to zero (for both IV and V). For ε, both sigmoid and bi-linear methods presented extreme values depending on the method. For this strain-attribute, methods I and VII struggled for both sigmoid and bi-linear curves, while methods VI and VIII had more trouble with bi-linear curves. Methods IV and V also performed poorly for ε in bi-linear curves, whereas the intersection methods sometimes failed as well when VCLratio was low for this strain-attribute.

Method IX clustered along the load values applied during the compression tests (especially at 100, 200 and 400 kPa), indicating that this method was very sensitive to the applied loads during the tests. According to Arvidsson and Keller (2004), the semi-logarithmic representation of the compression curve forces it to bend at a certain stress level, and the spline was sensitive to this bending at particular loads. Adding more load steps to the compression tests may favor the application of this method, which has great flexibility in fitting increasing compression curves (that is for ρ_b and ε) regardless of its shape. This type of

regression may become a viable choice for calculating σ_p using the procedure for determining the point of maximum curvature from Lamandé et al. (2017).
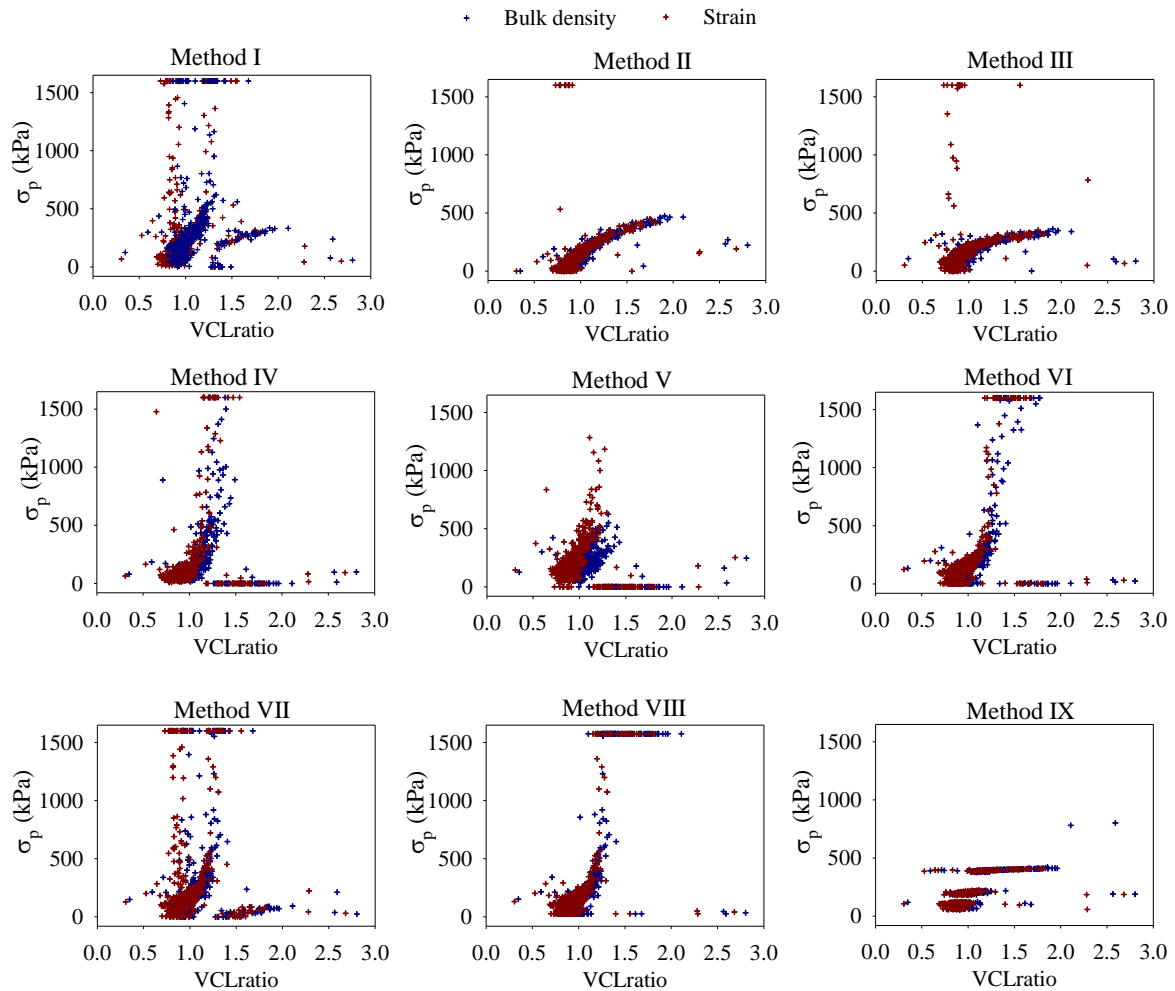
Figure 4. Effect of compression curve shape indicated by the VCLratio (ratio between the compression rates at 800-1600 kPa and 400-8000 kPa) on the determination of σ_p.

4 CONCLUSIONS

Determination method, strain-attribute and compression curve shape (affected by water potential) interacted in the calculation of precompression stress (σ_p). In addition to the nonlinear relation between some strain-attributes, we identified that σ_p may be also affected by the behavior of the strain-attribute during compression (whether increasing or decreasing).

Vertical strain (ε) should be preferred over void ratio (e) because although they are linearly related to each other, ε increases during compression as ρ_b, what favors the application of methods based on polynomial and spline regression.

A single method adequate for all of the experimental conditions tested could not be identified. Values of σ_p outside the range 10-1550 kPa were more or less common depending on the method, but were always present.

The methods based on sigmoid equation did not converge in steep virgin compression curves, which also compromised to different extents the methods based on fourth-degree polynomial.

The bi-linear intersection methods proved a reliable choice, but should be preferably applied to ρ_b. The inclusion of three points in the regression lines favored method-performance allowing for its use even with sigmoid equations

The spline method was very sensitive to the shape of the compression curve and the σ_p values clustered along the loads applied during the compression tests. Performing these tests with a larger number of load steps (instead of just seven, as in the present study) may favor not only this flexible method, but also the other methods based on regression analysis.

There is urgent need to acknowledge mathematical artifacts produced during the determination of σ_p in order to better allow for this soil attribute to be used in compaction prevention strategies.

5 ACKNOWLEDGEMENTS

6 REFERENCES

Ajayi, A.E., Dias Junior, M.S., Curi, N., Okunola, A., Souza, T.T.T., Pires, B.S., 2010. Assessment of vulnerability of oxisols to compaction in the Cerrado region of Brazil. Pedosphere 20, 252–260. doi:10.1016/S1002-0160(10)60013-6

Ajayi, A.E., Dias junior, M.S., Curi, N., Pais, P.S.M., Iori, P., 2014. Hydrophysical properties of Humic Latosols from Brazil. Int. Agrophysics 28, 395–402. doi:10.2478/intag-2014-0030

Andrade, M.L. C., Tassinari, D., Dias Junior, M. S., Martins, R.P., Rocha, W.W., Souza, Z.R., 2017. Soil compaction caused by harvest and logging operations in eucalyptus forests in coarse-textured soils from Northeastern Brazil. Ciência e Agrotecnologia 41, 191–200.

doi:10.1590/1413-70542017412036216

Arvidsson, J., Keller, T., 2004. Soil precompression stress I. A survey of Swedish arable soils. Soil Tillage Res. 77, 85–95. doi:10.1016/j.still.2004.01.003

Bowman, A.W., Azzalini, A., 2018. "sm": nonparametric smoothing methods (version 2.2-5.6).

Casagrande, A., 1936. The determination of pre-consolidation load and its practical significance, in: Proc. Int. Conf. Soil Mechanics and Foundation Engineering, v. III. Harvard University, Cambridge, MA, pp. 60–64.

Cavalieri, K.M.V., Arvidsson, J., Silva, A.P., Keller, T., 2008. Determination of precompression stress from uniaxial compression tests. Soil Tillage Res. 98, 17–26. doi:10.1016/j.still.2007.09.020

Dias Junior, M.S., Pierce, F.J., 1995. A simple procedure for estimating preconsolidation pressure from soil compression curves. Soil Technol. 8, 139–151. doi:10.1016/0933-3630(95)00015-8

Dias Junior, M.S., Martins, P.C.C., 2017. Ensaio de compressão uniaxial e modelos de capacidade de suporte de carga do solo, In: Teixeira, P.C., Donagemma, G.K., Fontana, A., Teixeira, W.G. (Eds.), Manual de métodos de análise de solo. Embrapa, Brasília, pp. 152–171.

Donagemma, G.K., Viana, J.H.M., Almeida, B.G., Ruiz, H.A., Klein, V.A., Dechen, S.C.F., Fernandes, R.B.A., 2017. Análise granulométrica, In: Teixeira, P.C., Donagemma, G.K., Fontana, A., Teixeira, W.G. (Eds.), Manual de métodos de análise de solo. Embrapa, Brasília, pp. 95–116.

FEAM - Fundação Estadual Do Meio Ambiente, 2010. Mapa de solos de Minas Gerais: legenda expandida. FEAM, Belo Horizonte, MG.

Fontana, A., Campos, D.V.B., 2017. Carbono orgânico, In: Teixeira, P.C., Donagemma, G.K., Fontana, A., Teixeira, W.G. (Eds.), Manual de métodos de análise de solo. Brasília, pp. 360–367.

Gompertz, B., 1825. On the nature of the function expressive of the law of human mortality, and on a new mode of determining the value of life contingencies. Philos. Trans. R. Soc. London B Biol. Sci. 182, 513–585.

Gregory, A.S., Whalley, W.R., Watts, C.W., Bird, N.R.A., Hallett, P.D., Whitmore, A.P., 2006. Calculation of the compression index and precompression stress from soil compression test data. Soil Tillage Res. 89, 45–57. doi:10.1016/j.still.2005.06.012

Gubiani, P.I., van Lier, Q.J., Reichert, J.M., Goulart, R.Z., Fontanela, E., 2015. Precompression stress and compression index depend on the property used to represent the soil deformation in the compression curve. Ciência Rural 46, 76–82. doi:10.1590/0103-8478cr20141495

Holthusen, D., Brandt, A.A., Reichert, J.M., Horn, R., 2018. Soil porosity, permeability and static and dynamic strength parameters under native forest/grassland compared to no-tillage cropping. Soil Tillage Res. 177, 113–124. doi:10.1016/j.still.2017.12.003

Horn, R., Lebert, M., 1994. Soil compactability and compressibility, in: Soane, B.D., van Ouwerkerk, C. (Eds.), Soil compaction in crop production. Elsevier Science, Amsterdam.

Imhoff, S., Silva, A.P., Ghiberto, P.J., Tormena, C.A., Pilatti, M.A., Libardi, P.L., 2016. Physical quality indicators and mechanical behavior of agricultural soils of Argentina. PLoS One 11, e0153827. doi:10.1371/journal.pone.0153827

INMET - Instituto Nacional de Meteorologia, 2018. Normais Climatológicas do Brasil: 1981-2010. INMET, Brasília, DF.

Kassambara, A., Mundt, F., 2017. factoextra: extract and visualize the results of multivariate data analyses.

Keller, T., Arvidsson, J., 2007. Compressive properties of some Swedish and Danish structured agricultural soils measured in uniaxial compression tests. Eur. J. Soil Sci. 58, 1373–1381. doi:10.1111/j.1365-2389.2007.00944.x

Keller, T., Arvidsson, J., Schjønning, P., Lamandé, M., Stettler, M., Weisskopf, P., 2012. In situ subsoil stress-strain behavior in relation to soil precompression stress. Soil Sci. 177, 490–497. doi:10.1097/Ss.0b013e318262554e

Keller, T., Lamandé, M., Schjønning, P., Dexter, A.R., 2011. Analysis of soil compression curves from uniaxial confined compression tests. Geoderma 163, 13–23. doi:10.1016/j.geoderma.2011.02.006

Koolen, A.J., Kuipers, H., 1983. Agricultural Soil Mechanics. Springer, Berlin.

Lamandé, M., Schjønning, P., Labouriau, R., 2017. A novel method for estimating soil precompression stress from uniaxial confined compression tests. Soil Sci. Soc. Am. J. 81, 1005. doi:10.2136/sssaj2016.09.0274

Martins, P.C.C., Dias Junior, M.S., Ajayi, A.E., Takahashi, E.N., Tassinari, D., 2018. Soil compaction during harvest operations in five tropical soils with different textures under Eucalyptus forests. Ciência e Agrotecnologia 42, 58–68. doi:10.1590/1413-

70542018421005217

Mcbride, R.A., 2007. Soil consistency: upper and lower plastic limits, In: Carter, M.R., Gregorich, E.G. (Eds.), Soil sampling and methods of analysis. Crc Press, Boca Raton, FL, pp. 761–770.

Mosaddeghi, M., 2003. Pre-compression stress and its relation with the physical and mechanical properties of a structurally unstable soil in central Iran. Soil Tillage Res. 70, 53–64. doi:10.1016/S0167-1987(02)00120-4

Mosaddeghi, M.R., Koolen, A.J., Hemmat, A., Hajabbasi, M.A., Lerink, P., 2007. Comparisons of different procedures of pre-compaction stress determination on weakly structured soils. J. Terramechanics 44, 53–63. doi:10.1016/j.jterra.2006.01.008

Nunes, M.R., Pauletto, E.A., Denardin, J.E., S. Suzuki, L.E.A., van Es, H.M., 2019. Dynamic changes in compressive properties and crop response after chisel tillage in a highly weathered soil. Soil Tillage Res. 186, 183–190. doi:10.1016/j.still.2018.10.017

Reichert, J.M., Mentges, M.I., Rodrigues, M.F., Cavalli, J.P., Awe, G.O., Mentges, L.R., 2018. Compressibility and elasticity of subtropical no-till soils varying in granulometry organic matter, bulk density and moisture. Catena 165, 345–357. doi:10.1016/j.catena.2018.02.014

RStudioTeam, 2016. RStudio: Integrated Development for R.

Rücknagel, J., Brandhuber, R., Hofmann, B., Lebert, M., Marschall, K., Paul, R., Stock, O., Christen, O., 2010. Variance of mechanical precompression stress in graphic estimations using the Casagrande method and derived mathematical models. Soil Tillage Res. 106, 165–170. doi:10.1016/j.still.2009.11.001

Rücknagel, J., Rademacher, A., Götze, P., Hofmann, B., Christen, O., 2017. Uniaxial compression behaviour and soil physical quality of topsoils under conventional and conservation tillage. Geoderma 286, 1–7. doi:10.1016/j.geoderma.2016.10.015

Schjønning, P., Lamandé, M., 2018. Models for prediction of soil precompression stress from readily available soil properties Geoderma 320, 115–125. doi:10.1016/j.geoderma.2018.01.028

Schjønning, P., Lamandé, M., Munkholm, L.J., Lyngvig, H.S., Nielsen, J.A., 2016. Soil precompression stress, penetration resistance and crop yields in relation to differently-trafficked, temperate-region sandy loam soils. Soil Tillage Res. 163, 298–308. doi:10.1016/j.still.2016.07.003

Silva, A.R., Lima, R.P., 2015. soilphysics: An R package to determine soil preconsolidation

pressure. Comput. Geosci. 84, 54–60. doi:10.1016/j.cageo.2015.08.008

Silva, R.P., Rolim, M.M., Gomes, I.F., Pedrosa, E.M.R., Tavares, U.E., Santos, A.N., 2018. Numerical modeling of soil compaction in a sugarcane crop using the finite element method. Soil Tillage Res. 181, 1–10. doi:10.1016/j.still.2018.03.019

Soil Survey Staff, 2014. Keys To Soil Taxonomy. Washington, Dc.

Rabot, E., Wiesmeier, M., Schlüter, S., Vogel, H.J., 2018. Soil structure as an indicator of soil functions: A review. Geoderma 314, 122–137. doi:10.1016/j.geoderma.2017.11.009

Tang, A., Cui, Y., Eslami, J., Défossez, P., 2009. Analysing the form of the confined uniaxial compression curve of various soils. Geoderma 148, 282–290. doi:10.1016/j.geoderma.2008.10.012

van Genuchten, M.T., 1980. A closed-form equation for predicting the hydraulic conductivity of unsaturated Soils. Soil Sci. Soc. Am. J. 44, 892–898.

Viana, J.H.M., Teixeira, W.G., Donagemma, G.K., 2017. Densidade de partículas, In: Teixeira, P.C., Donagemma, G.K., Fontana, A., Teixeira, W.G. (Eds.), Manual de métodos de análise de solo. Embrapa, Brasília, DF, pp. 76–81.

Watanabe, R., Figueiredo, G.C., Silva, A.P., Neves, J.C.L., Oliveira, T.S., 2017. Soil compressibility under irrigated perennial and annual crops in a semi-arid environment. Rev. Bras. Ciência Do Solo 41. doi:10.1590/18069657rbcs20160206

PREDICTION OF SOIL PRECOMPRESSION STRESS FROM WATER POTENTIAL, MOISTURE ATTRIBUTES AND MASS/VOLUME RATIOS

Preparado de acordo com as normas do periódico Soil and Tillage Research (versão preliminar)

ABSTRACT

Soil compressive properties are very important in soil compaction studies, being a common strategy for assessing soil mechanical strength. Precompression stress (σ_p), determined from soil compression curves, has been extensively investigated in order to determine how it is affected by other soil attributes. Nevertheless, a comprehensive effort in this sense is still lacking, aiming to properly address how the different soil moisture and mass/volume ratio attributes may be related to soil water tension (Ψ) in the prediction of σ_p. The present study aimed to fill this knowledge gap by developing prediction models for σ_p based on: Ψ; different soil moisture attributes, such as gravimetric water content (θ_g), volumetric water content (θ_v), degree of saturation (S), water ratio (*w*), and the ratios between θ_g and the optimum water content for compaction (θ_g/θ_{opt}), and the ratio between θ_g and the water content in the plastic limit (θ_g/θ_{PL}); and several expressions of soil mass/volume ratios, including bulk density (ρ_b), void ratio (*e*), total porosity (*n*), and degree of compaction (DC). Analyses of variance indicated that the factors sampling field and depth affected differently the soil physical attributes. The relative measures of both mass/volume ratios (DC) and moisture attributes (θ_g/θ_{opt} and θ_g/θ_{PL}) were less affected by the variation in intrinsic soil attributes among the sampled fields and depths. The different predictors for σ_p interacted in complex ways and the relative importance of each attribute (moisture vs. mass/volume ratio) varied according to the attribute (whether absolute measures, as bulk density, or relative, as degree of compaction) and Ψ. At $\Psi = 10$ kPa, σ_p increased more for each unitary change in ρ_b and DC than at $\Psi = 100$ kPa. For each 1% increase in DC, σ_p increases on average 3.2 kPa and 4.4 kPa for Ψ equals to 100 kPa and 10 kPa respectively.

Keywords: water content, degree of compaction, bulk density, water ratio, degree of saturation.

1 INTRODUCTION

Soil compaction poses a threat to soil quality and crop production (Rabot et al., 2018). The prevention and assessment of soil compaction may greatly benefit from considering soil compressive behavior and its mechanical strength (Imhoff et al., 2016; Keller et al., 2013; Lebert et al., 2007), since these are tightly linked to structural changes due to compaction and are also related to plant growth (Nunes et al., 2019; Schjønning et al., 2016).

Soil compressive strength has been assessed by many different methods, including field methods, such as vertical stress transmission (Holthusen et al., 2018a; Naveed et al., 2016) and plate-sinkage (Keller et al., 2004; Naderi-Boldaji et al., 2018); and laboratory methods, most commonly confined uniaxial compression tests performed under different conditions and methodologies (Holthusen et al., 2018b; Nunes et al., 2019; Reichert et al., 2018; Dias Junior and Martins, 2017; Rücknagel et al., 2017; Watanabe et al., 2017).

Soil compression is most commonly adopted as a strength measurement in croplands under wet climate conditions, such as in Northern Europe (Keller et al., 2012; Rücknagel et al., 2017; Schjønning and Lamandé, 2018) and Southern Brazil (Nunes et al., 2019; Reichert et al., 2018); in the study of vulnerable soils, such as Oxisols, Mollisols and others (Ajayi et al., 2010; Imhoff et al., 2016; Mosaddeghi et al., 2007; Severiano et al., 2013, 2011); and in forestry studies (Andrade et al., 2017; Martins et al., 2018).

In these soil compaction studies, the most common mechanical strength parameter is the precompression stress (σ_p), which indicates the maximum load a soil could withstand without suffering additional compaction, that is, the pressure value that separates elastic from plastic deformations (Horn and Lebert, 1994; Koolen and Kuipers, 1983).

The relation between σ_p and other soil physical properties is currently under scrutiny, in order to understand how different parameters may affect soil strength (Lima et al., 2018; Reichert et al., 2018) and also aiming to develop pedotransfer function for predicting σp from more easily available attributes (Imhoff et al., 2016; Schjønning and Lamandé, 2018). Most commonly σ_p is predicted from bulk density, water potential, granulometric distribution (clay content) and organic matter content.

The present study aimed to evaluate different combinations of moisture attributes and mass/volume ratios for prediction of σ_p, investigating how varying intrinsic soil properties may affect the performance of the different predictors.

2 MATERIAL AND METHODS

2.1 Characterization of the studied sites and sampling

The present study was conducted with soil samples collected from three fields annually cultivated with maize for silage production located in the municipality of Lavras, Southern Minas Gerais state, Southeastern Brazil (Figure 1). The fields belong to two different dairy farms and are managed under conventional tillage (annual disk-harrowing before seeding, with occasional subsoiling). The predominant soils classes in the studied sites are Oxisols (mainly Hapludox) and Inceptisols (Dystrudept) (FEAM - Fundação Estadual Do Meio Ambiente, 2010; Soil Survey Staff, 2014). Local climate is classified as Cwa (mesothermic with rainy summer and warm winter) with mean annual precipitation of 1470 mm and average annual temperature of 22,3 °C (INMET-Instituto Nacional de Meteorologia, 2018). Sampling (Feb-Mar 2017) was performed prior to harvesting, in order to capture the soil physical condition to which the crop was submitted during most of the growing season.

Figure 1. Location of the sampling points in the municipality of Lavras, southern Minas Gerais state, Southeastern Brazil.

The samples were collected according to a spatially-stratified design, aiming to systematically coverage the soil spatial variation. In each sampling point, six undisturbed soil samples were collected (within metallic cylinders 2.5 cm high and 6.4 cm wide), a replicate pair in each of the sampling depths: 0-5 cm, 10-15 cm, and 20-25 cm. A set of 76 sampling

points was distributed in the three fields (field 1A: 22 points in 6.2 ha; field 1B: 29 points in 15.6 ha; field 2A: 25 points in 7.6 ha), totaling 456 samples.

2.2 Laboratory analysis and soil physical attributes

The undisturbed samples were initially prepared by removing the exceeding soil from the cylinders. This spare soil was air-dried and sieved (2.0 mm) for further analysis. Organic carbon was determined by wet combustion with $K_2Cr_2O_7$ and titration (Fontana and Campos, 2017). Soil granulometric distribution was determined after dispersion with 1.0 mol L^{-1} NaOH and 16h agitation (30 rpm) by the pipette method (Donagemma et al., 2017). Particle density was determined with deaerated water by the pycnometer method (Viana et al., 2017). Soil consistency was assessed by determining the plastic limit with soil sieved < 0.4 mm according to the procedure from McBride (2007).

Table 1. Soil texture (clay, sand and silt contents), organic carbon content (SOC), particle and bulk densities (ρ_p and ρ_b respectively), average water content at the water tensions of 10 and 100 kPa (θ_{10kPa} and θ_{100kPa}), and water content at the plastic limit (PL).

Field and depth	Clay	Sand	Silt	SOC	ρ_p	ρ_b	θ_{10kPa}	θ_{100kPa}	PL
	--------------- g kg^{-1} ---------------				---- Mg m^{-3} ----		---------- (g g^{-1}) ----------		
1A 0-5 cm	394	497	109	20.1	2.49	1.28	0.28	0.23	0.26
1A 10-15 cm	405	484	111	11.3	2.57	1.48	0.22	0.18	0.25
1A 20-25 cm	433	445	122	7.3	2.60	1.45	0.23	0.20	0.24
1B 0-5 cm	500	377	123	17.8	2.59	1.27	0.29	0.24	0.31
1B 10-15 cm	524	349	127	16.8	2.60	1.32	0.28	0.23	0.30
1B 20-25 cm	518	331	151	12.8	2.63	1.33	0.27	0.24	0.30
2A 0-5 cm	579	178	243	18.0	2.58	1.13	0.32	0.25	0.29
2A 10-15 cm	575	174	251	15.3	2.59	1.21	0.31	0.25	0.30
2A 20-25 cm	575	174	251	14.7	2.60	1.18	0.32	0.24	0.31

Following preparation, a nylon cloth was attached to the samples, which were put to saturate in plastic trays with distilled water. When saturation was reached, the samples were weighed and set to equilibrate at a water tensions of 10 or 100 kPa (half the samples at each water potential) in porous plate extractors (Soil Moisture, USA). These water tensions were chosen because silage harvesting usually occurs during the rainy season and the soil is therefore expected to be moist. After equilibrium, the undisturbed samples were weighed and

submitted to drained, confined uniaxial compression tests on electric-pneumatic consolidometers (model S-450, Durham GeoSlope, USA) according to Dias Junior and Martins (2017). A stress sequence of 25, 50, 100, 200, 400, 800 and 1,600 kPa was applied to the samples for eight minutes per load step without decompression between each step. The resultant deformation was recorded by a dial gauge. This compression time was chosen because it ensures at least 90% of the maximum deformation per load step according to the square-root of time method (Taylor, 1948). Following compression, the samples were oven-dried (48 h at 105 °C) for determination of the soil dry mass, and then used to calculate the soil mass/volume ratios and water content. Precompression stress was determined by a modification of the linear intersection method from Dias Junior and Pierce (1995), considering three points for each regression line instead of two as originally.

2.3 Relation between σ_p and soil physical properties

Soil σ_p was predicted by different combinations of soil physical attributes. These comprised soil water potential (Ψ), included in the regression models as a categorical dummy variable (with values equal to zero for Ψ = 100 kPa and to one for Ψ = 10 kPa), and several attributes which characterize soil moisture and mass/volume ratios.

The soil moisture attributes (M) encompassed: (i) gravimetric water content (θ_g), calculated as the ratio between the mass of water and the mass of dry soil; (ii) volumetric water content (θ_v), given as the ratio between the volume of water and the volume of soil; (iii) degree of saturation (S), calculated as the ratio between θ_v and total porosity (n); (iv) soil water ratio (w), which is similar to void ratio (e), but consists in the ratio between θ_v and the volume of solids; (v) the ratio between θ_g and the optimum water content for compaction (θ_g/θ_{opt}) derived from the Proctor test as given by the pedotransfer function by Dias Junior and Miranda (2000) for soils within the same region; and (vi) the ratio between θ_g and the water content in the plastic limit (θ_g/θ_{PL}) as given in Table 1.

The mass/volume ratios (R) included: (i) bulk density (ρ_b), given as the ratio between the mass of dry soil and its volume; (ii) void ratio (e), calculated as the ratio between the volumes of soil pores and solids; (iii) total porosity (n), given by the expression $n = 1 - \rho_b/\rho_p$, where ρ_p is the particle density (Table 1); and (iv) degree of compaction (DC), calculated as the ratio between ρ_b and the maximum bulk density from the Proctor test as given by the pedotransfer function by Dias Junior and Miranda (2000).

Initially, the effects of sampling field and depth were tested for each of these attributes by analyses of variance (ANAVA). The M and R attributes were normalized (by subtracting the minimum value from each observation and dividing this difference by the amplitude) in order to allow for direct comparisons of the regression coefficients regardless of the different measurement units. The relation between σ_p, Ψ, M and R were investigated by means of linear regression models. A principal components analysis was also performed in order to allow for better visualization of the relations between the attributes. All the statistical procedures were performed on RStudio (RStudioTeam, 2016).

3 RESULTS AND DISCUSSION

3.1 Soil attribute variation between sampling fields and depths

In order to better analyze the influence of different moisture and mass/volume ratio attributes (M and R, respectively) on precompression stress (σ_p), we first investigated the influence of sampling field, sampling depth and water tension over these predictor variables. Analyses of variance (results depicted in Tables 2 and 3) were performed considering the interacting factors field and depth for the mass/volume attributes (bulk density, ρ_b, degree of compaction, DC, void ratio, e, and total porosity, n) and field, depth and water tension for the water content attributes (gravimetric water content, θ_g, volumetric water content, θ_v, degree of saturation, S, water ratio, w, water content in relation to the optimum water content for compaction, θ_g/θ_{opt}, and water content in relation to the plastic limit, θ_g/θ_{PL}).

The attributes ρ_b, e and n portrayed similar results (Table 2), what is expected since they are conceptually related to each other. These attributes were strongly affected by the sampling field, which retained around 40% of the total sum of squares (SSq), since this factor comprises not only differences on texture (clay content ranging from 39 up to 58%) and organic matter content (Table 1), but also on management history. DC was much less affected by sampling field (only 8.5% of the total SSq retained in this factor) and also presented a lower total SSq, meaning less variation (total SSq values can be directly compared between attributes since these were normalized prior to the analyses). In comparison to ρ_b, e and n, DC was much less affected by the differences in intrinsic soil attributes (texture and organic matter content), resulting in a much weaker dependence on sampling field. This demonstrates that DC more properly represents the differences arising from differences in management history between fields, while ρ_b, e and n overestimate the effect of sampling field, which could be erroneously credited to differences in soil management.

These results indicate that DC may be more appropriate for predicting σ_p when data comes from differently-textured soils. By constructing a model of $\sigma_p = f(\rho_b)$, the predictor ρ_b is affected not only by the compaction state of the soil, but also by its intrinsic properties. If predictions based on ρ_b are intended, one should therefore fit a different model for each experimental unit, add field as a predictor variable if they are of different textures, or include additional predictors such as clay or organic matter content as was done by Schjønning and Lamandé (2018). The use of DC in soil quality studies has long been recognized as an alternative for coping with soils of different textures (Hakansson and Lipiec, 2000; Reichert et al., 2009), although this attribute originated and is more commonly employed by Soil Mechanics within a geotechnical scope (e.g. Holtz and Kovacs, 1981). Nevertheless, current research on mechanics of agricultural soils still relies more heavily on ρ_b (e.g. Lima et al., 2018; Schjønning and Lamandé, 2018).

Table 2. Partitioning of the sum of squares (SSq) from the analyses of variance for bulk density (ρ_b), void ratio (e), total porosity (n) and degree of compaction (DC) according to de sources of variation sampling field, depth and their interaction.

Sources of variation	Partitioning of the SSq (%)			
	ρ_b	e	n	DC
Field	37.1^{**}	40.1^{**}	42.0^{**}	8.5^{**}
Depth	8.18^{**}	5.57^{**}	5.10^{**}	15.3^{**}
Field*Depth	2.62^{**}	0.75^{ns}	1.17^{*}	4.10^{**}
Residuals	52.1	53.6	51.7	72.0
Total SSq	22.5	21.2	21.7	15.2

[**]: significant at 1%; [*]: significant at 5%; [ns]: non-significant.

The soil moisture attributes (M) were significantly affected by both field and depth, but also by the additional factor Ψ (Table 3), which accounted for most of the SSq among the tested sources of variation (from 23.3 to 41.0%). Weight-basis and volume-basis water contents (θ_g and θ_v respectively) behaved very distinctly, with the former being better explained by sampling field than the latter, which retained most of the SSq in the residue. These differences most likely arise from the effect of an additional factor not included as a source of variation that is ρ_b. The correlation coefficient between ρ_b and θ_g was -0.60, with less water retained the denser the soil since the samples were equilibrated at higher water potentials (-10 and -100 kPa), more dependent on structural porosity, and because ρ_b itself

was very dependable on sampling field (Table 2). While θ_v is conceptually related to ρ_b (being defined as the product between θ_g and ρ_b), their correlation coefficient was very low (0.04) because ρ_b acted in opposing ways (decreasing θ_g but also acting to increase the product θ_g x ρ_b). Therefore, the effect of sampling field, which actually accounted for the effect of ρ_b, was much weaker for θ_v than for θ_g.

Degree of saturation (S) also behaved distinctly, with a slightly higher sum of squares, from which 64.8% remained in the residue (that is, unaccounted for by the considered sources of variation). S also correlated more strongly to ρ_b as θ_g, but in an inverse way, with a correlation coefficient of 0.67. S is doubly affected by ρ_b, both on its numerator ($\theta_v = \theta_g$ x ρ_b) and its denominator ($n = 1 - \rho_b/\rho_p$). Water ratio (w) and θ_g behaved very similarly both on their total variability (similar sum of squares) and their distributions among the sources of variation (water tension, sampling field and depth). The former has recently been acknowledged as an option for predicting σ_p (Schjønning and Lamandé, 2018), although its determination is not as straightforward because it depends on particle density, whereas θ_g does not. Similarly to DC, the ratios θ_g/θ_{opt} and θ_g/θ_{PL} also presented lower variability (lower total sum of squares) and were less affected by sampling field since they are also relative measures of water content. Since their relative nature is based on moisture attributes strongly affected by soil texture (soil consistency and compactability), sampling field accounted for only a small fraction of the SSq.

Table 3. Partitioning of the sum of squares (SSq) from the analyses of variance for gravimetric water content (θg), volumetric water content (θv), degree of saturation (S), water ratio (w), and the ratios between θg and the water optimum water content for compaction (θg/θopt) and between θg and the plastic limit (θg/θPL) according to de sources of variation sampling field, depth and their interaction.

Sources of variation	Partitioning of the SSq (%)					
	θ_g	θ_v	S	w	θ_g/θ_{gopt}	θ_g/θ_{gLP}
Ψ	28.2[**]	41.0[**]	23.3[**]	27.9[**]	33.7[**]	34.0[**]
Field	25.8[**]	5.0[**]	9.83[**]	29.2[**]	1.59[**]	6.1[**]
Depth	3.88[**]	0.02[ns]	1.55[*]	2.5[**]	7.55[**]	3.5[**]
Field*depth	3.57[**]	2.5[**]	0.51[ns]	2.5[**]	6.51[**]	5.1[**]
Residuals	38.6	51.5	64.8	37.9	50.7	51.3
Total SSq	15.6	15.1	17.2	16.7	9.7	11.6

[**]: significant at 1%; [*]: significant at 5%; [ns]: non-significant.

The biplot from the principal components analysis (PCA) helped to better grasp all the variation in the data (Figure 2), since it was able to represent approximately more than 90% of the total variability in just two principal components (PC) as many of the attributes are correlated to each other. Although not included as a variable in the PCA, Ψ was a major factor affecting the soil attributes, as can be seen from the segregation it promoted in the observation points. The moisture attributes θ_g, w, θ_g/θ_{opt} and θ_g/θ_{PL} behaved very similarly (arrows clustered together) and were strongly correlated to σ_p but in an inverse manner. This was also observed for θ_v, but with a much weaker association to the cluster formed by the previously mentioned attributes and also to σ_p. Although Schjønning and Lamandé (2018) advocated for the use of w as a predictor for σ_p, we did not confirmed its usefulness in the present study and further discourage its use since it is not as directly interpretable as θ_g. Also θ_v is often adopted as a predictor for σ_p (Ajayi et al., 2014; Andrade et al., 2017; Martins et al., 2018), but care should be taken because of how it is influenced by ρ_b (the arrow for θv was displaced in the direction of higher ρ_b values in the biplot) and thus might portray a weaker relation to σ_p than θ_g. This same trend was observed for S but more intensively, with its arrow being displaced in the direction of higher ρ_b and DC even further.
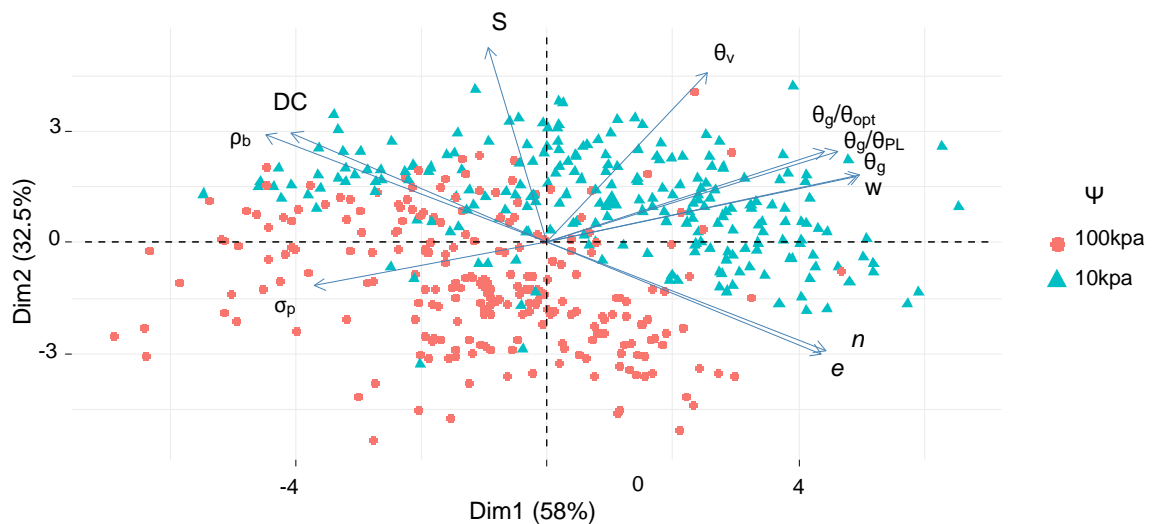
Figure 2. Principal component analysis biplot. Depicted variables are: precompression stress (σ_p); gravimetric water content (θ_g); volumetric water content (θ_v); degree of saturation (S); water ratio (w); ratio between θ_g and the optimum water content for compaction (θ_g/θ_{opt}); ratio between θ_g and the plastic limit (θ_g/θ_{PL}); bulk density (ρ_b), total porosity (*n*), void ratio (*e*) and degree of compaction (DC). Points colored according to soil water tension (Ψ).

3.2 Prediction of σ_p from soil moisture attributes and mass/volume ratios

Predictions based on a single attribute varied substantially for M (Table 4), with coefficient of determination (R^2) values ranging from 0.006 to 0.469 (model $\sigma_p = a + bM$ in Table 4), while predictions based on a single R attribute (model $\sigma_p = a + bR$ in Table 4) resulted in R^2 values always below 0.22. Although water content is often considered the major factor affecting soil mechanical strength (e.g. Ajayi et al., 2014; Andrade et al., 2017; Martins et al., 2018), in the present study the M attributes alone did not explain more than half of the variation in σ_p. This may be related to the narrower range of variation in water contents in the present study (average water content ranging from 0.18 to 0.28 g g^{-1}, Table 1), since we evaluated only two water tensions, 10 and 100 kPa.

The best predictions based on models with a single predictor were obtained for θ_g/θ_{opt} and θ_g/θ_{PL} (R^2 values of 0.469 and 0.419 respectively), while θ_g and θ_v performed more poorly (R^2 values of 0.378 and 0.173 respectively). Adding Ψ to the models based on M attributes improved predictions (reaching a maximum R^2 value of 0.542), since Ψ was the major factor affecting the variability in these attributes (Table 3 and Figure 2). Nevertheless, there was virtually no benefit from allowing Ψ to interact with the M attributes (Table 4), with a negligible increase in R^2 but also associated to an increase in AIC values (indicating an inflated model, with uninformative predictors). For the R attributes, even though prediction accuracy was lower at first (for the single-attribute models), it substantially increased by adding Ψ to the models and increased even further when Ψ and R were allowed to interact. The best predictor among the R attributes was DC, which resulted in models with higher R^2 and lower AIC values.

Although θ_v and ρ_b are the most common predictors used for modeling σ_p (Andrade et al., 2017; Lima et al., 2018; Martins et al., 2018; Schjønning and Lamandé, 2018), these were not the best predictors within its respective groups (M and R). The best predictions were obtained by the attributes that constitute relative measures obtained in relation to some reference variable that depends on intrinsic soil properties, such as DC, θ_g/θ_{opt} and θ_g/θ_{PL}. Although this presents an additional effort in order to obtain this reference variable, it could be easily done from available pedotransfer functions, such as those from the studies by Dias Junior and Miranda (2000) for soils within our study region, Marcolin and Klein (2011) for soils from Southern Brazil and Keller and Håkansson (2010) for Swedish soils. Since these relative measures may enhance prediction models, efforts in developing these pedotransfer functions should be intensified in order to make predictions available for a broader range of

soils. Because DC performed the best for predicting σ_p (since the data came from different soils and were analyzed together) and because ρ_b is the most common mass/volume ratio for predicting σ_p, only these two mas/volume ratios were kept in the following analyses.

Table 4. Performance of the fitted linear models for predicting soil precompression stress (σ_p) from different moisture attributes, mass/volume ratios and water tension (Ψ) as given by their coefficients of determination (R^2) and Akaike information criteria (AIC) values.

Prediction of σ_p from soil moisture attributes (M = θ_g, θ_v, θ_g/θ_{opt}, θ_g/θ_{PL}, w or S)						
Model	θ_g	θ_v	θ_g/θ_{opt}	θ_g/θ_{PL}	w	S
expression	R^2					
$\sigma_p = a + bM$	0.378	0.173	0.469	0.419	0.352	0.006
$\sigma_p = a + bM + c\Psi$	0.496	0.382	0.542	0.507	0.481	0.446
$\sigma_p = a + bM\Psi$	0.488	0.346	0.529	0.497	0.473	0.300
$\sigma_p = a + bM + c\Psi + dM\Psi$	0.497	0.388	0.544	0.507	0.481	0.492
	AIC					
$\sigma_p = a + bM$	4952.2	5082.0	4880.0	4921.0	4971.0	5166.2
$\sigma_p = a + bM + c\Psi$	4858.0	4951.2	4814.3	4848.7	4872.3	4901.5
$\sigma_p = a + bM\Psi$	4866.1	4977.2	4827.5	4857.8	4878.8	5008.4
$\sigma_p = a + bM + c\Psi + dM\Psi$	4859.8	4949.1	4815.2	4850.6	4873.5	4864.3
Prediction of σ_p from soil mass/volume ratios (R = ρ_b, DC, e or n)						
Model	ρ_b	DC	e	n		
expression	R^2					
$\sigma_p = a + bR$	0.160	0.219	0.142	0.136		
$\sigma_p = a + bR + c\Psi$	0.410	0.532	0.522	0.530		
$\sigma_p = a + bR\Psi$	0.543	0.604	0.524	0.519		
$\sigma_p = a + bR + c\Psi + dR\Psi$	0.561	0.613	0.543	0.539		
	AIC					
$\sigma_p = a + bR$	5089.5	5056.1	5099.2	5102.3		
$\sigma_p = a + bR + c\Psi$	4930.1	4824.7	4834.5	4827.0		
$\sigma_p = a + bR\Psi$	4813.5	4748.4	4832.2	4837.1		
$\sigma_p = a + bR + c\Psi + dR\Psi$	4797.5	4739.8	4815.6	4819.9		

M: soil moisture attributes: gravimetric water content (θ_g); volumetric water content (θ_v); degree of saturation (S); water ratio (w); ratio between θ_g and the optimum water content for compaction (θ_g/θ_{opt}); ratio between θ_g and the plastic limit (θ_g/θ_{PL}). R: soil mass/volume ratios: bulk density (ρ_b), void ratio (e), total porosity (n) and degree of compaction (DC). a, b, c and d: equation parameters.

For the soil moisture attributes (M), there was little difference in considering Ψ as an independent predictor or allowing it to interact, meaning that there was very little performance gain by allowing the moisture attributes to display different slopes depending on Ψ. Although σ_p is frequently described by nonlinear models (Ajayi et al., 2014; Andrade et al., 2017; Martins et al., 2018), thus by equations in which the slope varies according to the predictor value, the single-slope linear equations we fitted may have sufficed given the narrower range of variation in soil moisture in the present study (since only two Ψ values were employed). As for the mass/volume ratios (R), there was a notable increase in model performance by allowing these attributes to interact with Ψ, indicating that the effect of compaction in making the soil stronger acts at different rates depending on Ψ. Although this interaction had a substantial effect in the models based on R attributes from Table 4, it was not as strong when the three predictors (M, R and Ψ) were combined (Table 5).

When all three predictor variables (M, R and Ψ) were considered together, R^2 values reached a maximum of 0.597 for ρ_b and 0.638 for DC (Table 5). This difference arises from the effect that DC has on controlling the variation between fields that arise from differences in their intrinsic soil attributes (Table 1). The best predictions were obtained from the models that combined a moisture attribute and the interaction of DC and Ψ. In the models from Table 5, θ_g/θ_{opt} and θ_g/θ_{PL} were not always as superior to the other moisture attributes as was observed for the models on Table 4. In the previous models (models based on M and Ψ, Table 4), these attributes were the only control for the influence of differences in intrinsic attributes across fields. In Table 5, θ_g/θ_{opt} and θ_g/θ_{PL} remained superior when combined to ρ_b, but were not better than the others when DC was adopted.

The results of this section indicate that prediction of soil properties from moisture and mass/volume ratio attributes may suffer several setbacks which need to be properly addressed by the statistical analysis. The majority of soil physical properties were strongly affected by field and depth (Tables 2 and 3), since these factors incurred in differences in intrinsic attributes (Table 1). The alternatives to cope with this may include (i) adding field and depth as predictor variables, what would affect the usefulness of the statistical parameters related to the soil attributes and hamper the application of the model to other sites; (ii) fit models separately according to the experimental units, what would narrow the variation of the observed values and drastically reduce the number of degrees of freedom in the residue; (iii) add soil texture, organic matter content or other attributes as predictor variables to address the variation between experimental units, although these attributes have complex relations to

virtually every soil aspect of soil behavior (water retention, bulk density, organic matter content, and so on); or (iv) employ physical attributes which are less affected by these variations since they are calculated in relation to some variable that already deals with intrinsic differences, such as the employed variables DC, θ_g/θ_{opt} and θ_g/θ_{PL}. Therefore, we may recommend that at least one predictor variable should be a relative measurement, whether of mass/volume ratio or water content, when data from different fields that differ on their intrinsic properties are compared together.

Table 5. Performance of the fitted linear models for predicting soil precompression stress (σ_p) from different moisture attrinutes, mass/volume ratios and water tension (Ψ) as given by their coefficients of determination (R^2) and Akaike information criteria (AIC) values.

Model expression	Soil moisture attributes (M)					
	θ_g	θ_v	θ_g/θ_{opt}	θ_g/θ_{PL}	w	S
	R^2					
$\sigma_p = a + bM\rho_b$	0.413	0.376	0.495	0.450	0.392	0.376
$\sigma_p = a + bM + c\rho_b$	0.379	0.349	0.480	0.442	0.355	0.376
$\sigma_p = a + bM + c\Psi + d\Psi\rho_b$	0.563	0.562	0.597	0.584	0.561	0.567
$\sigma_p = a + bM + c\Psi\rho_b$	0.469	0.450	0.540	0.514	0.455	0.458
$\sigma_p = a + bM + c\Psi + d\rho_b$	0.549	0.546	0.590	0.574	0.545	0.550
$\sigma_p = a + bM(DC)$	0.450	0.488	0.499	0.463	0.437	0.498
$\sigma_p = a + bM + c(DC)$	0.423	0.472	0.497	0.463	0.409	0.495
$\sigma_p = a + bM + c\Psi + d\Psi DC$	0.620	0.627	0.633	0.623	0.619	0.638
$\sigma_p = a + bM + c\Psi DC$	0.567	0.579	0.597	0.579	0.562	0.589
$\sigma_p = a + bM + c\Psi + d(DC)$	0.614	0.621	0.629	0.618	0.612	0.631
	AIC					
$\sigma_p = a + bM\rho_b$	4929.9	4958.2	4861.3	4900.2	4945.7	4957.5
$\sigma_p = a + bM + c\rho_b$	4953.3	4975.3	4872.5	4905.1	4970.9	4955.7
$\sigma_p = a + bM + c\Psi + d\Psi\rho_b$	4797.5	4798.4	4760.1	4775.2	4799.3	4793.1
$\sigma_p = a + bM + c\Psi\rho_b$	4884.7	4900.6	4818.7	4844.0	4896.2	4893.5
$\sigma_p = a + bM + c\Psi + d\rho_b$	4810.1	4813.1	4766.7	4783.7	4813.7	4808.5
$\sigma_p = a + bM(DC)$	4900.7	4867.7	4858.1	4889.1	4911.1	4859.1
$\sigma_p = a + bM + c(DC)$	4919.9	4879.7	4857.1	4887.3	4931.2	4859.2
$\sigma_p = a + bM + c\Psi + d\Psi DC$	4733.3	4724.7	4718.4	4729.7	4735.5	4711.7
$\sigma_p = a + bM + c\Psi DC$	4791.0	4778.0	4758.8	4778.2	4796.5	4767.4
$\sigma_p = a + bM + c\Psi + dDC$	4738.5	4730.0	4720.7	4733.5	4741.3	4718.6

M: soil moisture attributes: gravimetric water content (θ_g); volumetric water content (θ_v); degree of saturation (S); water ratio (w); ratio between θ_g and the optimum water content for compaction (θ_g/θ_{opt}); ratio between θ_g and the plastic limit (θ_g/θ_{PL}). ρ_b: bulk density. DC: degree of compaction. a, b, c and d: equation parameters.

3.3 Prediction accuracy and interpretation of model coefficients

Prediction accuracy for the best-performance model from the previous section (σ_p = a + bM + cΨ + dΨR) fitted to ρ_b and DC (respectively the most common and the best predictor of the R attributes) was assessed graphically (Figure 3) and by calculating the RMSE (Table 6). As indicated previously, predictions based on DC were more accurate than those based on ρ_b, as indicated by the points closer to the 1:1 line (Figure 3) and the lower RMSE values (Table 6), which were on average 42.7 kPa for DC and 46.1 for ρ_b. Figure 3 and Table 6 also indicate that prediction accuracy was higher for Ψ = 10 kPa than for Ψ = 100 kPa, although this difference was more evident for the models based on ρ_b.

The chosen model (σ_p = a + bM + cΨ + dΨR) was fitted to the data with and without normalization. The normalization sets all the predictor variables to the same scale (from 0 to 1) and thus gives a measure of the importance of each predictor, while the model adjusted without normalization is more easily interpreted since it makes use of the predictor variables at their original units. Ψ entered the models as a categorical dummy variable, and its value is 0 for 100 kPa and 1 for 10 kPa. Therefore, the models differ according to Ψ both on the intercept (given by "a" for Ψ = 100 kPa and by "a" + "c" for Ψ = 100 kPa) and on the coefficient that multiplies the R variables (parameter "d" has different values according to Ψ).

Table 6. Root-mean-square error (RMSE) values for the model σ_p = a + bM + cΨ + dΨR, where σ_p is the soil precompression stress (kPa), M is the soil moisture attribute, Ψ is the soil water tension and R is the mass/volume ratio (bulk density, ρ_b, and degree of compaction, DC).

M attribute[1]	ρ_b		DC	
	Ψ (kPa)		Ψ (kPa)	
	10	100	10	100
θ_g	43.2	50.0	39.8	46.4
θ_v	43.1	50.4	40.3	45.1
θ_g/θ_{opt}	43.4	45.7	40.9	43.7
θ_g/θ_{PL}	42.6	48.0	40.2	45.6
w	43.0	50.5	39.7	46.7
S	43.5	49.6	41.4	43.1

[1]M attributes: gravimetric water content (θ_g); volumetric water content (θ_v); degree of saturation (S); water ratio (w); ratio between θ_g and the optimum water content for compaction (θ_g/θ_{opt}); ratio between θ_g and the plastic limit (θ_g/θ_{PL}).
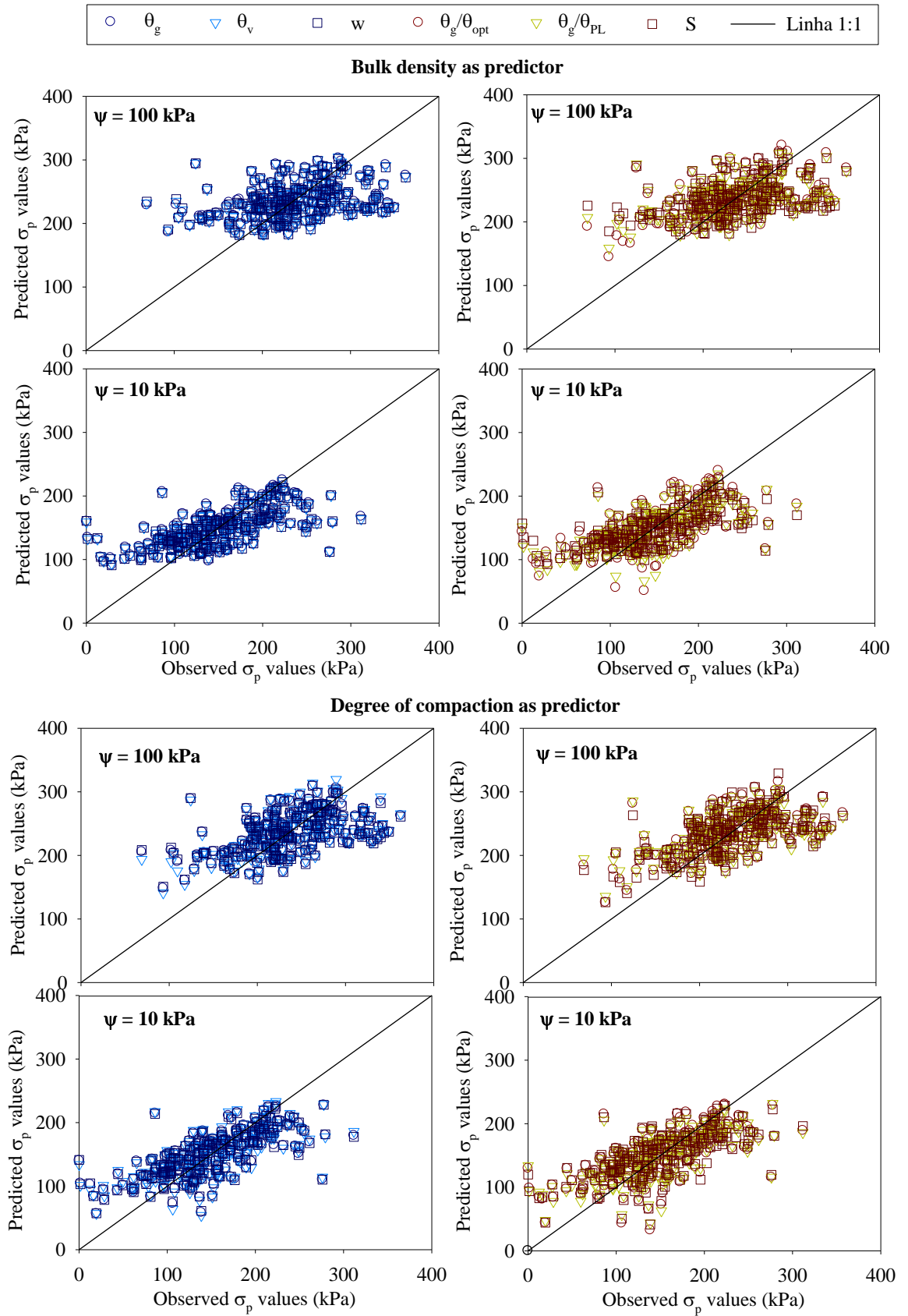
Figure 3. Observed and predicted precompression stress values ($\sigma_p = a + bM + c\Psi + d\Psi R$).

The effect of water tension can be noted from the parameter "c" in Table 7, which represents the decrease (since it is negative) in σ_p when the soil is equilibrated at 10 kPa (this parameter multiplies the dummy variable Ψ, which is 0 for 100 kPa and 1 for 10 kPa). When the soil dries from 10 kPa to 100 kPa, there is an average increase in mechanical strength of approximately 100 kPa (overall average for the model parameter "c" from the normalized models in Table 7). This increase is approximately the double of what Severiano et al. (2013, 2011) found for Oxisols of similar textures in the Brazilian Cerrado under natural vegetation, and also higher than what Oliveira et al. (2003) observed for annually tilled Oxisols.

In terms of the relative importance of the R and M attributes, the parameters from the equations adjusted to the normalized predictors indicate there is no absolute superiority of one over the other and that the relative importance of each predictor also depended on Ψ and on the R attribute itself (whether ρ_b or DC). For this comparison, the coefficient for Ψ ("c" in Table 7) was summed to that of the M attributes ("b" in Table 7) because they both relate to water content and they both vary from zero to one.

By doing so, it was noted that the effect of Ψ and M combined (given by "b" + "c" in Table 7) ranged from -129.7 to -226.1 for the models based on ρ_b and from -150.3 to -202.9 for the models based on DC (these coefficients indicate the variation in σ_p when Ψ = 10 kPa and the M attribute is at its maximum value, which is 1 since the predictors were normalized). As for the ρ_b and DC, their effect (given by the parameter "d" in Table 7) was on average respectively 152.2 and 203.7 for Ψ = 10 kPa and 78.9 and 145.7 for Ψ = 100 kPa. These coefficients indicate that the R attributes contribute more to σ_p when the soil is at Ψ = 10 kPa than when the soil is at Ψ = 100 kPa. Additionally, DC also contributed more to σ_p than ρ_b, but this difference is due to their different performance as predictors for σ_p (as discussed earlier, DC was a better predictor than ρ_b in this study).

When ρ_b was used as a predictor variable, Ψ and M had a much higher importance in determining σ_p values ("b" + "c" was on average 2.3 and 1.7 times higher than "d_{10kPa}" and "d_{100kPa}" respectively). When DC was adopted as the predictor variable, the summed effects of Ψ and M (given by the summed coefficients "b" + "c") were on average only 1.2 and 0.88 of that for DC at 10 kPa and 100 kPa respectively. These results also seem to be linked to the performance of each predictor variable: ρ_b was a worse predictor for σ_p than was DC, therefore the former indicated a smaller importance than the latter in comparison to the moisture attributes (Ψ and M). Overall, our results indicate that neither mass/volume ratios nor moisture attributes can be regarded as the absolute most important single factor

controlling mechanical strength. This comparison is biased by the statistical importance of each attribute in improving model performance and is also affected by the significant interaction between Ψ and the R attributes.

Table 7. Values of the adjusted parameters for the linear regression models which predict soil precompression stress (σ_p) from water tension (Ψ), moisture attributes (M), bulk density (ρ_b) and degree of compaction (DC).

| Moisture variables | Normalized predictors | | | | | | | | | |
| | $\sigma_p = a + bM + c\Psi + d\Psi\rho_b$ | | | | | $\sigma_p = a + bM + c\Psi + d\Psi DC$ | | | | |
	a	b	c	d_{100kPa}	d_{10kPa}	a	b	c	d_{100kPa}	d_{10kPa}
θ_g	214.4	-28.2	-116.1	72.4	149.2	185.3	-45.3	-110.8	126.8	187.3
θ_v	203.3	-15.9	-119.7	85.1	165.8	176.1	-61.5	-105.0	158.3	218.0
θ_g/θ_{opt}	256.4	-137.1	-88.9	56.7	113.1	206.3	-102.7	-94.5	116.6	163.1
θ_g/θ_{PL}	237.2	-95.8	-97.4	65.6	128.6	187.8	-65.7	-104.2	125.9	180.5
w	201.6	-7.3	-122.4	80.3	161.9	180.2	-36.8	-113.6	130.0	192.9
S	202.9	-49.6	-114.4	113.3	194.6	155.7	-99.5	-103.3	216.3	280.6

| Moisture variables | Predictors in original units | | | | | | | | | |
| | $\sigma_p = a + bM + c\Psi + d\Psi\rho_b$ | | | | | $\sigma_p = a + bM + c\Psi + d\Psi DC$ | | | | |
	a	b	c	d_{100kPa}	d_{10kPa}	a	b	c	d_{100kPa}	d_{10kPa}
θ_g	126.4	-109.5	-225.0	105.5	217.4	44.3	-175.9	-189.4	2.7	4.1
θ_v	93.9	-58.7	-234.2	124.1	241.7	14.2	-226.7	-182.5	3.4	4.7
θ_g/θ_{opt}	242.8	-117.5	-168.9	82.6	164.8	105.0	-88.1	-154.9	2.5	3.5
θ_g/θ_{PL}	199.4	-100.8	-186.7	95.6	187.4	62.3	-69.1	-175.1	2.7	3.9
w	91.7	-11.4	-238.2	117.0	236.0	31.3	-57.1	-195.1	2.8	4.2
S	69.5	-73.5	-229.8	165.2	283.7	-70.3	-147.5	-186.8	4.7	6.1

M: gravimetric water content (θ_g); volumetric water content (θ_v); degree of saturation (S); water ratio (w); ratio between θ_g and the optimum water content for compaction (θ_g/θ_{opt}); ratio between θ_g and the plastic limit (θ_g/θ_{PL}). a, b, c and d: equation parameters. Ψ was included as a categorical variable and its coefficient ("b") relates to water tension at 10 kPa.

Considering the models without normalization, which can be more easily interpreted, an increase in θ_g of 0.01 g g^{-1} (1%) decreases σ_p in approximately 2 kPa. When the soil is ate the optimum moisture for compaction ($\theta_g/\theta_{opt} = 1$), σ_p may decrease in more than 100 kPa, whereas the average reduction for the soil in the plastic limit ($\theta_g/\theta_{PL} = 1$) is of 85 kPa (considering both the models for ρ_b and DC). For each increase in ρ_b of 0.1 Mg m^{-3}, there is

an average increase in σ_p of approximately 11 kPa for $\Psi = 100$ kPa and 22 kPa for $\Psi = 10$ kPa. Similarly, for each 1% increase in DC, there is an average increase in σ_p of 3.2 kPa for $\Psi = 100$ kPa and of 4.4 kPa for $\Psi = 10$ kPa. It was also observed by Reichert et al. (2018) that ρ_b has a stronger effect upon σ_p for $\Psi = 10$ kPa in comparison to $\Psi = 100$ kPa.

4 CONCLUSIONS

Soil bulk density (ρ_b), total porosity and void ratio were strongly affected by sampling field and depth, while degree of compaction (DC) was much less affected by these. The moisture attributes were greatly influenced by soil water tension (Ψ), whereas gravimetric water content and water ratio were also affected by sampling field and depth.

Variation in intrinsic soil attributes (such as soil texture) affected the performance of the different predictors, while relative measures such as degree of compaction (DC) usually resulted in more accurate predictions for precompression stress (σ_p).

The normalized prediction models indicated that the different predictors for σ_p interacted in complex ways and the relative importance of each attribute (moisture vs. mass/volume ratio) varied according to attribute (whether absolute measures, as ρ_b, or relative, as DC) and water potential (Ψ).

For $\Psi = 10$ kPa, ρ_b and DC had a stronger effect over σ_p than at $\Psi = 100$ kPa, while the contribution from the moisture attributes behaved inversely (greater importance at $\Psi = 100$ kPa). DC contributed more strongly to σ_p than ρ_b because the formed was a better predictor than the latter.

5 ACKNOWLEDGEMENTS

6 REFERENCES

Ajayi, A.E., Dias Junior, M.S., Curi, N., Okunola, A., Souza, T.T.T., Pires, B.S., 2010. Assessment of vulnerability of oxisols to compaction in the Cerrado region of Brazil. Pedosphere 20, 252–260. doi:10.1016/S1002-0160(10)60013-6

Ajayi, A.E., Dias Junior, M.S., Curi, N., Pais, P.S.M., Iori, P., 2014. Hydrophysical properties

of Humic Latosols from Brazil. Int. Agrophysics 28, 395–402. doi:10.2478/intag-2014-0030

Andrade, M.L. C., Tassinari, D., Dias Junior, M.S., Martins, R.P., Rocha, W.W., Souza, Z.R., 2017. Soil compaction caused by harvest and logging operations in eucalyptus forests in coarse-textured soils from Northeastern Brazil. Ciência e Agrotecnologia 41, 191–200. doi:10.1590/1413-70542017412036216

Dias Junior, M.S., Martins, P.C.C., 2017. Ensaio de compressão uniaxial e modelos de capacidade de suporte de carga do solo, In: Teixeira, P.C., Donagemma, G.K., Fontana, A., Teixeira, W.G. (Eds.), Manual de métodos de análise de solo. Embrapa, Brasília, DF, pp. 152–171.

Dias Junior, M.S., Miranda, E.É.V., 2000. Comportamento da curva de compactação de cinco solos da região de Lavras (MG). Cienc. e Agrotecnologia 24, 337–346.

Dias Junior, M.S., Pierce, F.J., 1995. A simple procedure for estimating preconsolidation pressure from soil compression curves. Soil Technol. 8, 139–151. doi:10.1016/0933-3630(95)00015-8

Donagemma, G.K., Viana, J.H.M., Almeida, B.G., Ruiz, H.A., Klein, V.A., Dechen, S.C.F., Fernandes, R.B.A., 2017. Análise granulométrica, In: Teixeira, P.C., Donagemma, G.K., Fontana, A., Teixeira, W.G. (Eds.), Manual de métodos de análise de solo. Embrapa, Brasília, DF, pp. 95–116.

FEAM - Fundação Estadual Do Meio Ambiente, 2010. Mapa de solos de Minas Gerais: legenda expandida. FEAM, Belo Horizonte, MG.

Fontana, A., Campos, D.V.B., 2017. Carbono orgânico, In: Teixeira, P.C., Donagemma, G.K., Fontana, A., Teixeira, W.G. (Eds.), Manual de métodos de análise de solo. Brasília, DF, pp. 360–367.

Hakansson, I., Lipiec, J., 2000. A review of the usefulness of relative bulk density values in studies of soil structure and compaction. Soil Tillage Res. 53, 71–85. doi:10.1016/S0167-1987(99)00095-1

Holthusen, D., Brandt, A.A., Reichert, J.M., Horn, R., 2018b. Soil porosity, permeability and static and dynamic strength parameters under native forest/grassland compared to no-tillage cropping. Soil Tillage Res. 177, 113–124. doi:10.1016/j.still.2017.12.003

Holthusen, D., Brandt, A.A., Reichert, J.M., Horn, R., Fleige, H., Zink, A., 2018a. Soil functions and in situ stress distribution in subtropical soils as affected by land use, vehicle type, tire inflation pressure and plant residue removal. Soil Tillage Res. 184, 78–

92. doi:10.1016/j.still.2018.07.009

Holtz, R.D., Kovacs, W.D, 1981. An Introduction to Geotechnical Engineering. Prentice-Hall: Englewood Cliffs.

Horn, R., Lebert, M., 1994. Soil compactability and compressibility, In: Soane, B.D., Van Ouwerkerk, C. (Eds.), Soil Compaction In Crop Production. Elsevier Science, Amsterdam.

Imhoff, S., Silva, A.P., Ghiberto, P.J., Tormena, C.A., Pilatti, M.A., Libardi, P.L., 2016. Physical quality indicators and mechanical behavior of agricultural soils of Argentina. Plos One 11, E0153827. doi:10.1371/Journal.Pone.0153827

INMET - Instituto Nacional de Meteorologia, 2018. Normais Climatológicas do Brasil: 1981-2010. INMET, Brasília, DF.

Keller, T., Arvidsson, J., Dawidowski, J.., Koolen, A.., 2004. Soil precompression stress II. A comparison of different compaction tests and stress–displacement behaviour of the soil during wheeling T. Soil Tillage Res. 77, 97–108. doi:10.1016/j.still.2003.11.003

Keller, T., Arvidsson, J., Schjønning, P., Lamandé, M., Stettler, M., Weisskopf, P., 2012. In situ subsoil stress-strain behavior in relation to soil precompression stress. Soil Sci. 177, 490–497. doi:10.1097/Ss.0b013e318262554e

Keller, T., Håkansson, I., 2010. Estimation of reference bulk density from soil particle size distribution and soil organic matter content. Geoderma 154, 398–406. doi:10.1016/j.geoderma.2009.11.013

Keller, T., Lamandé, M., Peth, S., Berli, M., Delenne, J.Y., Baumgarten, W., Rabbel, W., Radja, F., Rajchenbach, J., Selvadurai, A.P.S., Or, D., 2013. An interdisciplinary approach towards improved understanding of soil deformation during compaction. Soil Tillage Res. 128, 61–80. doi:10.1016/J.Still.2012.10.004

Koolen, A.J., Kuipers, H., 1983. Agricultural Soil Mechanics. Springer-Verlag, Berlin.

Lebert, M., Böken, H., Glante, F., 2007. Soil compaction—indicators for the assessment of harmful changes to the soil in the context of the German Federal Soil Protection Act. J. Environ. Manage. 82, 388–397. doi:10.1016/j.jenvman.2005.11.022

Lima, R.P., Silva, A.P., Giarola, N.F.B., Silva, A.R., Rolim, M.M., Keller, T., 2018. Impact of initial bulk density and matric suction on compressive properties of two Oxisols under no-till. Soil Tillage Res. 175, 168–177. doi:10.1016/j.still.2017.09.003

Marcolin, C.D., Klein, V.A., 2011. Determinação da densidade relativa do solo por uma função de pedotransferência para a densidade do solo máxima. Acta Sci. Agron. 33, 349–

354. doi:10.4025/actasciagron.v33i2.6120

Martins, P.C.C., Dias Junior, M.S., Ajayi, A.E., Takahashi, E.N., Tassinari, D., 2018. Soil compaction during harvest operations in five tropical soils with different textures under Eucalyptus forests. Ciência e Agrotecnologia 42, 58–68. doi:10.1590/1413-70542018421005217

Mcbride, R.A., 2007. Soil consistency: upper and lower plastic limits, In: Carter, M.R., Gregorich, E.G. (Eds.), Soil sampling and methods of analysis. Crc Press, Boca Raton, FL, pp. 761–770.

Mosaddeghi, M.R., Koolen, A.J., Hemmat, A., Hajabbasi, M.A., Lerink, P., 2007. Comparisons of different procedures of pre-compaction stress determination on weakly structured soils. J. Terramechanics 44, 53–63. doi:10.1016/j.jterra.2006.01.008

Naderi-Boldaji, M., Hajian, A., Ghanbarian, D., Bahrami, M., 2018. Finite element simulation of plate sinkage, confined and semi-confined compression tests: A comparison of the response to yield stress. Soil Tillage Res. 179, 63–70. doi:10.1016/j.still.2018.02.003

Naveed, M., Schjønning, P., Keller, T., de Jonge, L.W., Moldrup, P., Lamandé, M., 2016. Quantifying vertical stress transmission and compaction-induced soil structure using sensor mat and X-ray computed tomography. Soil Tillage Res. 158, 110–122. doi:10.1016/j.still.2015.12.006

Nunes, M.R., Pauletto, E.A., Denardin, J.E., S. Suzuki, L.E.A., van Es, H.M., 2019. Dynamic changes in compressive properties and crop response after chisel tillage in a highly weathered soil. Soil Tillage Res. 186, 183–190. doi:10.1016/j.still.2018.10.017

Oliveira, G.C., Dias Junior, M.S., Resck, D.V.S., Curi, N., 2003. Alterações estruturais e comportamento compressivo de um Latossolo Vermelho distrófico argiloso sob diferentes sistemas de uso e manejo. Pesqui. Agropecuária Bras. 38, 291–299. doi:10.1590/S0100-204X2003000200017

Rabot, E., Wiesmeier, M., Schlüter, S., Vogel, H.J., 2018. Soil structure as an indicator of soil functions: A review. Geoderma 314, 122–137. doi:10.1016/j.geoderma.2017.11.009

Reichert, J.M., Mentges, M.I., Rodrigues, M.F., Cavalli, J.P., Awe, G.O., Mentges, L.R., 2018. Compressibility and elasticity of subtropical no-till soils varying in granulometry organic matter, bulk density and moisture. Catena 165, 345–357. doi:10.1016/j.catena.2018.02.014

Reichert, J.M., Suzuki, L.E.A.S., Reinert, D.J., Horn, R., Håkansson, I., 2009. Reference bulk density and critical degree-of-compactness for no-till crop production in subtropical

highly weathered soils. Soil Tillage Res. 102, 242–254. doi:10.1016/j.still.2008.07.002

RStudioTeam, 2016. RStudio: Integrated Development for R.

Rücknagel, J., Rademacher, A., Götze, P., Hofmann, B., Christen, O., 2017. Uniaxial compression behaviour and soil physical quality of topsoils under conventional and conservation tillage. Geoderma 286, 1–7. doi:10.1016/j.geoderma.2016.10.015

Schjønning, P., Lamandé, M., 2018. Models for prediction of soil precompression stress from readily available soil properties. Geoderma 320, 115–125. doi:10.1016/j.geoderma.2018.01.028

Schjønning, P., Lamandé, M., Munkholm, L.J., Lyngvig, H.S., Nielsen, J.A., 2016. Soil precompression stress, penetration resistance and crop yields in relation to differently-trafficked, temperate-region sandy loam soils. Soil Tillage Res. 163, 298–308. doi:10.1016/j.still.2016.07.003

Severiano, E. C., Oliveira, G.C. , Dias Junior, M.S., Costa, K.A.P., Silva, F.G., Ferreira Filho, S.M., 2011. Structural changes in latosols of the cerrado region: I - relationships between soil physical properties and least limiting water range. Rev. Bras. Ciência do Solo 35, 773–782. doi:10.1590/S0100-06832011000300013

Soil Survey Staff, 2014. Keys to Soil Taxonomy. Washington, DC.

Viana, J.H.M., Teixeira, W.G., Donagemma, G.K., 2017. Densidade de partículas, In: Teixeira, P.C., Donagemma, G.K., Fontana, A., Teixeira, W.G. (Eds.), Manual de métodos de análise de solo. Embrapa, Brasília, DF, pp. 76–81.

Watanabe, R., Figueiredo, G.C., Silva, A.P., Neves, J.C.L., Oliveira, T.S., 2017. Soil compressibility under irrigated perennial and annual crops in a semi-arid environment. Rev. Bras. Ciência Do Solo 41. doi:10.1590/18069657rbcs20160206